AIX-MARSEILLE UNIVERSITÉ
ÉCOLE DOCTORALE SCIENCES POUR L'INGÉNIEUR 353
Mécanique, Physique, Micro et Nanoélectronique

Laboratoire de Mécanique et d'Acoustique, UMR7031 AMU CNRS Centrale Marseille

Thèse présentée pour obtenir le grade universitaire de docteur

Discipline : Sciences pour l'ingénieur
Spécialité : Acoustique

Héctor GARCÍA MAYÉN

Characterization of open toneholes of woodwind instruments

Presented the 13 of December 2021 the jury :

Jean-Pierre DALMONT	Professeur, LAUM, Le Mans, France	Rapporteur
Alexandre GARCIA	Professeur, CNAM, Paris, France	Rapporteur
Jean-Baptiste DOC	Maitre de Conférence, LMSSC, Paris, France	Examinateur
Pauline EVENO	CEO, Syos, Paris, France	Examinatrice
Christophe VERGEZ	Directeur de Recherche CNRS, LMA, Marseille, France	Directeur de thèse
Jean KERGOMARD	Directeur de recherche émérite CNRS, LMA, Marseille France	Encadrant de thèse
Michael JOUSSERAND	Ingénieur, Buffet-Crampon, Mantes-la-Ville, France	Invité

Acknowledgments

I would like to thank Michaël Jousserand and the Buffet Crampon society for having me as an employee during this thesis work, I was very happy to get into the heart of the fabrication of the legendary Buffet Crampon woodwind instruments.

My gratefulness to the ANRT for the CIFRE scholarship No 2017/1600, the main funding of the thesis. Also to the Mexican council of science, CONACYT scholarship 707987, without this funding I couldn't have my family with me during all these years.

Thanks to my tutor Christophe Vergez, for helping me with all the administrative situations, that is not a small endeavor, overall with the funding without which I couldn't have provided for my family. Also his insightful revisions that always contributed to have better results.

I'm grateful to Patrick Sanchez for all his disposition in every aspect, scientific or not, that I had to deal with from the very first moment me and my family arrived in Marseille.

Many thanks to Fabrice Silva for being my accomplice in the COMSOL simulations. And for all the useful scientific discussions, advise and support, it was nice that he had a lot of disposition to do it in Spanish.

Thanks to all the sound team of the LMA that made me feel welcome.

Thanks to my parents who have been with me since the day I was born and have never let me down. My mother and my friend Victor had suffered from cancer during these years, they have fully recover, thanks to all the support of the family. I'm glad that we will meet again to continue enjoying life.

My gratefulness to my beloved wife Maricarmen, for her support and love. And to my children Emilio, Sofia and Benjamin. It has been an amazing adventure so far.

Throughout these three years my uncles Gilberto and Sigfrido, my aunt Aida and my friend Omar have passed away. I know that there is no other reality where we will meet again, in which we will talk about all the things that you have missed. But I'm happy that we have share this life together, that we haven't miss the chance to celebrate life as it is. I don't remember the last day we saw each other, but I remember vividly all the times when we were happy together with our family and friends. A memory for you.

Contents

Introduction **3**
Framework . . . 4
Buffet Crampon Society . . . 4
Mechanics and Acoustics Laboratory (LMA) . . . 4
LIAMFI . . . 5
CIFRE . . . 5
Woodwinds and the clarinet . . . 6
Woodwinds . . . 7
The clarinet . . . 8
Acoustics of the tonehole . . . 9
Linear behavior of the tonehole . . . 9
Nonlinear behavior of the tonehole . . . 13
Topic of the PhD . . . 14
Outline of the manuscript . . . 14
Chapter 1 . . . 14
Chapter 2 . . . 15
Chapter 3 . . . 15
Conclusion and Appendix . . . 16

1 Impedance measurements in straight tubes **20**
1.1 Introduction . . . 20
1.2 Impedance Sensor (*Capteur-Z)* . . . 21
1.3 Model of uncertainties of input impedance measurements . . . 25
1.3.1 Electrical noise . . . 26
1.3.2 Modeling the uncertainty . . . 27
1.4 Some quantities extracted from the input impedance for different closed terminations 28
1.4.1 Input impedance . . . 29
1.4.2 Reflection coefficient moduli and effective length . . . 30
1.4.3 Terminal impedance . . . 32
1.4.4 Transfer impedance . . . 34
1.4.5 Conclusion of sec. 1.4 . . . 35
1.5 Radiation and input impedance measurement in an open tube . . . 44
1.5.1 Radiation Impedance . . . 44
1.5.2 Input impedance . . . 46
1.5.3 Conclusion of sec. 1.5 . . . 47
1.6 Numerical simulation . . . 48
1.6.1 Finite Element Method (FEM) . . . 48
1.6.2 Quality of the model . . . 50
1.6.3 The use of FEM in musical instruments . . . 51
1.6.4 Modeled tubes . . . 52

1.6.5 Conclusion of sec. 1.6 . . . 59

2 Tube reversed method **65**
2.1 Submitted Article . . . 65

Appendix: Finite Element Model for the tube reversed method **77**
Input impedance results . . . 79
Derived quantities . . . 80
Conclusion . . . 85

3 Method of the input and transfer impedances **89**
3.1 Introduction . . . 89
3.2 Direct problem: model . . . 90
3.3 Inverse Problem . . . 94
3.4 Simulation of the experiment: effect of uncertainties on the main tube length . . . 98
3.4.1 Analytical and numerical errors induced by the length uncertainties . . . 99
3.5 Simulation of the experiment: effects of the influence of uncertainties in the input impedance . . . 104
3.6 Comparison between the two methods . . . 109
3.7 Conclusion of the theoretical part . . . 111
3.8 Finite Element Model and measurements for the method of the input and transfer impedances . . . 112
3.8.1 Losses in the Finite Element Method . . . 112
3.9 Measurement vs FEM . . . 114
3.9.1 Reconstruction . . . 117
3.9.2 Computing of the tonehole input impedance from the FEM model . . . 118
3.9.3 Conclusion of the FEM model and measurements . . . 119

4 Conclusion and perspectives **129**
4.1 Conclusion . . . 129
4.2 Perspectives . . . 132

Appendices **135**

A Nonlinear behavior of the tonehole **135**

B Air physical properties **141**

C Bibliography **146**

D Abstracts **150**

Introduction

This work is a collaboration between Buffet Crampon, one of the most prestigious musical wind instruments makers and the Sounds Team of the Mechanics and Acoustics Laboratory (LMA[1]). That a musical instrument has gained a place in the musical tradition, does not mean that its development is over. Players will, depending on necessities, ask for improvements to their instruments. Traditionally the musical instrument making was lead by the tradition, with trial and error as the base including players feedback. Nowadays, science has been gaining importance in the design of musical instruments. In particular, for wind instruments, large companies like Buffet Crampon, Selmer or Yamaha for instance, have their own in-house R&D department, while collaborating with academic research laboratories. In this work, scientific collaboration between Buffet Crampon and the Laboratory of Mechanics and Acoustics is conducted on clarinet's lateral holes. More precisely, research is focused on how undercut techniques used by Buffet Crampon impact the produced sound. The framework of this work is detailed below, as well as the topic of this PhD.

[1] Laboratoire de Mécanique et d'Acoustique

Framework

Buffet Crampon Society

Wind instrument manufacturer based in Mantes-la-Ville France, it was founded in 1825 when the french instrument maker Denis Buffet-Auger set up his workshop in the heart of Paris, where he produced 13-keys clarinets. In 1836 Jean-Louis Buffet, son of Denis, married Zoé Crampon and creates Buffet Crampon brand. In 1850 the workshop is established in Mantes-la-Ville and the Buffet Crampon Boehm system is created [1][2]. This corresponds to the set of principles for making toneholes on woodwinds, that laid the foundation for modern instrument making (see details in the section devoted to the clarinet). The company produces the whole game of wind instruments: woodwinds, brass, transverse flute and saxophones. It also has a research and development department that is in close contact with acousticians to continually improve their instruments with scientific basis [1].

Mechanics and Acoustics Laboratory (LMA)

The LMA [2][3] is a Research Unit of CNRS[4] (National Center of the Scientific Research, Institute of Engineering Science and Systems INSIS), attached to the Aix-Marseille University (AMU), and to the Ecole Centrale de Marseille. The LMA has as objective to ensure the continuity between fundamental research in engineering and technology, within the Acoustics and Mechanics domains of knowledge. The LMA develops original research from the comprehension of the phenomena to the development of systems with high technological or societal stake, through their design or the development of basic concepts and technologies. The LMA has national and international known

[2] https://www.buffet-crampon.com/en/about-us/

[3] http://www.lma.cnrs-mrs.fr/

[4] Centre National de la Recherche Scientifique

skill set, in the domains of the Solid Mechanics and in Acoustics. It is structured in three research teams: Materials and Structures, Waves and Imagery, and Sounds [2]. This work is framed by the common laboratory: Interface Laboratory of Acoustic-Music-Instrument Making (LIAMFI[5]) between Buffet Crampon and the LMA.

LIAMFI

This common laboratory sponsored by the Research National Agency (ANR[6]) started working the first of March of 2017 and was formally inaugurated in 2019 [3]. Its objective is to establish a durable synergy on the topic of acoustic wind instruments but also digital ones. It aims to bring Buffet Crampon and the LMA closer together to better enable the Company to contribute to the specification and transfer of existing tools and skills or to be developed at the LMA, within the framework of previous collaborative projects between these two partners. The scientific issues considered are related to the design of new instruments and the evaluation of their objective sound quality, using experimental tools, but also subjective, calling on the judgment of the musician or the listener [4][7].

This thesis work is framed in common laboratory LIAMFI in the form of a Industrial Convention for the Formation to the Research (CIFRE[8]) scholarship.

[5] Laboratoire d'Interface Acoustique-Musique-Facture Instrumentale

[6] Agence National de la Recherche.

[7] https://liamfi.cnrs.fr/

[8] Convention Industrielle de Formation par la Recherche.

CIFRE

The Industrial Convention for the Research Formation is a frame implemented with the aim of promote the development of public-private partnership research. As mentioned in the official internet site of the CIFRE [5][9] "The vocation of industrial convention for the formation to the research, is to strengthen exchanges between public research laboratories and socioeconomic circles, promote the employment of doctors in companies and contribute to the innovation process of companies established in France. It is financed by the Superior Education, Research and Innovation Ministry, it was created in 1981. The CIFRE allows the company to benefit from financial assistance to recruit a young doctoral student whose research work, supervised by a public research laboratory, will lead to the defense of a thesis. Praised by companies as well as by laboratories and doctoral students, this flagship partnership research device constitutes a lever for initiating and strengthening public-private cooperation in R&D and promoting the employment of doctors." It contributes to the innovation process of French companies and to their competitiveness [5].

Woodwinds and the clarinet

The sources of information on the early history of musical instruments are often nebulous. Among the few instruments that have survived from the prehistoric period are bone end-blown flutes with notched mouthpieces and finger holes that show technical skills. There are many conjectures concerning the origin of wind instruments, and, because they are found widely scattered over the face of the Earth, it is quite likely that the process of vibrating the lips against a hole in a branch, a bone, a shell, an animal horn, or a tusk may have been discovered independently in many early cultures. Their origin may, in fact, have transcended even the first lip buzzing [6]. Musical instruments evolve in time depending on the place, historic moment and cultural context but the physical and

[9] https://www.enseignementsup-recherche.gouv.fr

acoustical principles can be applied to every instrument.

In the case of wind instruments based on straight tubes, the acoustic modes of the and the oscillation eigen-frequencies air column produce oscillations regimes or registers that are the notes played for a given tube length, to be used for music. The frequencies that can be played are, in a simple first approximation close to, either the harmonic series if the tube has two open ends or the odd harmonics if one end is closed or it resembles a physically closed end. There is not a perfect match with the harmonics and there is a cut-off frequency for which the harmonic content stops, but for the first notes it is a good approximations for certain tubes.

Besides the cylindrical tubes, animal horns or marine snail shells were also used as wind instruments, they have different timbres, that depend on the way of the excitation and on the internal bore. Further development of the horns gave birth to brass instruments. In this work, we are interested only in cylindrical bore pipes.

Woodwinds

Since the main material for wind instruments with cylindrical bores have traditionally been wood, these became called woodwinds. There are two traditional ways to reach the notes in between the natural modes of resonances of the woodwinds tube in order to play scales. Either, placing together tubes of several lengths, as in the case of the Pan flute, or to drill side holes (named hereafter toneholes) of suitable size and position in order to vary the acoustical length of the tube. The playing frequency is determined by the length of the air column when the tonehole is open, obtaining by this the desired tone [7]. Toneholes are closed and open by the action of the fingers. The number of toneholes was at first limited to the reach of the player fingers. With the invention

of the keys, more toneholes were available in a single instrument. Toneholes that are too large to be directly closed by the fingers and those that are out of reach for a direct control are closed and opened by the action of keys. Keys where introduced somewhere in the XVIIth century, overall for the tonehole that was closed with the pinky finger. As the XVIIIth century passed, the number of keys also increased [8].

The clarinet

The clarinet was invented in Nuremberg, about the year 1690, by the stringed instruments maker John Christopher Denner. It had only one key and there was no regularity in the change of register, this clarinet had at first very little attention. However, some musicians were attracted by its particular timbre. Thus, by degrees from one improvement to another, the number of keys was increased to five, remaining like that for a long time. Then, Ivan Müller made improvements reaching thirteen keys around 1812 (Fig. 1). This clarinet was the standard for half a century. Nevertheless, at that time the holes were pierced according to the natural separation of the fingers. This resulted in a faulty tone, the notes being frequently dull, feeble, or too shrill. The mechanism of the keys caused insurmountable difficulties of fingering, making impossible to play the clarinet in all different scales, and hence arose the necessity for three clarinets, *C*, *B♭* and *A* [9].

Figure 1: *B♭* clarinet by Piatet in Lyon, 13 brass keys, circa 1840. Boxwood and ivory mounts [10].

Around 1840, Hyacinthe E. Klosé came with the idea of the movable rings as an efficacious manner to solve the problem of the tuning (Fig. 2). It was in collaboration with Auguste Buffet

Jr. (younger brother of Denis Buffet-Auger) that they arrived to the Boehm system, that owes its name to the inspiration they got from Theobald Boehm's system for the flute. Klosé's patent for the Boehm clarinet was granted in 1844, and his method was published about the same time [11].

Figure 2: *B♭* ebony, ivory mounts 15 keys by Euler in Frankfurt [10].

Nowadays, the Boehm system is the basis for every clarinet made by Buffet Crampon (Fig. 3).

Figure 3: *B♭* Model Conservatoire Buffet Crampon [1].

Acoustics of the tonehole

There is a first collaborative thesis between Buffet Crampon and the LMA, the one from A. Guilloteau in 2015 [12], devoted to the Conception of a Logical Clarinet. However, this thesis work is the first in, which the CIFRE frame is implemented. We will start by introducing the acoustic behavior of the toneholes since it is the topic of this PhD. Baring in mind that the linear behavior is the most important when reaching playing frequencies of the instrument.

Linear behavior of the tonehole

The physical first order effect of the tonehole is to effectively shorten the vibrating air column in order to obtain a higher pitch. An open tonehole can be characterized by two impedances, one in

series and one in parallel. The most important effect comes from the impedance in parallel. Since pipe and and tonehole are both short, length corrections at both, end of the tube and end of the tonehole are comparable to main quantities of the tube, and they have, therefore, a perceptible influence on the resulting resonance frequency [13]. The Boehm system, which is the full system of keys to achieve a full chromatic scale, had at first the aim to bear one large tonehole for every note in the first register and that every tonehole in the upstream of the first open tonehole is closed [14].

It has been observed that the behavior of the instrument is strongly affected by the tonehole position, diameter and height. It is therefore of main interest to understand the acoustical properties of a single tonehole and also the whole instruments tonehole network. Therefore, toneholes have been developed differently for every instrument and have also different geometries depending on the maker which is based on tradition but also on a feedback from musicians. In 1982 Keefe [15] said that the assumptions underlying the validity of the mathematical formulation of the tonehole behavior are that the excitation is described by linearized equations of acoustics, and that the impedance parameters associated with each tonehole are independent of those of other toneholes. Dalmont stated that if the tonehole diameters is large enough (comparable to the main tube diameter) the acoustic principle is simple and it is called the length correction, like if the instrument was cut at the level of the first open tonehole, then the downstream has relatively negligible influence [14]. As said by Nederveen [16], since the tonehole diameters are less than those of the main tube and they also have a certain height (often the wall thickness of the main tube) their effect can not simply be described as cutting off the main tube at the position of an open tonehole [16]. Therefore, every aspect of the tonehole should be taken into account in order to achieve good understanding of its influence in the final sound of the given instrument.

The difference in timbre between instrument without and with keywork is that the latter, with

larger size toneholes, are explained by Dalmont [14] by two fundamental phenomena: The first concerns the cut-off frequency from which the waves are no longer reflected from the first open tonehole in an instrument with several toneholes. There are not, theoretically, more resonances beyond the cut-off frequency. In the instruments with small toneholes, the cut-off frequency due to the open toneholes network is lower in comparison to instruments with large toneholes. In consequence a smaller number of resonances contributes to the oscillation; the playing frequency is then less assertive, that is to say it is more subject to fluctuations and harder to anticipate, as for the musicians as for the instrument makers. It has to be mentioned that the cut-off frequency influences largely to the radiated sound, since roughly speaking frequencies beyond the cut-off limit are propagated in the tube downstream and are then radiated by subsequent open toneholes or at the end of the instrument [17] [18]. The other phenomenon related to the size of the toneholes is a nonlinear phenomenon, this will be explained in the next section.

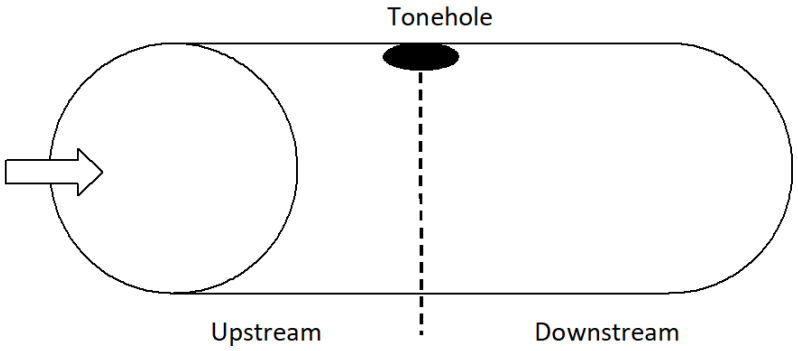

Figure 4: Schematic representation of a tube with tonehole blown from the left.

To a first approximation, a tube blown from the left with a single open tonehole (Fig. 4) can be described as a straight tube piece (upstream of the tonehole) terminated by two tube pieces in parallel (Fig. 5). The tonehole input impedance is determined by its length and diameter. This approach neglects, among other things, changes in compliance and inertance due to closed toneholes and due to the partition of the flow, from the downstream and the open tonehole. For an open tonehole, there are transitional correction at the inside as well as at the outside where the

flows and the acoustical wave adapt to another geometry. At the outside this is determined by the imaginary part of the radiation impedance, accurately known for only some geometries [19]. The real part of the tonehole impedance depends strongly to the physical dimensions, since this represents the losses in the tonehole.

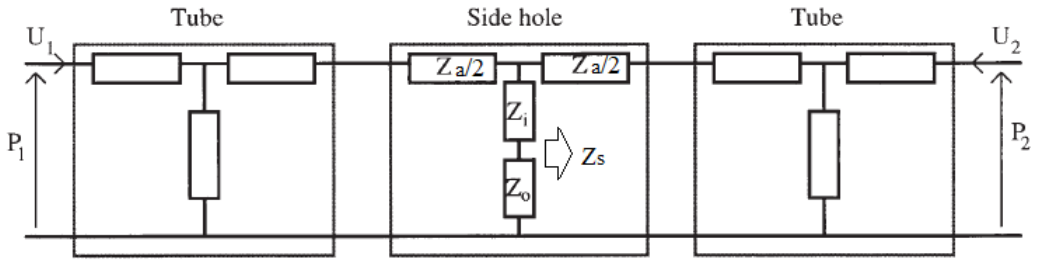

Figure 5: Equivalent circuit of the tube in Fig. 4 blown from the left, it is composed of two cylindrical tube sections and an open tonehole (side hole) in the middle. Z_a is the series impedance of the plane mode in the tonehole, it is divided in two equal parts at each side of the tonehole ($Z_a/2$). The shunt impedance Z_s is composed of: Z_o the input impedance of the tonehole and Z_i the impedance due to inner corrections. Figure adapted from Dalmont et al. [13].

At the tonehole position, a convenient mathematical description of wave propagation within the main bore uses transmission-line theory. Therefore, the acoustic effect of the tonehole may be represented by means of a lumped circuit in the transmission-line equations. The most general form of this circuit may be represented as a T circuit (Fig. 5) with series (Z_a) and shunt (Z_s) impedance elements. The series impedance acts in conjunction with the longitudinal particle velocity standing wave along the axis of the main air column at the tonehole location, while the shunt impedance is related to the pressure standing wave directly under the tonehole. If the longitudinal flow is zero at the tonehole location, then the pressure standing wave is symmetrical about the tonehole center. For this symmetrical pressure distribution, only the shunt impedance Z_s in the lumped circuit plays a role, and the subscript s denotes symmetry. If there is a pressure node

directly under the tonehole, then the series impedance Z_a is important. The connection of the antisymmetry of the pressure standing wave with the series impedance is denoted with the subscript a [15]. The series impedance is splitted in two equal parts flanking the tonehole. The imaginary part of Z_a is a negative quantity; it represents the reduction of acoustic mass due to the widening of the tube at the tonehole. The shunt impedance consist of three parts: the impedance Z_h that corresponds to the cylindrical part of the tonehole; a matching impedance Z_m takes into account the volume between the cylinders of the tube and the tonehole; and the terminal impedance Z_r, infinite for a closed tonehole and equal to the radiation impedance for an open tonehole [19].

Nonlinear behavior of the tonehole

Several studies have been conducted on the nonlinear behavior of the tonehole. Most of them devoted to metamaterials [20], [21], Helmholtz resonators [22], [23], [24] or microperforated plates [25], [26], [27]. Nevertheless, similar characteristics are expected to be found in musical instrument toneholes, to know: the high sound pressure level at the interior and at the exterior of the hole, the formation of jets and vortices, the particle velocity and its relation to the tonehole effective height in the form of the imaginary part of the shunt impedance.

The nonlinear phenomenon related to the toneholes - this is, it depends on the sound intensity - in relation to the fact that the air velocity in small holes can be relatively high. When the velocity in a tonehole is high, a jet is formed when the air exits the tonehole and the kinetic energy of the jet is dissipated by the vortices generated by the mixing of the jet with the air at the exterior. The consequence is an effect of saturation: beyond certain level it is difficult for the air to exit the tonehole which behaves at the limit as if it were closed [14].

For a longer discussion of nonlinear behavior in holes and orifices, see Annex A. This work is devoted to the linear behavior of the tonehole.

Topic of the PhD

The aim of this PhD thesis is the study of various types of undercut as used by the instrument maker, Buffet Crampon. The expected outcome of this research is the development of simplified models that can be used in design and optimization software for woodwinds. To achieve this, two experimental indirect methods will be used and compared, one is a method developed by Jean Pierre Dalmont et al. [13], this method is based on the measurement of the input and transfer impedances. A second method, that is new, is proposed and is the core of this work. It is based only on the measurement of two input impedances. It is expected that, regardless the tonehole geometry, these methods will allow to obtain the tonehole parameters to be used in the design of woodwinds.

Further work that can be developed in the long term from the results of this thesis are:

- Characterization of the acoustical behavior of any other kind of tonehole, not treated in this study, whatever its geometry or even for unknown undercuts or geometries.
- To be able to integrate these results in software to compute the input impedance.
- To be able to integrate these results in woodwinds optimization software.

Outline of the manuscript

Chapter 1

The first chapter is devoted to the measurement of the input and transfer impedance in tubes for which the analytical formulas are well known. First the impedance sensor *Capteur-Z*, is described and explored, and measures on cylindrical tubes are conducted. Then, an exploration on the measurement uncertainty is performed using also, cylindrical tubes. To verify that the measured quantities are in accordance with the theory, several extracted quantities are also obtained and explored, the reflection coefficient, effective length, terminal and transfer impedances are obtained for closed end tubes. Then, an open ended tube is also measured and extracted quantities are compared with analytical formulas of the input and radiation impedances. Finally numerical simulations with the finite element method are performed to explore and asses this tool as an aide in determining input and transfer impedances.

Chapter 2

This chapter is devoted to a new method for the indirect measurement of the tonehole impedance. This method is first constructed theoretically and then uncertainties are introduced to the model in order to verify the possible outcomes from the measurements. Then, measurements are performed and compared with the theory. It is found that this is a suitable method for the computation of the shunt impedance, despite the fact that, depending on the sample tube, there is a restricted frequency band. The main part of this chapter is an article submitted to the Journal of the Acoustical Society of America.

Chapter 3

This chapter is devoted to the method developed by Dalmont et al. [13], a method based on the measurement of the input and transfer impedances. It is first written in the form of direct and inverse problems. Then a simulation of the experiment is performed, and uncertainties in the length of the tube are added to verify the possible outcomes from a real measurements. A second simulation of the experiment is performed in order to observe the effect of the influence of uncertainties in the input impedance.

Also, a comparison between methods is performed by means of a simulation.

Conclusion and Appendix

After concluding on the outcome of this work and some perspectives are given for the continuation. Then some Appendices are added where nonlinear discussion in holes and orifices, analytical formulas, physical constants and relations are given.

Bibliography

[1] B. C. Societé, "Buffet crampon about us," 2021.

[2] L. de Mécanique et d'Acoustique, "Home page," 2021.

[3] LMA, "Inauguration liamfi," 2019.

[4] L. d'Interface Acoustique-Musique-Facture Instrumentale, "Liamfi," 2019.

[5] d. l. R. e. d. l. Ministère de l'Enseignement supérieur, "Conventions industrielles de formation par la recherche (cifre)," 2021.

[6] E. Britannica, "The history of western wind instruments," 2021.

[7] T. De Olazábal and R. C. de Arias, *Acústica musical y organología.* Ricordi, 1954.

[8] M. Thrasher, "The clarinetist-composers of nineteenth-century italy: An examination of style, repertoire, and pedagogy," *Proceedings of the Thirteenth Annual ClarinetFest (Atlanta, GA, 2006, accessed 30 January 2007)*, 2006.

[9] H. Klosé, *Celebrated Method for the Clarinet: Complete Edition.* Carl Fischer Music Dist, 1946.

[10] O. Shop, "Orphée music shop," 2021.

[11] E. A. K. Ridley, "Birth of the'boehm'clarinet," *The Galpin Society Journal*, pp. 68–76, 1986.

[12] A. Guilloteau, "Conception d'une clarinette logique," *Design of a logical clarinet"), Ph. D. thesis, Aix-Marseille Université, Marseille, France*, 2015.

[13] J.-P. Dalmont, C. J. Nederveen, V. Dubos, S. Ollivier, V. Meserette, E. te Sligte, *et al.*, "Experimental determination of the equivalent circuit of an open side hole: linear and non linear behaviour," *Acta Acustica united with acustica*, vol. 88, no. 4, pp. 567–575, 2002.

[14] J.-P. Dalmont, "Acoustique des instruments à anches," in *Musique et Technique 2010*.

[15] D. H. Keefe, "Theory of the single woodwind tone hole," *The Journal of the Acoustical Society of America*, vol. 72, no. 3, pp. 676–687, 1982.

[16] C. J. Nederveen, "Acoustical aspects of woodwind instruments," 1969.

[17] E. Petersen, *Comment le facteur d'instruments du musique a anche equilibre-t-il la production et le rayonnement?* PhD thesis, Aix-Marseille Univ, 2020.

[18] E. Petersen, T. Colinot, J. Kergomard, and P. Guillemain, "On the tonehole lattice cutoff frequency of conical resonators: applications to the saxophone," *Acta Acustica*, vol. 4, no. 4, p. 13, 2020.

[19] C. Nederveen, J. Jansen, and R. Van Hassel, "Corrections for woodwind tone-hole calculations," *Acta Acustica united with Acustica*, vol. 84, no. 5, pp. 957–966, 1998.

[20] X. Jing and X. Sun, "Sound-excited flow and acoustic nonlinearity at an orifice," *Physics of Fluids*, vol. 14, no. 1, pp. 268–276, 2002.

[21] N. Dickey, A. Selamet, and J. Novak, "The effect of high-amplitude sound on the attenuation of perforated tube silencers," *The Journal of the Acoustical Society of America*, vol. 108, no. 3, pp. 1068–1081, 2000.

[22] B. T. Zinn, "A theoretical study of non-linear damping by helmholtz resonators," *Journal of Sound and Vibration*, vol. 13, no. 3, pp. 347–356, 1970.

[23] D. A. Bies and O. Wilson Jr, "Acoustic impedance of a helmholtz resonator at very high amplitude," *The Journal of the Acoustical Society of America*, vol. 29, no. 6, pp. 711–714, 1957.

[24] U. Ingard, "On the theory and design of acoustic resonators," *The Journal of the acoustical society of America*, vol. 25, no. 6, pp. 1037–1061, 1953.

[25] M. A. Temiz, I. Lopez Arteaga, G. Efraimsson, M. Åbom, and A. Hirschberg, "The influence of edge geometry on end-correction coefficients in micro perforated plates," *The Journal of the Acoustical Society of America*, vol. 138, no. 6, pp. 3668–3677, 2015.

[26] A. Komkin, A. Bykov, and M. Mironov, "Experimental study of nonlinear acoustic impedance of circular orifices," *The Journal of the Acoustical Society of America*, vol. 148, no. 3, pp. 1391–1403, 2020.

[27] A. Komkin, A. Bykov, and M. Mironov, "Acoustic resistance of an orifice at high sound pressure levels," *Acoustical Physics*, vol. 64, no. 5, pp. 563–566, 2018.

Chapter 1

Impedance measurements in straight tubes

1.1 Introduction

In this chapter, the impedance sensor *Capteur-Z*, that is the measurement tool for this work, is described and explored. Since for this thesis work, several measurements on tubes that have never been measured before are going be performed, measurements on straight tubes for which the analytical formulas are well known, are first performed. This in order to trace the well functionality of the sensor and in case that unexpected results arose, we can be sure that it is not a measurement issue.

Measurements on straight cylindrical tubes are performed. And, an exploration on the impedance measurement uncertainty is done. In order to verify that the measured quantities are in accordance with the theory, several extracted quantities are also obtained and explored, the reflection coefficient, effective length, terminal and transfer impedances are obtained for tubes with the end opposite to the sensor position closed. Then, tubes with the end opposite to the sensor position open is also measured and extracted quantities are compared with analytical formulas of the input and radiation impedances. Finally numerical simulations with the finite element method are per-

formed and are compared with theory and measurements of the input and transfer impedances.

1.2 Impedance Sensor (*Capteur-Z)*

The *Capteur-Z* is an impedance sensor that allows to measure the acoustic impedance of an object to which it is connected. It was initially conceived to characterize acoustical wave guides, notably wind musical instruments. However it can be used for other applications such as: characterization of acoustics materials, surface impedance, absorption coefficient, dimensional control, among others. It was developed by the Center of Transfer of Technology of Mans (CTTM) and by the Acoustics Laboratory of the University of Maine (LAUM) [1].

The impedance is computed analytically from a measurement of the transfer function between two microphones, which are mounted in front and on back of a sound transducer that generates the acoustic excitation (Fig. 1.1). Thanks to an adequate signal post-processing the implementation does not require more than a partial calibration (measurement with the sensor closed by a rigid wall) [1]. The *Capteur-Z* is constituted of a sensor with a piezoelectric loudspeaker and two microphones, a rigid plate for the partial calibration, a compatible signal conditioner for the microphones, a four way data acquisition card (DAQ), and one way power amplifier [1].

Impedance measurement principle described by Macaluso and Dalmont [2]

The impedance measurement of the sensor is based upon a principle, that is described by Macaluso and Dalmont [2], in which the pressure in the back of a cavity of the source is measured by a microphone. This microphone gives an estimation of the volume velocity of the source, that is a piezoelectric buzzer. A second microphone measures the pressure in a small open cavity in the

front of the buzzer (Fig. 1.1).

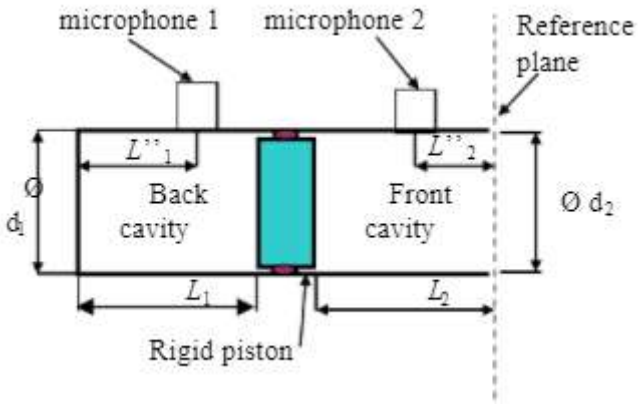

Figure 1.1: Schematic drawing of the impedance sensor and notations [2]

The pressure in the back of the cavity is at first order proportional to the flow U delivered by the source and the pressure P in the front open cavity is at first order equal to the pressure at the input of the pipe. The input impedance of the pipe $Z = P/U$ is thus at first order proportional to the transfer function between the two microphones. At first order it can be written as.

$$\frac{P_1}{P_2} = -jC\omega Z, \tag{1.1}$$

where P_1 and P_2 is the pressure measured by the microphones 1 and 2 at the back and front cavities of the sensor respectively (Fig. 1.1); $C = V/\rho c^2$ is the acoustic compliance of the back cavity of volume V, with ρ the air density and c the speed of sound; ω is the angular frequency and Z is the acoustic input impedance of the pipe.

In practice Eq. 1.1 is not sufficient and is only valid for low frequencies. Moreover, it is necessary to take the relative sensitivity of the two microphones into account, since the measured transfer function is $H_{12} = (P_2/P_1)(s_2/s_1)$ with s_1 and s_2 being the respective sensitivities of microphones 1 and 2. Due to the fact that the signal at each microphone is a linear function of the pressure p and the acoustical velocity u, the ratio of the signals (or the transfer function H_{12}) depends on

parameters that are imposed by the geometry of the system. Then, it is possible to calculate more precisely the expression of the impedance by taking into account the geometrical dimensions of the sensor, and a more precise value of the acoustical impedance is obtained by inverting the expression (Eq. 1.2):

$$H_{12} = K\frac{Z+\beta}{1+\delta Z} \tag{1.2}$$

where $K = -j\frac{1}{Z_{c1}}\frac{s_2}{s_1}\frac{\sin(kL_1)\cos(kL_2'')}{\cos(kL_1'')\cos(kL_2)}$, $\beta = jZ_{c2}\tan(kL_2'')$, $\delta = j\tan(kL_2)/Z_{c2}$, with $k = \omega/c$ the wave number [2].

Lengths L_1, L_2, L_1'' and L_2'' (Fig. 1.1) are dimensions related to the impedance sensor and to the position of the microphones. $Z_{c1} = \rho c/S_1$ and $Z_{c2} = \rho c/S_2$ are the respective characteristic impedances of plane waves in the front and back cavities, with $S_1 = \pi d_1^2/4$ and $S_2 = \pi d_2^2/4$ the cross sections of the back and front cavities (d_1 and d_2 the respective diameters).

The relative sensitivity of the sensors does not depend on the geometrical dimensions of the sensor. So, these geometrical dimensions being accurately measured, complex functions β and δ are known analytically and no calibration is needed for these parameters, since the influence of the temperature can be neglected. As functions β and δ are analytically known, a calibration with a single load is sufficient to determine parameter K and, consequently, the relative sensitivity ratio of the microphones. To do this, a metal disk is placed at the end of the front cavity that coincides with the reference plane (Fig. 1.1).

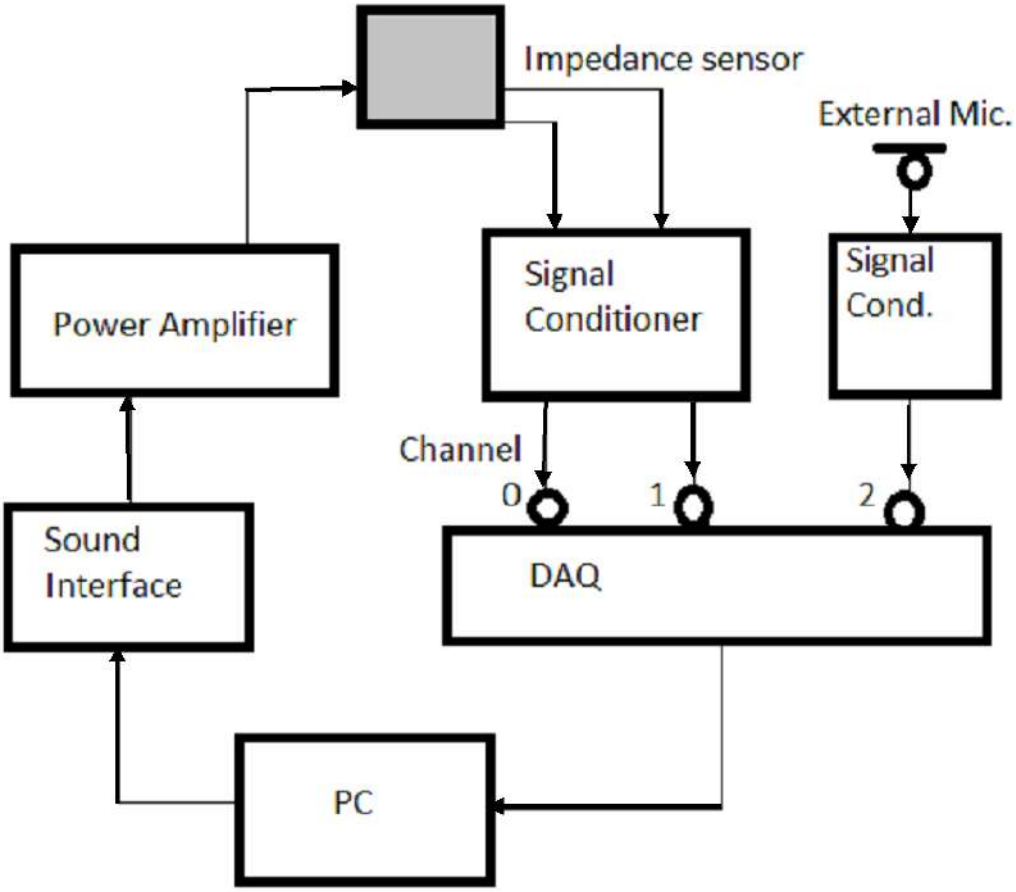

Figure 1.2: Schematic of the connectivity of the sensor impedance.

Measurement configuration with the impedance sensor

The elements in Fig. 1.2 are: a sound interface Focusrite Scarlet Solo Serial number T664234019793, a power amplifier Canfor S/N 904789, a signal conditioner C2 V4 17004 connected to the sensor, DAQ National Instrument type NI 9234 cDAQ-9171 S/N 1E2848A, and a sensor *Capteur-Z* v. 2.5. The software used to drive the sensor (v. 2.9) is also provided by the Center of Transfer of Technology of Mans (CTTM).

The general procedure in order to perform a measurement is: connect the sensor elements, check the configuration of the acquisition channels, create a new project, carry out a new calibration of the sensor, enter the measurement parameters, start the measurement, validate and save

the results, and visualize the results.

1.3 Model of uncertainties of input impedance measurements

Every time a measurement is performed the results are slightly different among them due to uncertainties associated to the measurement, even though the system in not perturbed and measurements are done one after another. Several types of uncertainties are present, for instance: electrical noise, small variations of temperature, either ambient or in the electronics, the capture hardware, signal amplifier, among others. Therefore, in order to quantify uncertainties associated with the sensor, one hundred measurements were performed, since no previous knowledge of the distribution is assumed, in order to quantify all the errors that are linked to repeatability as a whole.

Measurements of the input impedance using the *Capteur-Z* were carried out on a steel cylindrical tube of 1 m length and internal radius $r = 8$ mm, the far end of the tube was closed. Since the aim is to observe the uncertainties associated with the sensor, the system was kept invariant, this is, once the tube was mounted no further dismount was done in between the measurements. The measurements were performed from 10 Hz to 4.5k Hz, it was noted that the measured signal had a lot of influence of background noise at low frequencies, therefore only frequencies above 97 Hz are considered in the results. Despite the fact that the tube has a lot of resonances, the phenomenological model was based in low frequencies (97-260 Hz). Nevertheless, it was noted that it suits well for the whole frequency range of interest in the present study ($\sim 100-4000$ Hz).

1.3.1 Electrical noise

There is a very noticeable influence of the electrical noise in the measurements carried on the cylindrical steel tube. Despite the fact that this is not a random noise, it is important to quantify it in case it becomes a problem during measurements. In Fig. 1.3a, the peaks multiples of 50 Hz can be appreciated, the most prominent at 100 Hz and at 250 Hz. In Fig. 1.3b, it can be observed that despite the fact that the mean is performed upon one hundred measurement, there is still a big influence of the electrical noise perturbation at 100 Hz. Therefore it is not really a random but a steady perturbation. After several attempts it was not possible to identify the source of the electrical noise perturbation. Nevertheless, by changing the measurement room, there were no more electrically induced components in the spectrum of subsequent measurements.

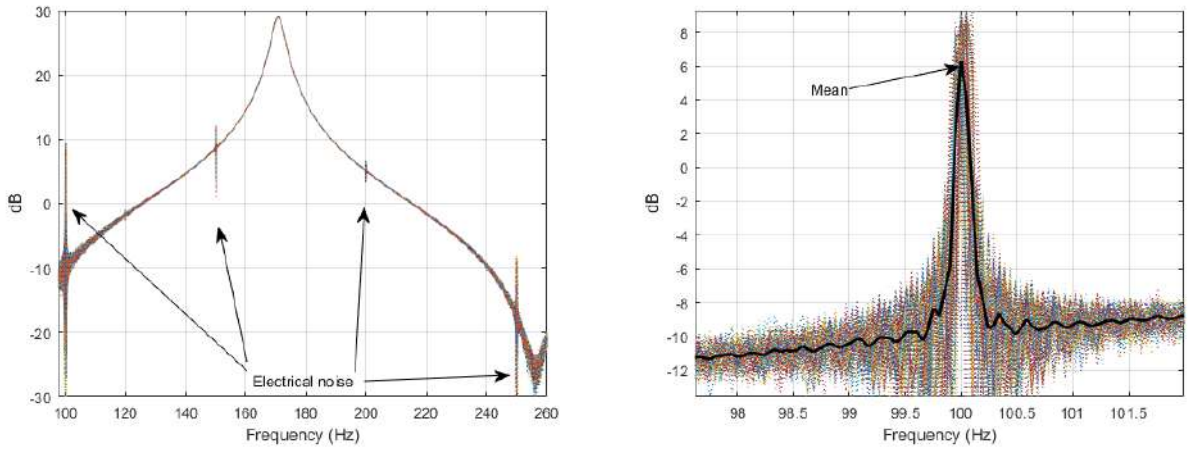

(a) (b)

Figure 1.3: Influence of the electrical noise in 100 measurements on a straight tube. (a) Modulus of the input impedance peak at 170 Hz, electrical noise peaks at 100, 150, 200, and 250 Hz. (b) Zoom at the electrical noise peak at 100 Hz. dB= $20\log_{10}(Z_{in}/Z_c)$

1.3.2 Modeling the uncertainty

Besides the electrical noise, which is not random and disappeared once the measurements are conducted in the anechoic chamber, other sources of error that can be regarded as random cannot be considered one by one, this kind of error appears every time a measurement is performed, and there are small variations in the output. Then based on several measurements and taking into account for the mean (μ) and the standard deviation (σ), a phenomenological model with a random error on the input impedance is proposed, this model takes into account the uncertainty introduced by every source of error during the impedance measurement. Eq. 1.3 is proposed, it takes into account the variations observed in either, the real and imaginary parts of the input impedance.

$$Z_B = \langle Z \rangle \, e^{j\phi_{\langle Z \rangle}} \{1 + 0.005\,[rand(N) - 0.5]\}, \tag{1.3}$$

where $\langle Z \rangle$ is the modulus and $\phi_{\langle Z \rangle}$ is the phase angle of the input impedance, Eq. 1.3 was constructed using the mean of the 100 measurements, but results can be applied to a single measurement or simulation. The 0.005 coefficient represents half amplitude of the random error, therefore $(0.005) * (2) * (100) = 1\%$, and $rand$ is a Matlab function that generates uniformly distributed pseudorandom numbers in the open interval $[0, 1]$.

In Fig. 1.4 the model in Eq. 1.3 considering a random variation of 1% is compared to the measure data dispersion, it can be observed that the phenomenological model (magenta curve) lies between the limits of the mean plus or minus two standard deviations ($\mu \pm 2\sigma$) which is also a good estimation of the dispersion of the experimental data. While the magenta curve in Fig. 1.4 is obtained for one realization of the random part, it is representative of what can be obtained when considering other realizations.

It can be concluded that there is a good correspondence between the experimental data dis-

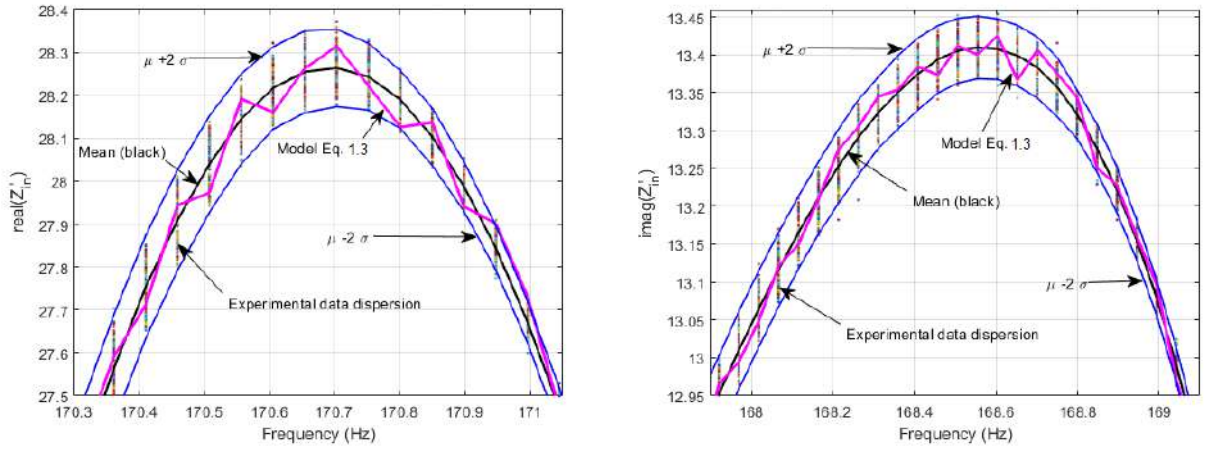

(a) (b)

Figure 1.4: Comparison among experimental data dispersion, model Eq. 1.3, mean of the experimental data, and $\mu \pm 2\sigma$. (a) real part, and (b) imaginary part of the input impedance. $Z'_{in} = Z_{in}/Z_c$ is the reduced impedance, measured value divided by the characteristic impedance of plane waves in the tube $Z_c = \rho c/\pi a^2$ with a the internal radius of the tube, ρ the air density and c the speed of sound.

persion ($\mu \pm 2\sigma$) and the equation proposed (Eq. 1.3) in which the uncertainty due to error sources in the measurement, is less than 1% of the measured quantity.

1.4 Some quantities extracted from the input impedance for different closed terminations

Several forthcoming experiments require to measure the transfer impedance between the input and the output of a tube. To do this the pressure at the closed end of the tube under study has to be measured. In order to decide the configuration to be used in the experiments as well as the effect of the measurement system in the results, cylindrical test tubes are constructed (Fig. 1.5a). The first tube ($P1$) of length $L = 6\ cm$ and internal radius $r = 7.3\ mm$ is open at the end opposite

to the sensor position, it has also an external diameter of 31.7 mm. The second tube ($P2$) with the same internal geometrical dimensions is closed at the end opposite to the sensor position (Fig. 1.5a). The tube $P1$ was tested in several conditions which are compared to the tube $P2$, because the latter is closer to an infinite impedance termination. The configurations are:

- Metal end (Fig. 1.5b), which consists of a metal disk at the the end of the tube opposite to the impedance sensor.
- Microphone 1/4" (Fig. 1.5c), which is a cap that holds a free-field microphone G.R.A.S 46BF-1 of 1/4" (6.35 mm) diameter microphone [3].
- Probe Microphone (Fig. 1.5d), which is also a cap but for a probe G.R.A.S 40SC microphone with 1.25 mm in diameter and a stainless-steel probe tube of 20 mm [4].

Microphones are placed on caps at the end of the tube making sure that there are no leaks, by the use of high vacuum grease in the case of the 1/4" microphone, and despite that there is lower risk of leaking in the probe microphone, since the diameter is 1.25 mm, dough is used at the interface microphone-cap to avoid leaking. The microphone front grid is lined up with the wall of the cap. It is observed that there is a gap between the microphone circumference and the holder in the case of the 1/4" microphone as it is seen in Fig. 1.5c.

1.4.1 Input impedance

The first quantity to be measured and compared for the various configurations is the input impedance, since this is directly obtained from the sensor software. The four configurations (Fig. 1.5) are compared to the theory and among them, theory of a perfectly closed termination is given by Eq. 1.4[1]

[1]The wavenumber k_a includes viscothermal losses, it is defined as $k_a = \frac{\Gamma_a}{j}$, where the propagation constant Γ_a is, among others, function of the tube radius a.

. It was expected to obtain close values of the input impedance measured for every configuration, meaning that these are similar to a rigid wall termination of infinite impedance. Results can be seen in Fig. 1.6.

$$Z_{in} = -jZ_c \tan^{-1}(k_a L) \tag{1.4}$$

In Fig. 1.6 it is observed that the input impedance measured from the tube $P2$ and from the tube $P1$ with metal end (Fig. 1.5b) and with probe microphone cap (Fig. 1.5d) at the end are very similar and are also very close to the theory. Around the first resonance peak, the difference in frequency between the theory and the measurement of the tube $P2$ (rigid end) is 1.2 $cents$ and 0.8 dB in amplitude. The difference between the theory and the tube $P1$ measured with the probe microphone is 1.8 $cents$ and 0.2 dB, for the same peak. Nevertheless, the measured input impedance from the tube $P1$ with the 1/4" microphone cap (Fig. 1.6b) is quite different from the other measured curves. The difference starts as low as 1000 Hz as seen in Fig. 1.6d, at the frequency peak the difference in frequency is 125 $cents$ and 12.5 dB in amplitude. There is also a peak that is not expected by the theory in the 1/4" microphone measurement at 3800 Hz. The case of the 1/4" microphone could be due to the gap between the microphone and the holder that is observed in Fig. 1.5c.

1.4.2 Reflection coefficient moduli and effective length

From the measurement of the input impedance, several quantities can be extracted by using the standard expressions of plane waves. Successively we compute the reflection coefficient at the input, the effective length of the tube, the reflection coefficient at the output, the impedance at the termination, and the transfer impedance of the tube.

The pressure and volume velocity are divided in outgoing wave and incoming waves as follows:

$$P(x) = P^{+}e^{-jk_a x} + P^{-}e^{jk_a x} \tag{1.5}$$

$$U(x) = \left[P^{+}e^{-jk_a x} - P^{-}e^{jk_a x}\right] / Z_c \tag{1.6}$$

where k_a is the complex wavenumber (which includes losses and dispersion in the tube) and Z_c is the characteristic impedance. The input impedance ($x = 0$) is:

$$Z_{in}/Z_c = \frac{P^{+}+P^{-}}{P^{+}-P^{-}} \tag{1.7}$$

and the reflection coefficient $R_{in} = P^{-}/P^{+}$:

$$R_{in} = \frac{Z_{in}/Z_c - 1}{Z_{in}/Z_c + 1} \tag{1.8}$$

At the output extremity $x = L$ the reflection coefficient R_{rad} is given by:

$$R_{rad} = \frac{P^{-}e^{jk_a L}}{P^{+}e^{-jk_a L}} = R_{in}e^{2jk_a L} \tag{1.9}$$

Fig. 1.7 and Fig. 1.9 show the modulus of the reflection coefficients at the input and at the output for different terminations. In Fig. 1.7a results for reflection coefficient modulus of tube $P1$ with metal end termination and for the tube $P2$ are very similar, the error is less than 1% with respect to the theory for both curves. In Fig. 1.7b the result fore the tube $P1$ with the probe microphone is closer to the theory in the low frequency range, below 500 Hz, then result for the same tube with 1/4" microphone are alike up to 1000 Hz with an error that is less of 1%. Then, after 1000 Hz, results for the 1/4" microphone diverge from both, the tube with microphone probe and the theory. For the tube $P2$ and for the tube $P1$ with metal end we can assume the theoretical value of a perfect closed end is $R_{rad} = 1$, then

$$R_{in}^{rigid} = e^{-2jk_a L} \tag{1.10}$$

In every other case, from Eq. 1.9 the complex effective length is:

$$L_{eff} = -\frac{j}{2k_a}\ln\left(\frac{R_{rad}}{R_{in}}\right) \tag{1.11}$$

Taking into account that the reflection coefficient is a complex number:

$$L_{eff} = -\frac{j}{2k_a}\left[ln|\frac{R_{rad}}{R_{in}}| + j * unwrap\left(angle\left(\frac{R_{rad}}{R_{in}}\right)\right)\right] \tag{1.12}$$

Where $angle(\cdot)$ denotes the phase of $\frac{R_{rad}}{R_{in}}$.

Fig. 1.8 shows the real part of the effective length $L_{effR} = Re(L_{eff})$ computed with Eq. 1.12. In the comparison of the tube $P1$ with metal end termination and the tube $P2$ we observe in Fig. 1.8athat results are very similar between them (< 1% of error) and around 2500 Hz there is good agreement with the geometrical length of $L = 60\ mm$. In Fig. 1.8a it is observed that the probe microphone termination over estimates the geometrical length by almost 15% and the 1/4" microphone under estimates this length for about the same amount. For every termination the length is well estimated around 2500 Hz.

Eq. 1.9 is used to compare the reflection coefficient modulus at the end of the tube for the different configurations. It can be appreciated that the cap for 1/4" microphone (Fig. 1.9b) gives very different results from the cap with probe microphone, which is within 1 % close to the theoretical value of one.

1.4.3 Terminal impedance

One of the quantities that will be important in this study is the transfer impedance, which relies on the measurement of the pressure at a rigid termination in the tested tube. There are several ways to measure this quantity, but since the tube's diameter is relatively small (compared to most regular microphones) the effect of the size of the microphone used could interfere with this measurement. Therefore, it is important to compare the microphone caps to real rigid terminations. To achieve this, the terminal impedance is first computed from the measured input impedance for the different closed terminations studied.

In order to deduce the terminal impedance from the input impedance, we use the classical formula (Eq. 1.13):

$$Z_{out} = Z_c \frac{-jtan(k_a L) + Z_{in}/Z_c}{1 - jtan(k_a L) Z_{in}/Z_c}. \tag{1.13}$$

Fig. 1.10 shows results from measurements of three studied configurations, it is noted that the difference between configurations in Fig. 1.10a in the low frequency range, up to 1000 Hz and after 3500 Hz is less than 5 dB (10%), between 2000 and 3500 Hz the difference, without the frequency peaks, is about 12 dB. Fig. 1.10b shows that results for the tube $P1$ with cap for 1/4" microphone are very different from the other configurations which are rather in accordance: the rigid termination tube $P2$, the tube $P1$ with metal end and the tube $P1$ with cap for probe microphone. The difference in the computed terminal impedance for the 1/4" microphone is as great as 35 dB. This means that, apart from the 1/4" microphone, the other terminations are close enough to a rigid acoustic wall (as for the tube $P2$) in the conditions of the present study.

From Fig. 1.10b it is noticeable that the termination for the 1/4" microphone is far from being a rigid termination in the studied frequency range. Moreover, it resembles an acoustic compliance. To assess this, the terminal impedance is plotted in linear scale (Fig. 1.11).

If we see the result in Fig. 1.11 as an acoustic compliance, then we can compute the coupled volume at the end of the tube trough Eq. 1.14.

$$V = \frac{\rho c^2}{j\omega Z_{out}} \tag{1.14}$$

In Fig. 1.12 we can see the plot of the computed volume through Eq. 1.14, since this equation is a low frequency model the value of the volume of the cavity is taken as the mean of the curve on

the frequency band [100-1000] Hz. Then we can conclude that the volume computed of the cavity around the 1/4" microphone is around 38 mm^3, even if the curve is noisy, this gives an order of magnitude of the volume of the cavity. This includes the cavity that is intrinsic to the microphone. This is in accordance with the difference in the measured impedance observed in Fig. 1.10 that resembles an acoustic impedance.

1.4.4 Transfer impedance

The transfer impedance Z_T is a quantity that will be used later in this study, it is defined in the frequency domain as the ratio between the pressure at the end of the tube and the volume velocity at the input $Z_T = P_{out}/U_{in}$. This quantity is directly measured by the impedance sensor with the use of a third microphone (Fig. 1.2).

Measurements of the transfer impedance Z_T of the tube $P1$ are performed with both microphones (Figs. 1.5d 1.5c). These measurements are directly taken from the sensor impedance software. The transfer impedance of the tube $P2$ (Fig. 1.5a) and tube $P1$ with metal end (Fig. 1.5b), cannot be directly measured, instead it is computed through Eq. 1.15 from the measurement of the input impedance. Results are in Fig. 1.13.

$$Z_T = \cos(k_a L) Z_{in} - j \sin(k_a L) Z_c \tag{1.15}$$

Results in Fig. 1.13 show that there is good agreement between transfer impedance computed for the tube $P2$ with rigid end, and the theoretical transfer impedance of a perfectly cylindrical tube of the same length, the difference is less than 4% in the amplitude and less than 2 $cents$ in frequency. Nevertheless, there is no agreement what so ever among these two results and the di-

rect measurement with the impedance sensor for neither of the microphones.

As a conclusion we can say that the measurement of the transfer impedance is not well performed by the impedance sensor, despite the fact that the cap made for the probe microphone gives results similar to an acoustic rigid wall in the studied frequency range, as seen in Section 1.4.2 and in particular in Fig. 1.10.

Table 1.1 shows a summary of the differences observed between measurements and analytical value for the input, transfer and terminal impedance for the closed tube terminations. Since the theoretical value for the terminal impedance is infinity at the closed end, the comparison is made among measurement results.

Table 1.1: Closed tube summary (Peak differences with respect to the analytical value).

	Closed Tube (P2)	Metal End (P1)	Microphone 1/4" (P1)	Probe Microphone
Input Impedance	1.2 *cents* 0.8 dB	0.6 *cents* 0.5 dB	125 *cents* 12.5 dB	1.8 *cents* 0.2 dB
Transfer impedance			125 *cents* 18 dB	2 *cents* 10 dB
Terminal impedance	5 dB	5 dB	35 dB	5 dB

1.4.5 Conclusion of sec. 1.4

- Measurements performed in the test tube $P2$ with rigid termination and without microphone, are in accordance with theoretical predictions in the studied frequency range.
- Input impedance results are in agreement with theoretical predictions, except for the cap with 1/4" microphone, which is notoriously different from $1k$ to 4 kHz.

- Probe microphone gives the closest results to the terminations without microphone in the cylindrical test tubes, in terms of the reflection coefficient and effective length.

- Terminal impedance computation shows that there is an acoustic compliance in the 1/4" microphone configuration, which is very likely to be the cause for the difference in results above 1 kHz.

- Despite small differences in the terminal impedance computations, there is good agreement between the probe microphone cap and the terminations without microphone. Therefore, this cap can be considered as a rigid wall end termination in the studied frequency range [80-4000] Hz.

- There is an unknown problem in the measurement of the transfer impedance.

(a)

(b)

(c)

(d)

Figure 1.5: Closed terminations studied. (a) Tube $P2$ closed end, (b) tube $P1$ closed at the end by a metal disk, (c) cap for 1/4" microphone, and (d) cap for probe microphone. Both caps are to be used with tube $P1$.

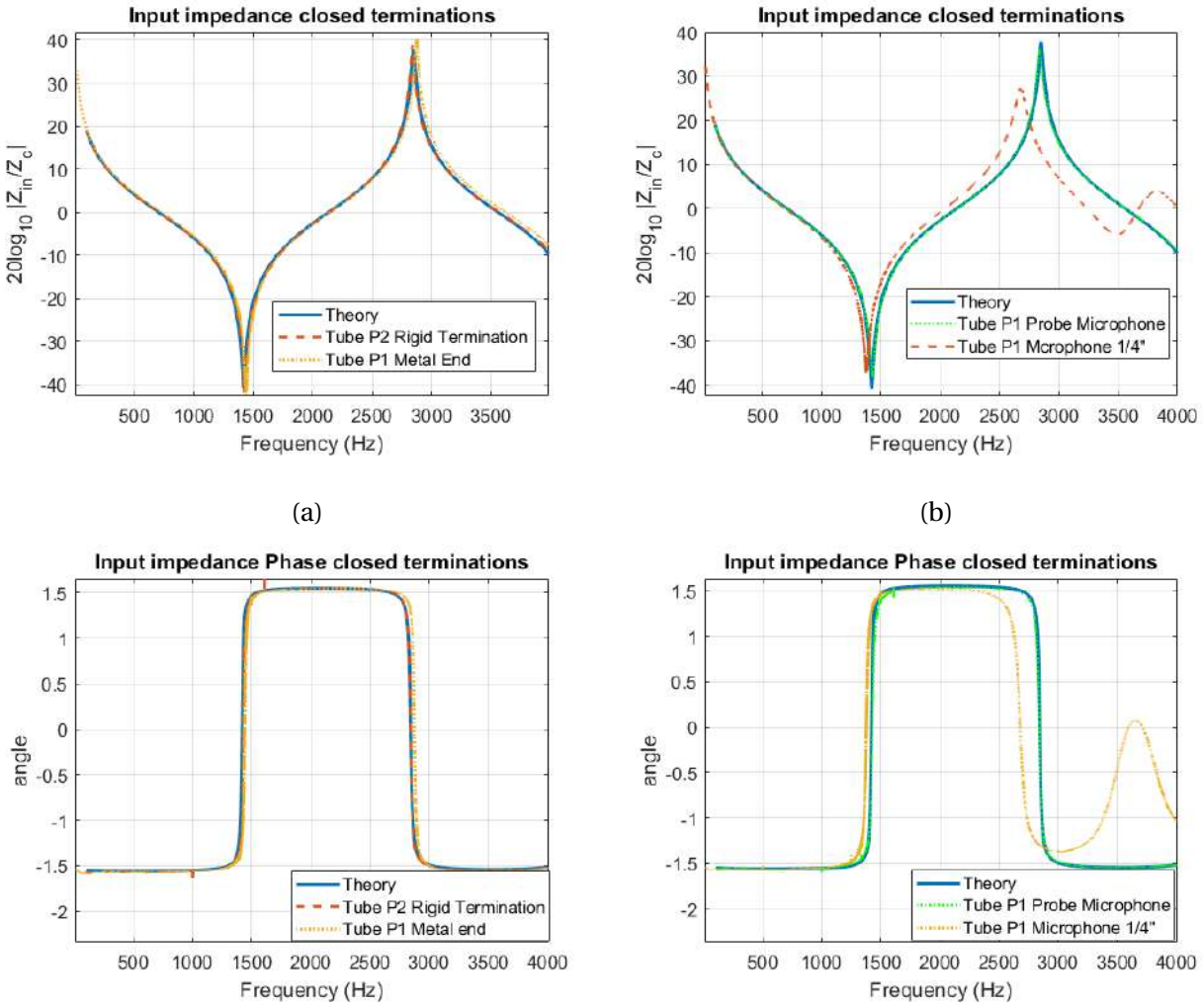

Figure 1.6: Input impedance comparison for different terminations. (a) Theory of a perfectly closed termination (Eq. 1.4), tube $P2$ and tube $P1$ with Metal End, (b) Theory, Probe and 1/4" microphone caps. Theory Eq. 1.4. (c) phase of Fig.1.6a, (d) phase of Fig. 1.6b.

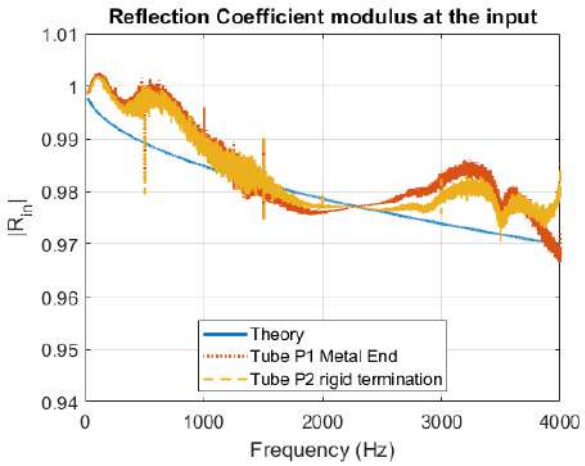

(a)

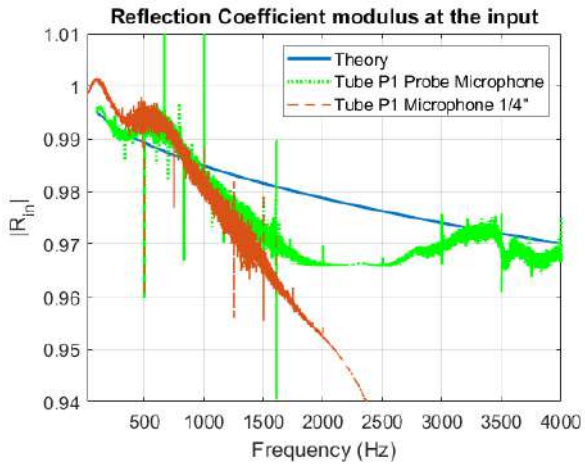

(b)

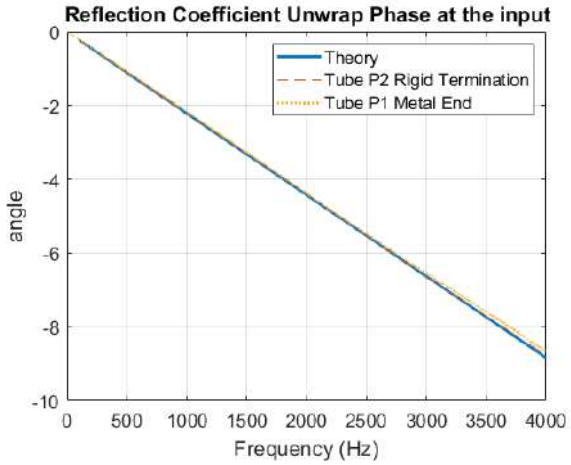

(c)

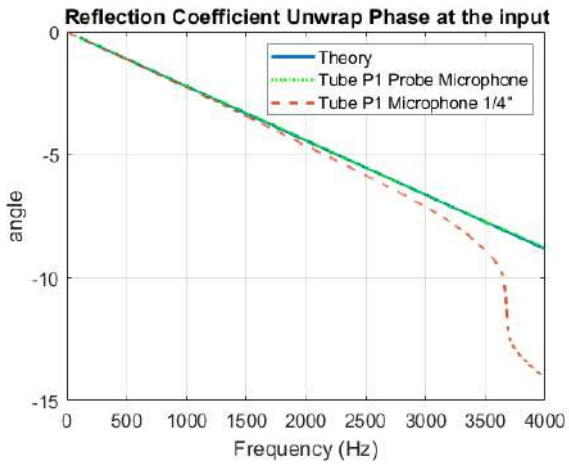

(d)

Figure 1.7: Reflection coefficient modulus (obtained through Eq. 1.10) at the input. Comparison for different terminations. (a) Tube $P2$, tube $P1$ with metal end and (through Eq. 1.10) (b) Tube $P1$ with probe and 1/4" microphone caps (through Eq. 1.10). Results greater than 1 are due to experimental errors in the low frequency range. (c) phase of Fig. 1.7a and (d) phase of Fig. 1.7b.

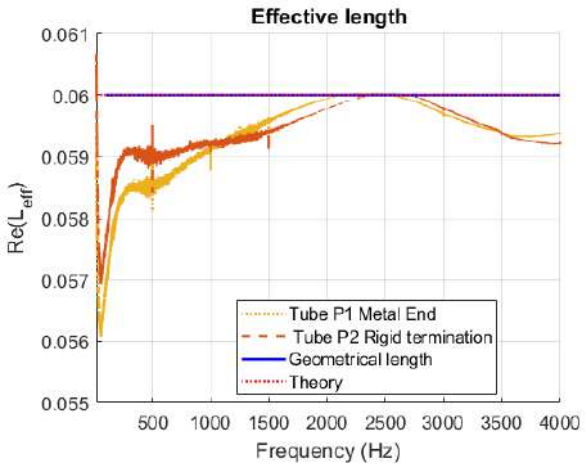

(a)

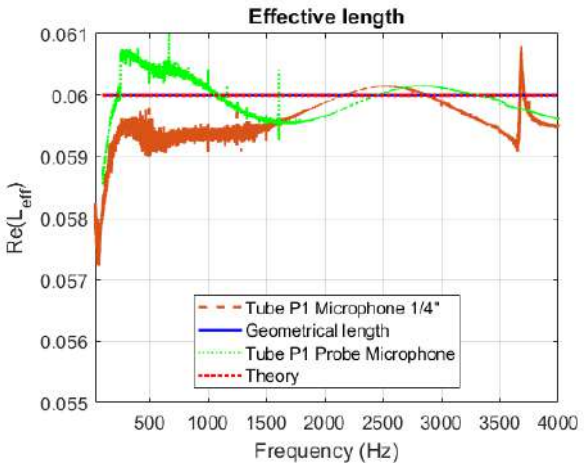

(b)

Figure 1.8: Real part of the effective length obtained through Eq. 1.12, comparison for different terminations. (a) Tube $P2$ and tube $P1$ with metal end and (b) Tube $P1$ with probe and 1/4" microphone caps. Geometrical length is measured with a caliper. Theory of a perfectly closed termination computed through Z_{in} from Eq. 1.4.

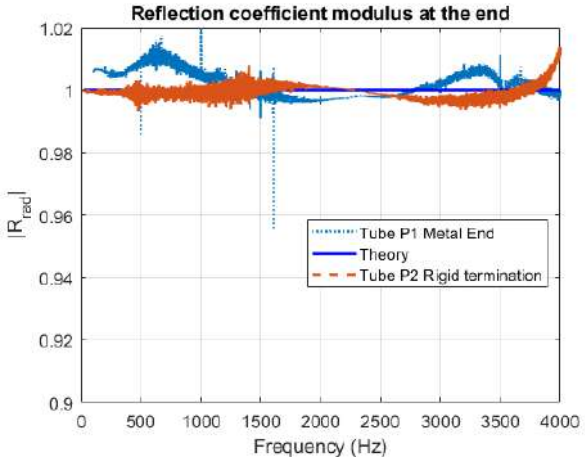

(a)

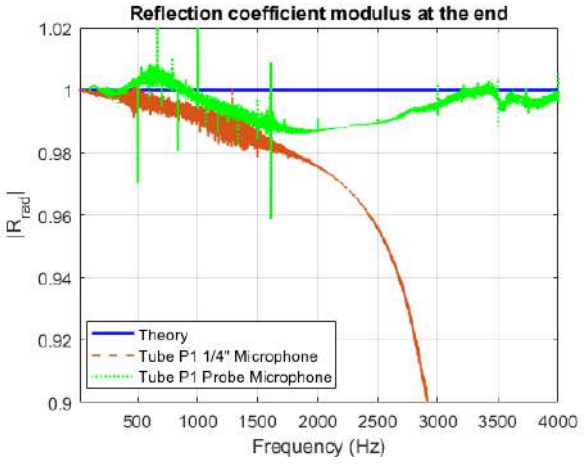

(b)

Figure 1.9: Reflection coefficient modulus at the end of the cylinder obtained through Eq. 1.9, comparison for different terminations. (a) Tube $P2$ and tube $P1$ with metal end, and (b) Tube $P1$ with probe and 1/4" microphone cap. Theory is given by $R_{rad} = 1$. Results greater than one are due to experimental errors.

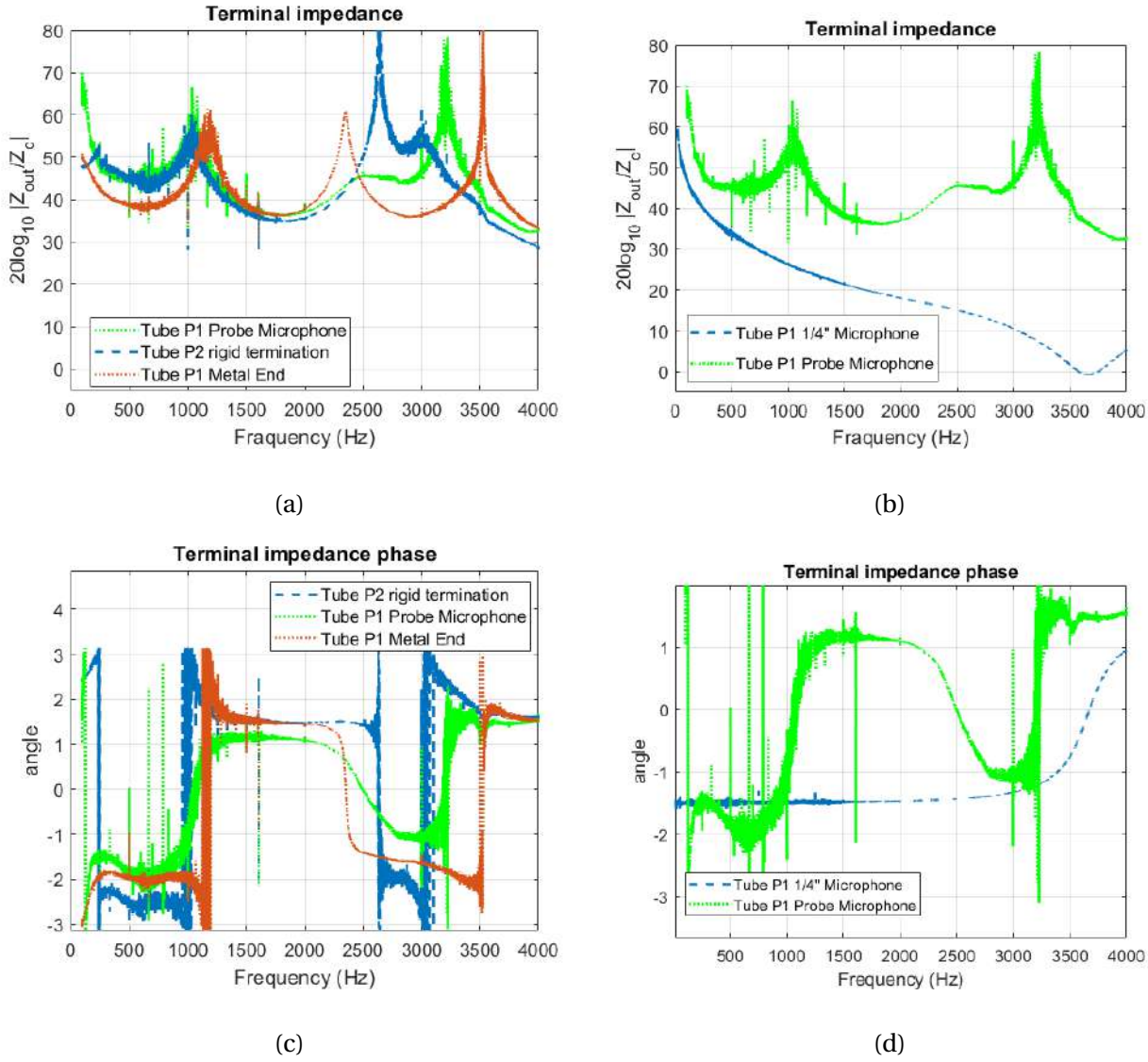

Figure 1.10: Modulus of the terminal impedance Z_{out}. (a) Tube $P2$ with rigid termination, tube $P1$ with Metal End, tube $P1$ with probe microphone. (b) Tube $P1$ with 1/4" and probe microphones (c) phase of Fig. 1.10b. (d) phase of Fig. 1.10a. Computed with Eq. 1.13 using the measured input impedance Z_{in} for the various configurations considered.

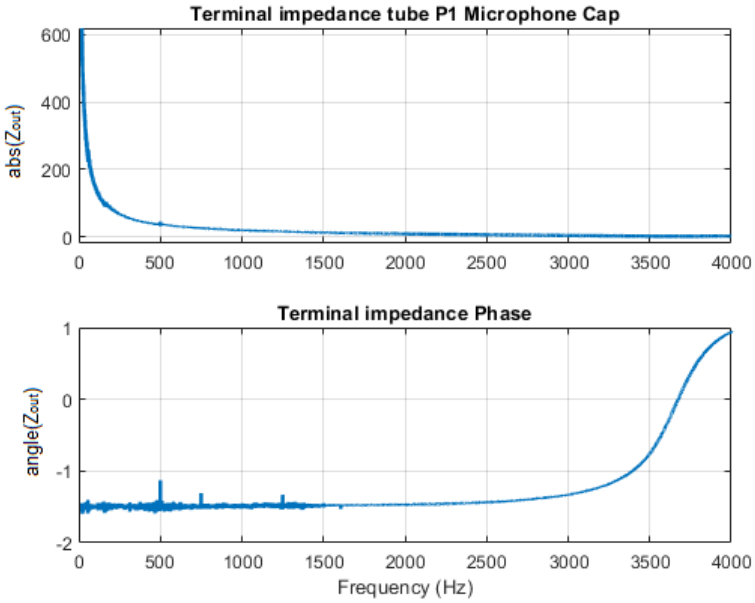

Figure 1.11: Terminal impedance Z_{out} modulus and phase at the 1/4" microphone cap in linear scale (Eq. 1.13) using the measured input impedance Z_{in}.

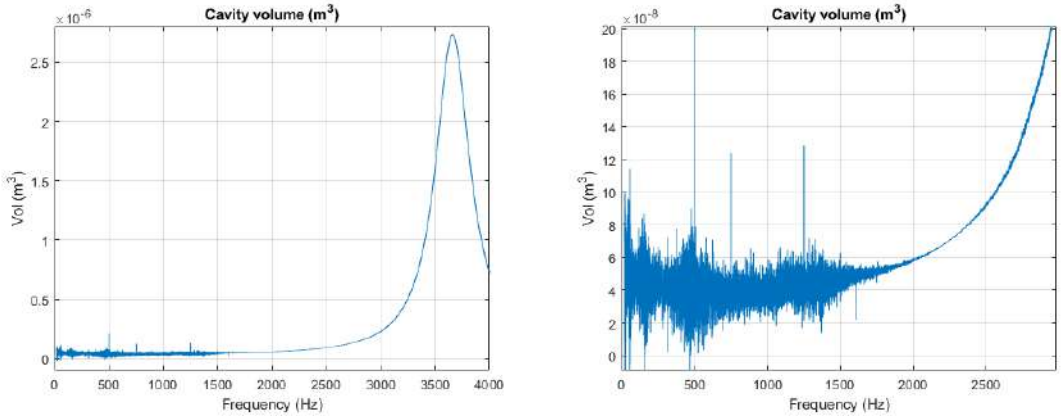

Figure 1.12: Computed cavity volume with Eq. 1.14.

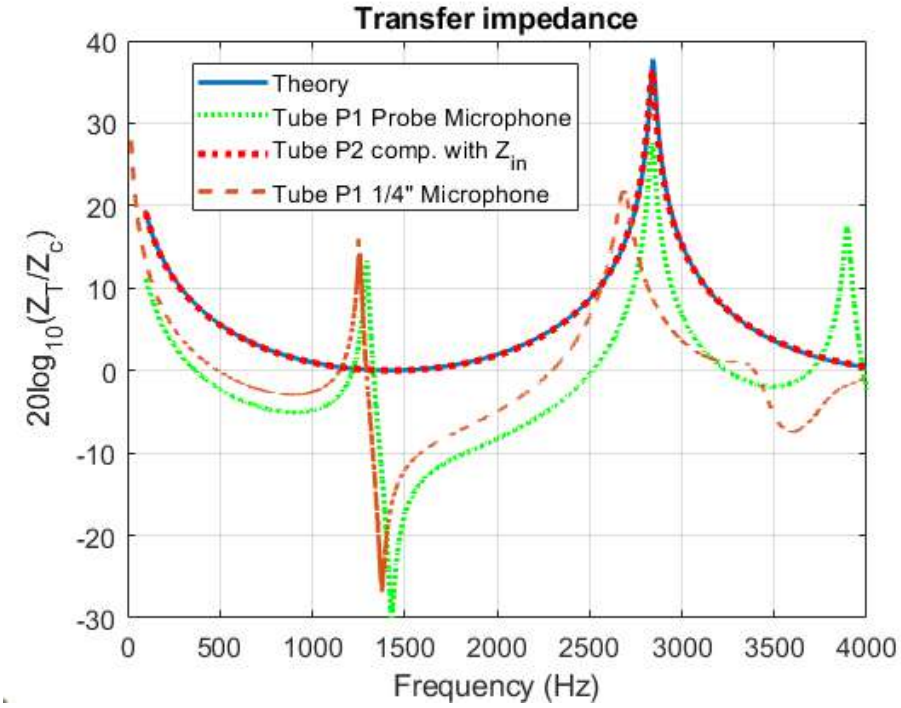

Figure 1.13: Transfer Impedance Z_T. Theory and tube $P2$ computed with Eq. 1.15; tube $P1$ measured with the impedance sensor for the 1/4" and probe microphones.

1.5 Radiation and input impedance measurement in an open tube

The open tube impedance will also have an important role later in this study. Therefore, it is important to accurately measure and quantify the input and radiation impedance. The test tube $P1$ is used without the rigid terminations studied in previous sections, but with the far end open. Measurement are performed in the anechoic chamber in LMA.

1.5.1 Radiation Impedance

The radiation impedance is the first quantity to be studied, since in the development of the theory is necessary to deduce the input impedance. No direct measurements of the radiation impedance are performed. However, comparisons are made between theoretical values of the radiation impedance and the impedance at the end of the tube deduced from the input impedance measurement with the sensor.

The theoretical radiation impedance is computed through Eq. 1.16 [5].

$$Z_r = Z_c \frac{j\delta ka + 0.5d_2(jka)^2}{1 + 0.5(n_1 + d_1)jka + 0.5d_2(jka)^2} \tag{1.16}$$

Where, for an unflanged tube:

$$\delta = 0.6133 \;\; n_1 = 0.167 \;\; d_1 = 1.393 \;\; d_2 = 0.457 \tag{1.17}$$

And, for the flanged tube:

$$\delta = 0.8236 \;\; n_1 = 0.182 \;\; d_1 = 1.825 \;\; d_2 = 0.649 \tag{1.18}$$

The input impedance of the open tube is theoretically computed as:

$$Z_{in}^{open} = \frac{\cos(k_a L)Z_r + jZ_c \sin(k_a L)}{jZ_c^{-1}\sin(k_a L)Z_r + \cos(k_a L)} \tag{1.19}$$

Results of this comparison of the real and imaginary parts of the radiation impedance Z_r are in Fig. 1.14.

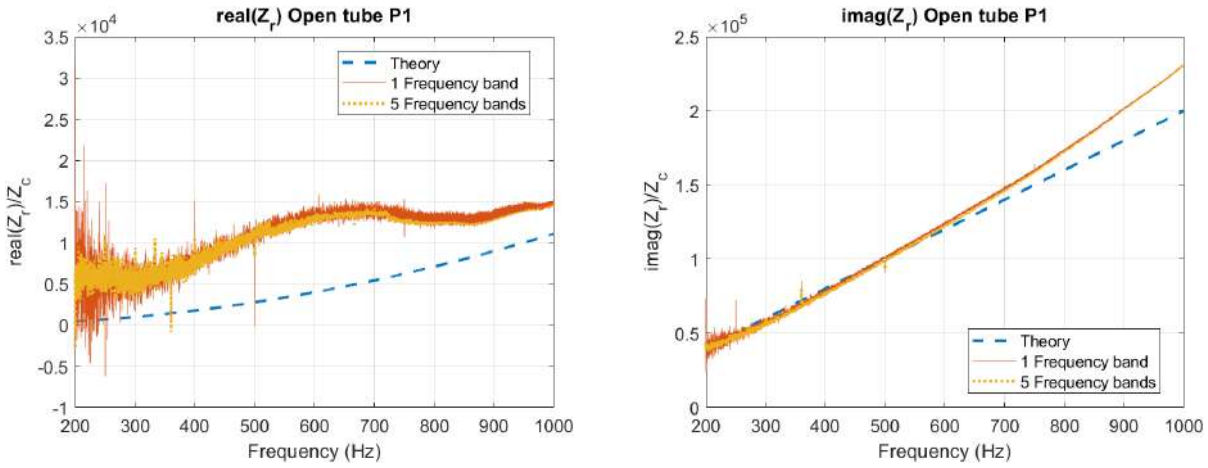

(a) (b)

Figure 1.14: Real (a) and imaginary (b) part of the radiation impedance obtained from the measured input impedance Z_{in} of the tube $P2$ (internal radius 7.3 mm, external radius 15.8 mm), theory computed through Eq. 1.13. Comparison with the model given by Eq. 1.16 with the coefficient of the tube unflanged (Eq. 1.17).

In Fig. 1.14a it is observed that there is a discrepancy, that it is not regular over the frequency, between theory and measurement. The difference increases up to 500 Hz, then decreases up to 750 Hz and then it is more or less stable up to 1000 Hz. This could be due to the fact that the tube $P1$ is quite thick in relation to an unflanged tube radiation, which is the theoretical curve depicted.The imaginary part of the radiation impedance in Fig. 1.14b is in good agreement from 200 to 800 Hz the discrepancy is less than 10 %. And it increases to 20 % at 1000 Hz.

The two experimental results labeled as 1 and 5 frequency bands in Fig. 1.14, are due to an option of the sensor impedance software, this feature is intended to obtain the lower signal to noise ratio in every measured frequency band. In this particular case it can be observed that there is no

significant difference between results, besides a small reduction in the noise and small discontinuities in the measured frequency bands. Therefore, for this particular case either of the measurements options can be used without significant difference in the results.

Conclusion:

- In low frequency there is not a very good agreement in the real part of the radiation impedance, the error is greater that 400 % below 500 Hz. It is around 330 % between 500 and 750 Hz. And after 750 Hz the discrepancy is less than 20 %.
- There is good agreement for the imaginary part of the radiation impedance, the difference is less than 10 % in the studied frequency range.
- There is not an unique frequency band that holds to the theory for every computed quantity. Therefore, the accuracy of the results will depend on the desired quantity to be measured.

1.5.2 Input impedance

In order to explore the frequency bands in which the *Capteur-Z* gives an accurate measurement for in the input impedance of the tube $P1$, several measurements were performed, it was noted that the results closer to theory are in the frequency range between 200 and 1000 Hz, results of measurements are compared with the theoretical result in Fig. 1.15. For the real part of the input impedance, up to 400 Hz the difference between the flanged and unflanged terminations is less than 10% and the measurement result is within this range. After 400 Hz and up to 650 Hz the measurement is closer to the flanged termination with a maximum deviation of 12%. Between 650 and 800 Hz there is a transitional zone, in which the measurement result passes from been closer to the flanged termination to be 10% over the unflanged termination, it continues uo to 1000 Hz. For the imaginary part of the input impedance (Fig. 1.15b) the measurement result is closer to the

unflanged termination for the whole frequency range, up to 860 Hz the difference is less than 1%, and after 860 Hz the difference goes up to 2%.

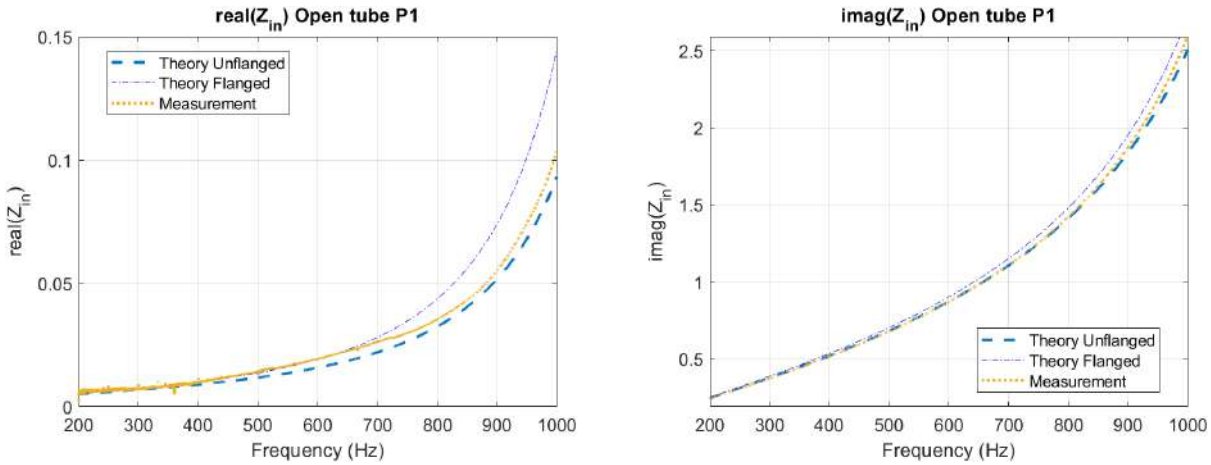

(a) (b)

Figure 1.15: Real and imaginary part of the input impedance computed through Eq. 1.19, comparison flanged - unflanged radiation impedance.

In Fig. 1.15a it is observed that up to 650 Hz result of the measurement is closer to the unflanged theoretical computing, the error is less than 10% of the theoretical value. Measurement result after 820 Hz is closer to the flanged theoretical result. As for the imaginary part (Fig. 1.15b) the result of the measurement is closer to the unflanged theoretical result in the studied frequency range.

1.5.3 Conclusion of sec. 1.5

- For the real part of the input impedance, at low frequencies (below 400 Hz) the difference between both theoretical curves and the experimental result is less than 10 %.
- There is a transitional zone between 650 and 800 Hz from which the real part of the input impedance passes from been closer to the unflanged termination to be closer o the flanged

termination.

- The imaginary part of the input impedance is closer to the unflanged termination with a maximum deviation of 2%.

1.6 Numerical simulation

Numerical simulations of the studied tubes in previous sections, is done with the use of COMSOL Multiphysics, which is a software based in the Finite Element Method (FEM). As pointed out by Gregory Bunting et al. [6] in acoustical problems when the geometry, boundary conditions, and/or given spatial distributions of material properties of the fluid are complex, the governing equations do not typically lend themselves to an analytical solution. In these scenarios, numerical solution of the wave equations can be a powerful tool for computing the acoustic quantities of interest because otherwise there is no other means of obtaining this information. Computational Acoustics has emerged as a subdiscipline of acoustics, concerned with combining mathematical and numerical solution algorithms to approximate acoustic fields with computer-based models and simulations. Using computational acoustics, acoustic propagation is mathematically modeled via the wave equation, a continuous partial differential equation that admits wave solutions. The numerical methods are focused on taking the continuous equation from calculus and turning them into discrete linear algebraic calculations, which are amendable to solution on digital computers.

1.6.1 Finite Element Method (FEM)

The FEM is a numerical computational technique initiated by Turner et al. in 1956, it approximates solutions of real problems in complex domains with boundary conditions. The base of the analysis lies in the division or discretization of the domain in a finite number of subdomains

or elements, for which a systematic approximated solution is built by solving partial differential equations (PDEs) turning them into linear algebra [7], [6]. The FEM reduces the problem from a continuous domain to a finite number of unknowns , dividing the domain in elements and expressing the variables in terms of approximated functions applied to each element. These functions, called interpolations functions, are defined in terms of the field variables values in specific points, called nodes. The nodes are in the boundary of each element and they connect adjacent elements [7].

The main steps to perform an analysis in FEM are:

- Discretization of the domain in elements.
- Selection of the interpolation functions.
- Element matrix development for each sub domain.
- Element matrix assembly to obtain a global domain matrix of the original geometry.
- Imposition of the boundary conditions.
- Solve equations.
- Results computation.

Once the domain is discretized, the elements are connected through the common nodes, in the matrix of the system equations, the unknowns are associated to the nodes in what it is known as nodal unknowns and these are the field variables. The filed variables are also called degrees of freedom (DOF) of an element. At each node the DOFs are applied at specific spatial location to which the physics of the problem are applied [7].

The FEM has been widely used as a tool for solving the acoustic wave equation. One of the earliest references is from Gladwell in 1965. More recent surveys on FEMs for acoustics and struc-

tural acoustics provide comprehensive technical reviews on the application of FEMs for solving acoustics problems in Atalla et al. [8] in 2017 [6].

In many acoustics applications, the FEM is an attractive numerical strategy. Some advantages of the method include:

- The ability to construct unstructured, body-fitted meshes that capture curved interfaces between complex fluid/structural domains;
- Sparse systems (i.e., matrices wherein most entries are zeros) of algebraic equations that, when combined with FEM of an elastic structure, render a coupled system of equations that are still sparse;
- The ability to solve either linear and/or nonlinear acoustic wave equations; and
- The ability to easily handle spatially varying material properties (e.g., capturing the speed of sound and density that vary with vertical position in underwater or atmospheric acoustics).

1.6.2 Quality of the model

In order to achieve good results that are closely related to the physical problem, a model with that represents accurately the geometry is important but, it also needs a suitable mesh with good quality elements. Some geometries with sharp edges are particularly difficult to be properly meshed, some times this part of the geometry is not crucial to resolve the problem, but some times one low-quality element is sufficient for the model to be not convergent, so no result can be obtained from it.

There are quality measures that allow to explore the elements to know where in the model problem related with the low-quality elements can arise. There are no absolute numbers that

indicates how good or bad an element is, but there are certain thumb rules that are useful. In COMSOL the quality of the elements is expressed in numbers ranging from zero to one, zero being a degenerated element that prevent the model to converge, and one the best possible element in the mesh. In general an element with quality lower than 0.1 is considered poor and if the quality is below 0.001 is considered as very low-quality. This range can be applied to different quality measures, such as: skewness, maximum angle, volume versus length, growth rate, among others. Each of one depending on the type of model and study, in general the skew of elements is a good indicative of the global models quality, the closest to one the average of the elements skewness the better the model convergence and results. The skewness is based on the equiangular skew that penalizes elements with large or small angles as compared to the angles in an ideal element [9]. Also, the maximum angle quality measure, penalizes elements with large angles, this may be well suited where an-isotropic elements are desired.

1.6.3 The use of FEM in musical instruments

The use of FEM in musical instruments started as early as in 1975, when Schwab and Sheng published a Finite Element Analysis of a guitar soundboard in the Catgut Acoustical Society Newsletter [10]. This open a path in the use of the FEM in musical instruments. Some examples of the use of FEM in the study of stringed instruments are: Bretos and Santamaria [11] studied the vibrational patterns and frequency responses of free plates and box of a violin; in 2001 [12] and 2002 [13] Elejabarrieta et al. published two papers in which they used FEM to study the vibrational behavior of the guitar body and the air in the interior of the box, it is to be noted that at the time it was not possible to model the coupling between the air and the guitar box in a single simulation, therefore they had to be model separately and then analyzed as coupled modes. In 2008 García-Mayén [14] used the FEM to study the modes of vibration of the guitar soundboard under different construc-

tion conditions, simulations where compared to measurements. More recently in 2020 Mihalcica et al. [15] used FEM and measurements to evaluate the effect of different bracing systems in the frequency response of guitar bodies.

The finite element model is also used to study wind instruments, some examples are: the use of FEM to determine the transmission-matrix parameters of woodwind instruments toneholes by Antoine Lefebvre in his PhD thesis at McGill University [16]. In 2012 Lefevbre ans Scavone used this approach to characterize open and closed woodwind instrument toneholes. They made the computation in two steps: first the tube is assumed to be lossless, then the velocity normal to the wall is derived, and the wall admittance. Then a new FEM is used for a tube with a finite admittance [17]. Previously, Dubos et al. [18] used the Boundary element method for the computation of toneholes. In 2015 Rucz et al. published a FEM of the tuning slots of labial organ pipes [19]. Tournemenne and Chabassier developed a computational tool for the calculation of wind instrument input impedance using a 1D FEM [20]. More recently, in 2020 Coaldrake used computed tomography scan images of a Japanese Koto as the basis of a mesh of a FEM, then vibrational behavior of the instrument was analyzed [21].

1.6.4 Modeled tubes

Tube with one closed end

First the tube *P*2 (Fig. 1.5a) is modeled. Due to the symmetry of the tube, the 2D axisymmetric geometry is used, triangular elements are used to model the air at the interior of the tube and rectangular elements models the thermal and viscous layers at the wall. These layers are essential when modeling sound propagation in geometries with relatively small dimensions, where attenuation because of thermal and viscous losses is important [22]. The skewness average element quality is

0.8474 and the average maximum angle element quality is 0.8671. The input end of the physical tube is placed on the impedance sensor and the far end is perfectly closed. In the FEM model, the tube is driven at the input by a *Port* boundary condition that models a plane wave mode at 0.0635 Pa (70 dB). To compute the input impedance the average pressure and the velocity integral are computed at the inlet of the tube and to compute the transfer impedance, the average pressure at the rigid end of the tube is computed.

Results are in Fig. 1.16, it is observed that there is a nearly perfect match between the analytical solution obtained through Eq. 1.4 for the input impedance and through Eq. 1.15 for the trasfer impedance and the results from the numerical simulation performed in COMSOL. The difference in frequency at the peak, for both the input and transfer impedance, is 2.7 $cents$ and there is no difference in amplitude. In Figs. 1.16c and 1.16d is observed that the phase is in accordance for the theory and the numerical simulation performed in COMSOL.

Tube with one open end

The tube $P1$ (Fig. 1.5b) is also modeled. In this case, one end of the physical tube is placed on the impedance sensor and the opposite end is open to the atmosphere, therefore the surrounding air has to be also modeled. The 2D axi-symmetric geometry used is in Fig. 1.17, the upper domain is a Perfectly Matched Layer (PML), a nearly perfect absorbent domain, that models the anechoic termination that is consistent with the anechoic chamber in which the measurement is performed. It is to be noted that the material of the tube is not in the model, only rigid walls are used, this is, in terms of the model, the space of the tube material is a void in the FEM model.

Fig. 1.18 shows the mesh used for the air inside and out the tube $P1$ and the PML. In Fig. 1.18b

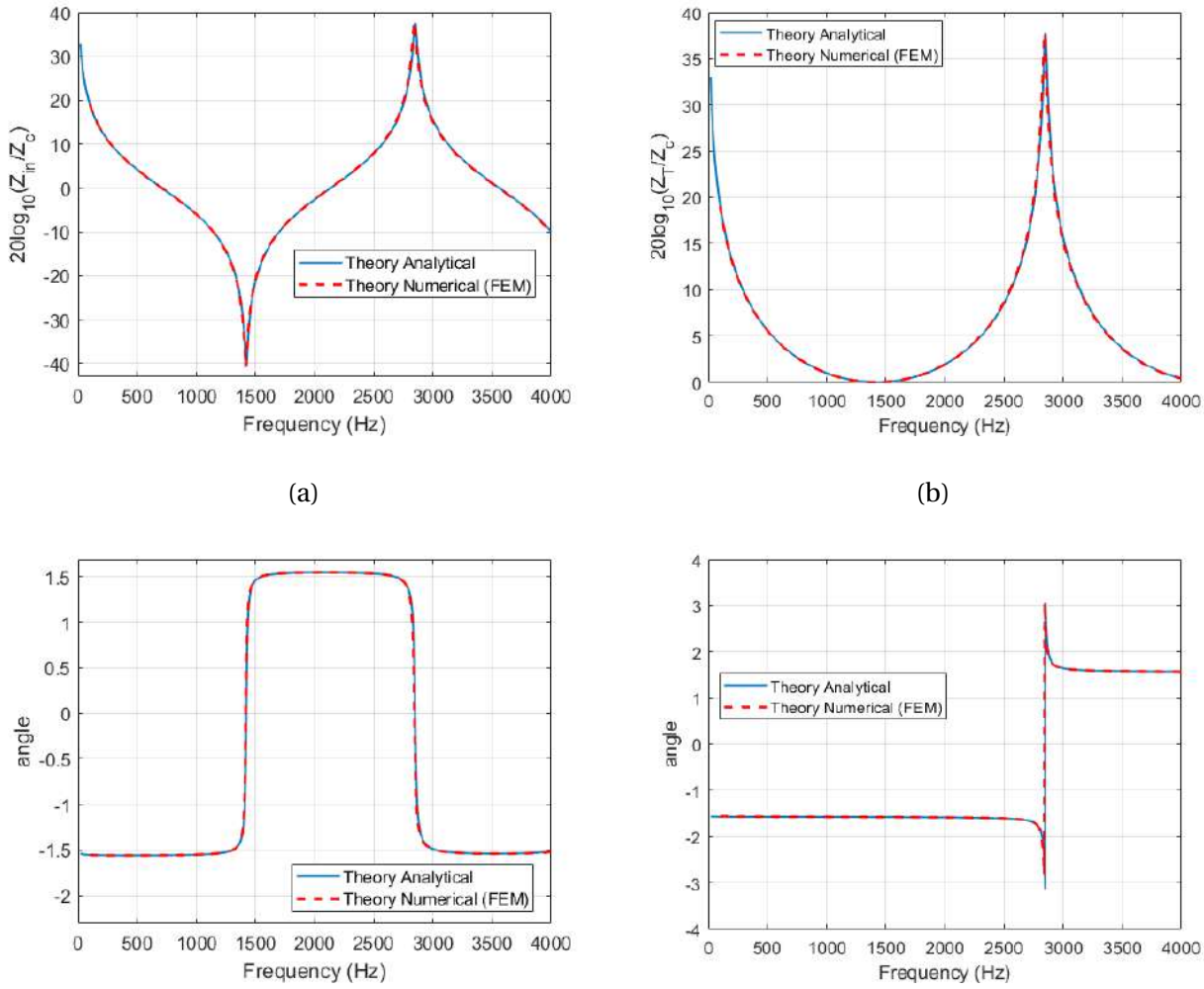

Figure 1.16: (a) Input and (b) transfer impedance of the tube *P*2. Analytical curve computed through Eq. 1.4 of a perfectly closed termination for the input impedance and through Eq. 1.15 for the transfer impedance. (c) phase of the input impedance and (d) phase of the transfer impedance.

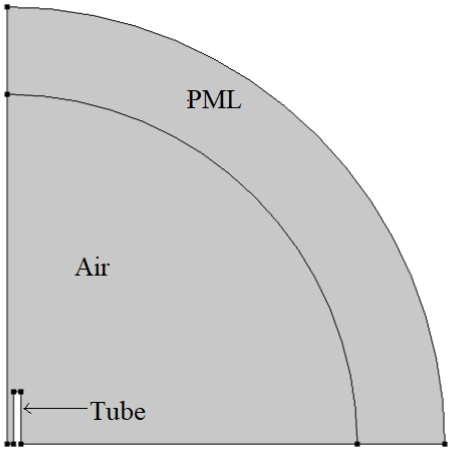

Figure 1.17: Axi-symmetric geometry of the tube $P1$ used for the numerical simulation in COMSOL. The domains are the air at the interior of the tube and at the surroundings, and a Perfectly Matched Layer (PML) domain that represent the anechoic domain of the chamber.

there is a detail of the mesh where the boundary layers can be seen, these rectangular elements models the thermoviscous layers at the wall of the tube, in contrast with the triangular elements used to model the air far from the tube walls. One advantage of using 2D axi-symmetric models is the efficiency in the computing time since the number of elements and DOFs is lower in comparison with a 3D model. In the case of the Fig. 1.18 there are 77 584 elements of which 14 834 are rectangular elements devoted to the viscous-thermal layers and the PML domain, the average skewness element quality is 0.8669 and the maximum angle quality average is 0.9239. This model takes about one hour to be solved in desk PC.

Results are in Fig. 1.19, there is a comparison between the direct measurement of the input impedance obtained with the sensor (*Capteur-Z*), the numerical simulation from COMSOL and the analytical solutions for a thin tube without flange and a tube with an infinite flange at the end (these are computed through Eq. 1.19 with the help of Eqs. 1.16, 1.18 and 1.17).

In fig. 1.19 it is observed that the numerical simulation through COMSOL is the closest to the

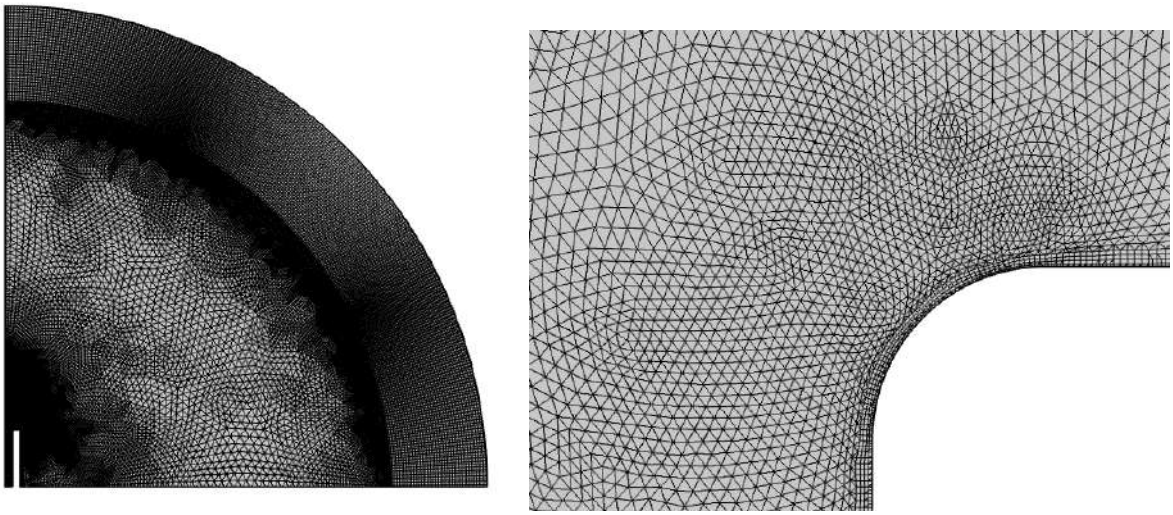

(a) (b)

Figure 1.18: Mesh used to compute the input impedance of the tube $P1$; (a) complete mesh and (b) detail of the mesh at the inner corner at the top of the tube.

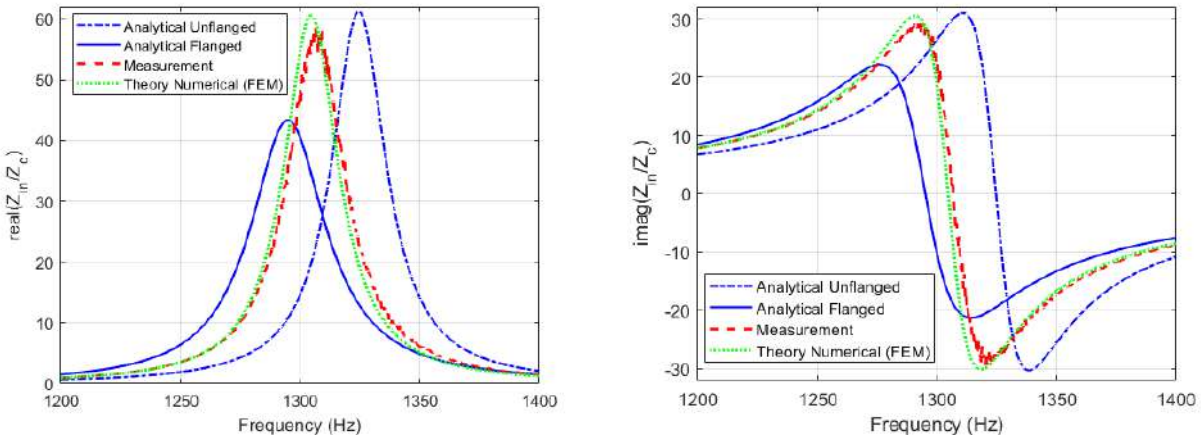

(a) (b)

Figure 1.19: (a) Real and (b) imaginary parts of the input impedance of the tube $P1$. Analytical computed through Eq. 1.19 with the radiation impedance computed through Eq. 1.16 for the flanged and unflanged conditions.

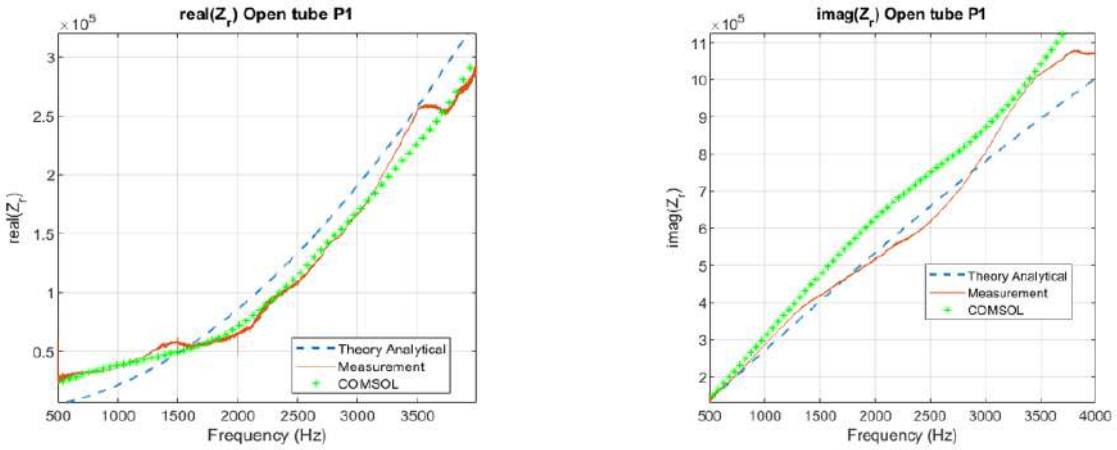

(a) (b)

Figure 1.20: (a) Real and (b) imaginary parts of the radiation impedance of the tube $P1$. Analytical computed through Eq. 1.16 for the flanged condition.

measurement. The difference at the peak between the measurement and the numerical simulation is 4.6 $cents$ in frequency and 2 dB in amplitude. While the difference regarding the measurement result with the theory analytical flanged end is 17.3 $cents$ in frequency and 25 dB in amplitude, also the difference with the theory unflanged end is 21.8 $cents$ in frequency and 3 dB in amplitude.

The radiation impedance was also computed from the input impedance measurement and result is compared with the simulated tube. Results are in Fig. 1.20. There is a very good agreement, less than 1% for the real part of the radiation impedance between measurement and simulation, apart of the 3.5 kHz where the difference is of about 10%. As for the imaginary part of the radiation impedance, there is a difference of less of 1% up to 1.5 kHz for the the plotted curves. This difference increases up to 15% around 2.5 kHz between measurement and numerical simulation. It has to be noted that there is no good agreement with the analytical result.

Figure 1.21: Tube $P1L$ placed on the sensor impedance for measurement.

Longer tube with one open end

In order to verify previous results, a tube similar to $P1$ was constructed also in PVC, but instead of 60 mm length, tube $P1L$ has a length of $L = 100$ mm. The tube was measured with the impedance sensor (Fig. 1.21) and modeled with analytical equations and numerical simulation through COMSOL. Results are in Figs. 1.22 and 1.23.

In Fig. 1.22 is observed that there is consistency between measurement and numerical simulation for the whole presented frequency range. In Fig. 1.23 is observed that the difference between measurement and numerical simulation is about 2 $cents$ and 0.5 dB in amplitude. While the difference regarding measurement results is 8.5 $cents$ in frequency and 1.4 dB in amplitude with the flanged result, as for the unflanged result the difference is 16.5 $cents$ in frequency and 0.1 dB in amplitude. For the second peak, the difference between measurement and numerical simulation is 0.5 dB in amplitude with no difference in frequency, with respect to the flanged analytical result, the difference is 7 $cents$ in frequency and 3.3 dB, and with respect to the unflanged end result is 17.4 $cents$ in frequency and 0.8 dB in amplitude. It also has to be noted that overall, the most similar curves are the measurement and the numerical simulation with COMSOL, as seen in Figs.

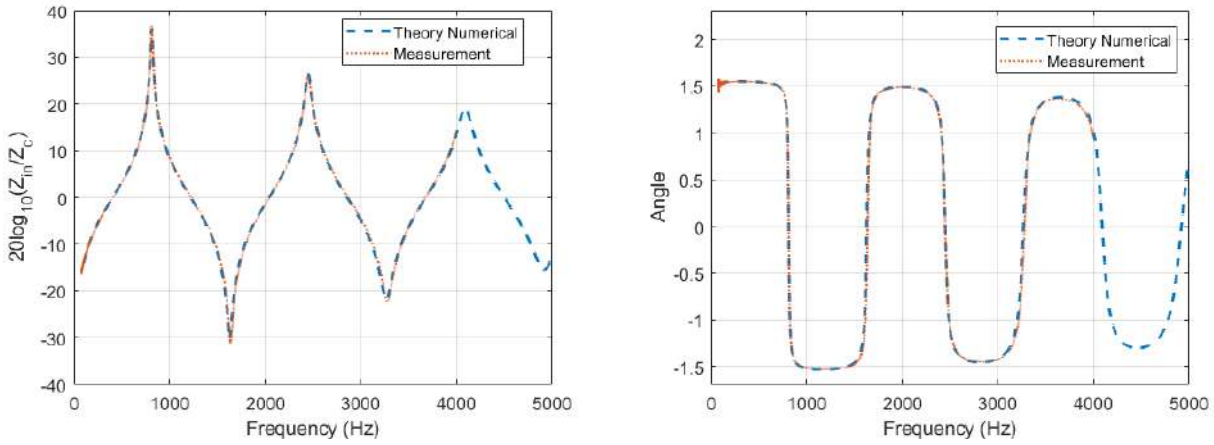

(a) (b)

Figure 1.22: Comparison between measurement (up to $4kHz$) and numerical simulation. (a) Input impedance modulus of the tube $P1L$ (b) input impedance phase of the tube $P1L$.

1.23c and 1.23d.

As for the short tube, the radiation impedance was also computed from the input impedance measurement and result is compared with the simulated long tube $P1L$. Results are in Fig. 1.24. For the real part of the radiation impedance, there is a very good agreement, less than 1% between measurement and simulation. There is agreement with the theoretical curve from 2.5 to 3 kHz for the flanged termination. As for the imaginary part of the radiation impedance, there is a difference of less of 1% among measurement, simulation and theoretical curve for flanged termination.

1.6.5 Conclusion of sec. 1.6

The numerical simulation through COMSOL Multiphysics provides results that can be matched with either the analytical solutions, when they exist, or with experimental results when analytical equations are not available. Therefore, COMSOL can be used as a tool for the analysis of the tone-holes with and without undercut.

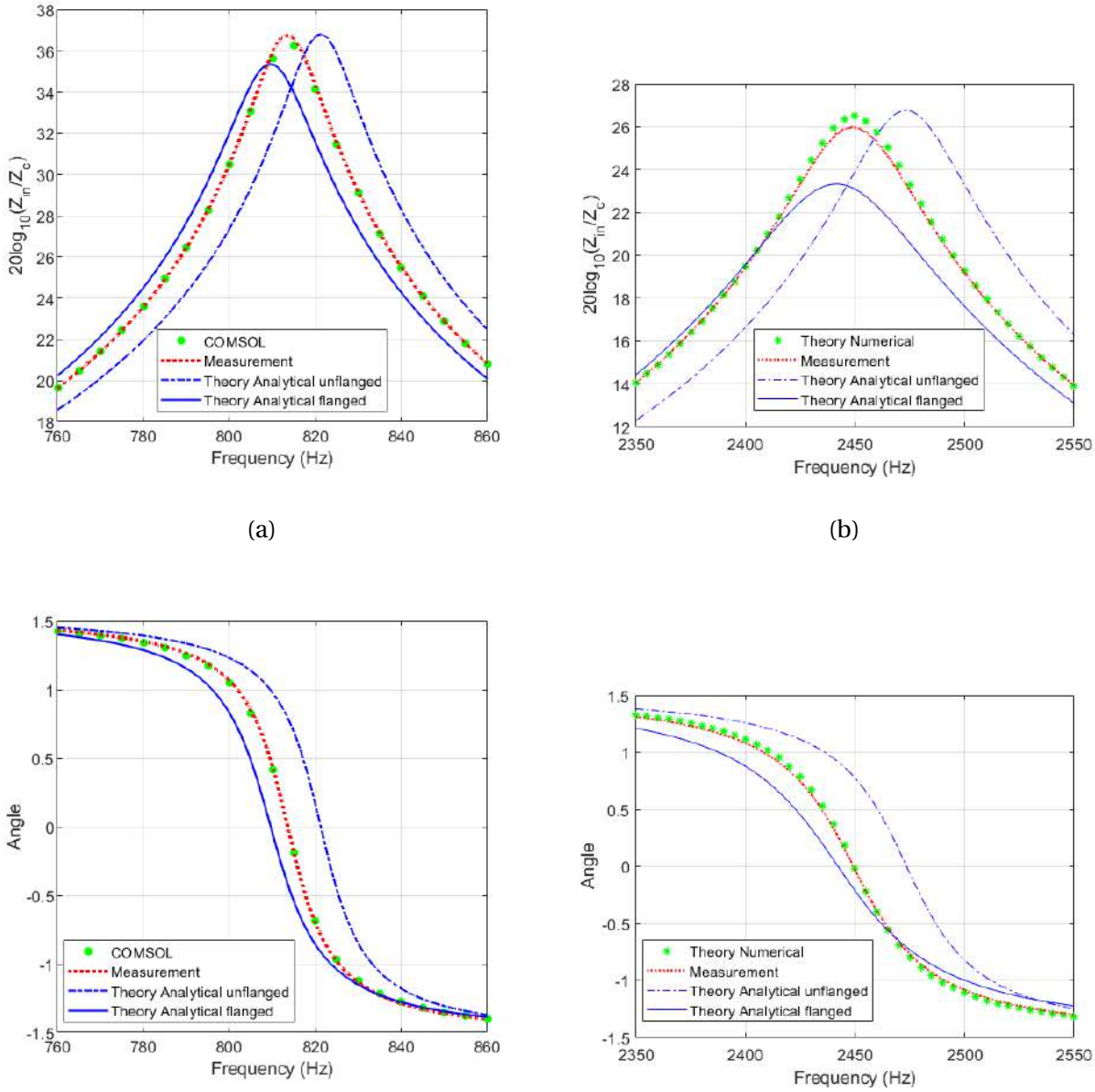

Figure 1.23: Comparison between measurement, analytical equation and numerical simulation. (a) First peak, (b) second peak of the input impedance modulus of the tube $P1L$. (c)First peak and (d) second peak of the input impedance phase of the tube $P1L$. Analytical curve computed through Eq. 1.19 with the radiation impedance computed through Eq. 1.16 for the flanged and unflanged conditions.

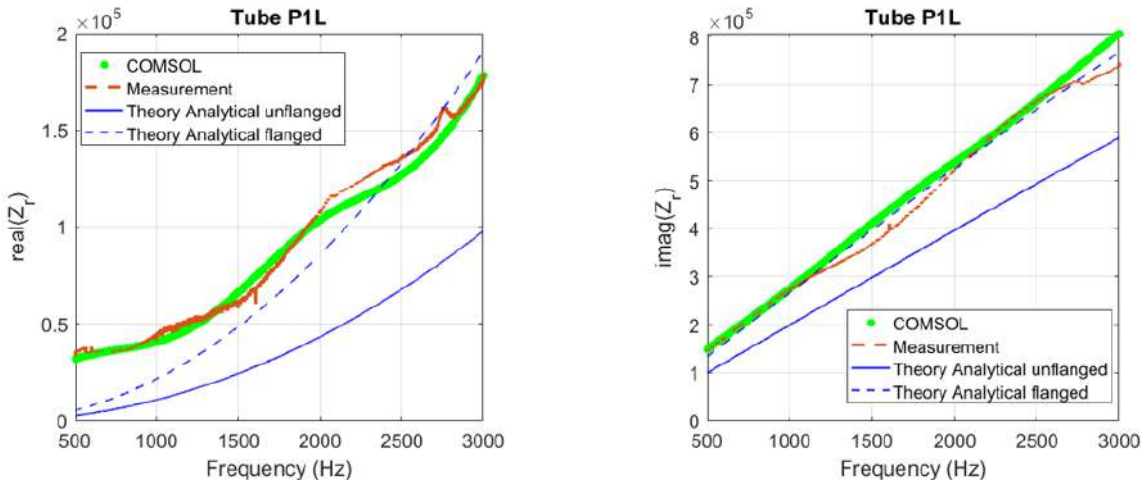

(a) (b)

Figure 1.24: (a) Real and (b) imaginary parts of the radiation impedance of the tube $P1L$. Analytical computed through Eq. 1.16 for the unflanged and flanged conditions.

Bibliography

[1] M. P. Le Roux Jean Christophe and D. J. Pierre, "Un capteur de nouvelle génération pour la mesure d'impédance acoustique en contexte industriel,"

[2] C. A. Macaluso and J.-P. Dalmont, "Trumpet with near-perfect harmonicity: Design and acoustic results," *The Journal of the Acoustical Society of America*, vol. 129, no. 1, pp. 404–414, 2011.

[3] G. Sound and Vibration, "Gras 46bf-1 1/4" lemo free-field," 2021.

[4] G. Sound and Vibration, "Gras 40sc ccp probe microphone," 2021.

[5] F. Silva, P. Guillemain, J. Kergomard, B. Mallaroni, and A. N. Norris, "Approximation formulae for the acoustic radiation impedance of a cylindrical pipe," *Journal of Sound and Vibration*, vol. 322, no. 1-2, pp. 255–263, 2009.

[6] G. Bunting, S. T. Miller, C. R. Dohrmann, and T. Walsh, "Solving complex acoustic problems using high performance computations.," *Acoustics Today*, vol. 16, no. SAND2020-3661J, 2020.

[7] E. Madenci and I. Guven, *The finite element method and applications in engineering using ANSYS®*. Springer, 2015.

[8] N. Atalla and F. Sgard, *Finite element and boundary methods in structural acoustics and vibration*. CRC Press, 2015.

[9] H. Gothall, "How to inspect your mesh in comsol multiphysics," tech. rep., COMSOL, 2017.

[10] H. Schwab and K. Chen, “Finite element analysis of a guitar soundboard,” *Catgut Acoust. Soc. Newsletter*, vol. 24, pp. 13–15, 1975.

[11] J. Bretos, C. Santamarıa, and J. A. Moral, “Vibrational patterns and frequency responses of the free plates and box of a violin obtained by finite element analysis,” *The Journal of the Acoustical Society of America*, vol. 105, no. 3, pp. 1942–1950, 1999.

[12] M. Elejabarrieta, A. Ezcurra, and C. Santamaría, “Vibrational behaviour of the guitar soundboard analysed by the finite element method,” *Acta Acustica united with Acustica*, vol. 87, no. 1, pp. 128–136, 2001.

[13] M. Elejabarrieta, A. Ezcurra, and C. Santamarıa, “Coupled modes of the resonance box of the guitar,” *The Journal of the Acoustical Society of America*, vol. 111, no. 5, pp. 2283–2292, 2002.

[14] H. García-Mayén, “Estudio del efecto de la unión entre la tapa y el diapasón en la radiación acústica de la guitarra clásica,” 2008.

[15] M. Mihălcică, M. D. Stanciu, and S. Vlase, “Frequency response evaluation of guitar bodies with different bracing systems,” *Symmetry*, vol. 12, no. 5, p. 795, 2020.

[16] A. Lefebvre, “Computational acoustic methods for the design of woodwind instruments,” 2011.

[17] A. Lefebvre and G. P. Scavone, “Characterization of woodwind instrument toneholes with the finite element method,” *The Journal of the Acoustical Society of America*, vol. 131, no. 4, pp. 3153–3163, 2012.

[18] V. Dubos, J. Kergomard, A. Khettabi, J.-P. Dalmont, D. Keefe, and C. Nederveen, “Theory of sound propagation in a duct with a branched tube using modal decomposition,” *Acta Acustica united with Acustica*, vol. 85, no. 2, pp. 153–169, 1999.

[19] P. Rucz, F. Augusztinovicz, J. Angster, T. Preukschat, and A. Miklós, "A finite element model of the tuning slot of labial organ pipes," *The Journal of the Acoustical Society of America*, vol. 137, no. 3, pp. 1226–1237, 2015.

[20] R. Tournemenne and J. Chabassier, "A comparison of a one-dimensional finite element method and the transfer matrix method for the computation of wind music instrument impedance," *Acta Acustica united with Acustica*, vol. 105, no. 5, pp. 838–849, 2019.

[21] A. K. Coaldrake, "A finite element model of the japanese koto constructed from computed tomography scans," *The Journal of the Acoustical Society of America*, vol. 148, no. 5, pp. 3153–3170, 2020.

[22] M. H. Jensen, "Theory of thermoviscous acoustics: Thermal and viscous losses," tech. rep., COMSOL, 2014.

Chapter 2

Tube reversed method

This chapter is composed of an integral article submitted to the Journal of the Acoustical Society of America (JASA), in relation of the new proposed method for the computing of the tonehole impedances. Additionally, there is a second part in the form of an Appendix, composed of a study in Finite Element Method (FEM) for the same proposed new method.

Submitted article

It is expected that the article will be accepted any day now, as the opinion of the associate editor before the new version was submitted was: "I am prepared to accept your manuscript JASA-06981R1, "Characterization of open woodwind toneholes by the tube reversed method," pending final minor revisions, which are appended below. If you address these minor revisions, your manuscript will be accepted."

Characterization of open woodwind toneholes by the tube reversed method

H. Garcia Mayén,[1] J. Kergomard,[2,a] C. Vergez,[2] P. Guillemain,[2] M. Jousserand,[3] M. Pachebat,[2] and P. Sanchez[2]
[1] *Buffet Crampon, 5 rue Maurice Berteaux, Mantes-la-Ville, 78711, France*
[2] *Aix Marseille Univ., CNRS, Centrale Marseille, LMA UMR 7031, Marseille, France*
[3] *Buffet Crampon, 5 rue Maurice Berteaux1, Mantes-la-Ville, 78711, France*

(Dated: 13 October 2021)

Woodwind tonehole's linear behavior is characterized by two complex quantities: the series and shunt acoustic impedances. A method to determine experimentally these two quantities is presented for the case of open toneholes. It is based on two input impedance measurements. The method can be applied to clarinet-like instruments, and can be used for undercut toneholes as well as toneholes with pads above their output, under the condition that a symmetry axis exists. The robustness of the method proposed is explored numerically through the simulation of the experiment when considering geometrical and measurement uncertainties. Experimental results confirm the relevance of the method proposed to estimate the shunt impedance. Even the effect of small changes in the hole's geometry, such as those induced by undercutting, are characterized experimentally. The main effect of undercutting is shown to be a decrease of the tonehole's acoustic mass, in agreement with theoretical considerations based on the shape of the tonehole. Investigation on the effects of pads will be studied in a further work. Experimental results also reveal that losses in toneholes are significantly higher than those predicted by the theory. Therefore the method is suitable for the experimental determination of the shunt impedance, but it is not convenient for the characterization of the series impedance.

 [https://doi.org(DOI number)]

[XYZ] Pages: 1–10

I. INTRODUCTION

For woodwind instruments, the effect of toneholes on the intonation and the ease of playing is essential. The present paper focuses on linear behaviour of open toneholes, which is especially important for the playing frequencies.

The characterization of holes can be independent of the geometry of the resonator (either cylindrical or conical, see e.g.[1]).

The first theory was given by Keefe[2], and completed by[4,7]. It is based on matching plane waves within the resonator and the tonehole. The tonehole is characterized by a transfer matrix of order 2. Because of reciprocity, only three elements of the matrix are necessary. Furthermore, in the present paper, the tonehole is assumed to be symmetrical, and two elements (i.e., two complex impedances) are sufficient (see[4]) for symmetrical toneholes. This can approximately happen for undercut toneholes. For toneholes with pads above their output, the radiation of the tonehole is modified, but it can be assumed that a symmetry axis exists, and two elements are also sufficient. The theory, based upon modal expansion, assumes the tonehole to be cylindrical, and this leads to a difficulty of the geometric matching between two cylinders. However, the number and nature of the matrix elements does not depend on the shape of the toneholes, and they can be determined either by experiment or numerical discretization (see e.g.[8–10]). The Finite Element Method can be used, but the geometric and acoustic modeling of boundary layers (see[9]) and nonlinear behaviour is not straightforward. Acoustic experiment can be also used for the computation of the input impedance of an instrument by using the transfer matrix method: the measurement of the two acoustic impedances make unnecessary the knowledge of the precise geometry. For the computation of the input impedance of an instrument, the acoustic characterization of the open toneholes is sufficient. We notice that the measured elements correspond to the pair tonehole-tube, because they depend on the tube diameter, and are useful for predicting (and maybe for optimizing) the input or transfer impedances. Moreover, the presence of pads located above the output of the open hole modifies their radiation, and therefore the shunt impedance. This paper is limited to open holes without pads, but the present method can be used for holes with pads.

Considering the equivalent circuit of an open tonehole, the elements are essentially acoustic masses. One is in series, modifying the acoustic pressure, and the other is in parallel, modifying the acoustic flow rate. They can be regarded as length corrections to the main tube and to the tonehole, respectively. Nevertheless, for high

[a] kergomard@lma.cnrs-mrs.fr

(i.e., long) toneholes, compressibility (and propagation) effects can appear. Moreover, for both the impedances in series and in parallel, losses (i.e., resistances) exist. Losses added to the series mass are generally ignored, and no theoretical determination exists, while experimental evidence was found by Dalmont et al[10] in a nonlinear regime. At low frequencies, the two masses are almost independent of frequency, but they increase when approaching the first cutoff of the main tube. This variation has been theoretically studied only for the 2D, rectangular case(see[4]), but it is general[5]. Other shunt acoustic masses intervene, in particular that of the plane mode in the hole, and a resonance of the total shunt mass can occur at high frequency: this is detailed in Section II.

Previous articles[6,10,14,15] used experiment devices for the measurement of the series and shunt impedances for open or/and closed toneholes, including the possibility of hole undercutting and pad existence[6,11–14]. They took advantage of the tonehole symmetry to limit the experiment to simultaneous measurement of two quantities, the input impedance of a tube with one tonehole at its middle, and a transfer impedance. This allows avoiding dismantling the apparatus during the measurement. The present paper aims at exploring another method. It limits the measurement to two input impedances, by reversing the cylindrical tube (see Fig. 1), the extremity being open. Thus the termination impedance is unchanged when turning the tube. The drawback is the need of dismantling the set up.

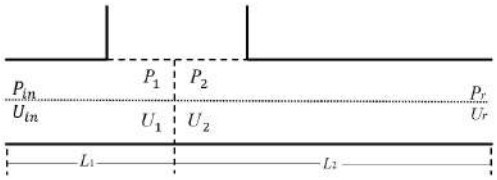

FIG. 1. Scheme of the tonehole geometry and acoustic variables. For the second situation, an apostrophe is added to the geometrical and acoustic quantities, and $L_1' = L_2$, and $L_2' = L_1$

In Sect. II, the calculation is performed by using the theoretical, known model of a cylindrical tonehole on a cylindrical tube. From the theoretical values of the two characteristics, the calculation determines the two input impedances of the tube in the two situations, the second being the reversed situation of the first. In Sect. III, the inverse problem (often called the crime inverse problem) is computed. It necessitates the determination of the two tonehole characteristics from the two input impedances of the tube in two different situations. In other words two input impedances become the starting point from which the two characteristics are derived. Therefore the tube reversed method consists in reversing the tube. If the calculations are correct, the two tonehole characteristics obtained by solving the inverse problem are identical to the initial values calculated from the model.
In practice there is a very small error because of the numerical computation (direct and inverse). If some data of the inverse problem are slightly wrong, the two characteristics obtained slightly differ from the initial values. The data of the inverse problem are either geometric data or measured input impedances. Modifying these data allows assessing the sensitivity of the method to uncertainties on these data. This is the purpose of Sect. IV, which discusses some parameter choices of the experiment, such as the main tube length and the location of the tonehole.

Sect. V describes the experiment including the measurement method of the input impedance and results for cylindrical toneholes, with dimensions similar to those of a clarinet. Sect. VI presents experimental results for examples of undercut toneholes. Sect. VII discusses the validity and interest of the method.

II. DIRECT PROBLEM: MODEL OF A TUBE WITH AN OPEN TONEHOLE

The radii of the main tube and the hole are denoted a and b, respectively. The wavenumber in free space is denoted $k = \omega/c$; ω is the angular frequency, and c is the sound speed in free space. The wavenumber involving viscous-thermal losses in the main tube is given by a standard expression[3] (p. 242):

$$k_a = k\left[1 + 1.044\sqrt{-2j}/r_v - 1.08j/r_v^2\right] \qquad (1)$$

where $r_v = a\sqrt{\omega\rho/\mu}$ for the main tube. ρ is the air density, and μ the air viscosity. The same formula holds for the tonehole, with the notations k_b and b. The characteristic impedances are $Z_c = \rho c/\pi a^2$ and $Z_{ch} = \rho c/\pi b^2$. The quantities at the left (resp. right) of the tonehole are denoted with subscript 1 (resp. 2). The lengths of the main tube on the two sides of the tonehole are L_1 and L_2. The height of the tonehole is t. The schematic of the tonehole geometry and the acoustic variables are shown in Fig. 1. In both the main tube and the tonehole, only the plane mode propagates, i.e., higher order modes are evanescent, i.e., the frequency is low enough ($k < 1.84/a$). The plane mode can be matched on the two sides of the tonehole symmetry axis by a second order transfer matrix[2]. The effect of the tonehole is described by the following equation:

$$\begin{pmatrix} P_1 \\ U_1 \end{pmatrix} = M_h \begin{pmatrix} P_2 \\ U_2 \end{pmatrix}, \qquad (2)$$

where acoustic pressure and volume velocity are denoted P and U, respectively. For the volume velocity, the axis

is oriented to the right. M_h is a symmetrical matrix with unity determinant[16]. It corresponds to the T-circuit (see[3,4]) shown in Fig. 2. It is written as follows:

$$M_h = \frac{1}{1 - Y_s Z_a/4} \begin{pmatrix} 1 + Y_s Z_a/4 & Z_a \\ Y_s & 1 + Y_s Z_a/4 \end{pmatrix} \quad (3)$$

The series impedance Z_a and the shunt impedance $Z_s = 1/Y_s$ are the impedances corresponding to the anti-symmetric and symmetric parts of the velocity at the input of the tonehole[2,3], respectively. For an open tonehole, they are given by the following equations[4]:

$$Z_a = jkZ_c t_a \quad (4)$$

$$Z_s = jZ_{ch}(kt_i + \tan[k_b t + k(t_m + t_r)]). \quad (5)$$

In the equivalent circuit and the transfer matrix the effective shunt impedance Z_h appears. It is defined by:

$$Z_h = Z_s - Z_a/4. \quad (6)$$

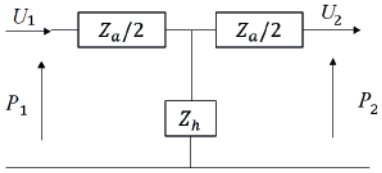

FIG. 2. Equivalent circuit for the tonehole

The lengths included in the above expressions are given hereafter. If $\delta = b/a$, the series length correction t_a is given by[4]:

$$t_a = -b\delta^2 / \left[1.78\tanh(1.84t/b) + 0.94 + 0.540\delta + 0.285\delta^2\right]. \quad (7)$$

This quantity is very small (a typical value is 0.5 mm). For this reason several authors neglect the corresponding term in Eq. 6. However, in the matrix M_h it is not consistent to ignore a quantity in one element while keeping it in the other elements. This remark can be related to the dual role of pressure and volume velocity in Eq. (3). An important remark is that the corresponding acoustic mass is negative[2]. No failure of causality is done, because causality is ensured by the complete matrix Eq. (3).

At low frequencies, the length t_i, due to evanescent modes, is independent of frequency and can be regarded as an internal length correction for the tonehole height. It can be written as (see[4], and[10] for a correction):

$$t_i = b(0.82 - 0.193\delta - 1.09\delta^2 + 1.27\delta^3 - 0.71\delta^4). \quad (8)$$

The length t_m is related to the matching volume between the tonehole and the main tube, and cannot be exactly computed with the modal matching method, except when the main tube is rectangular (in which case it vanishes). Its value is given by[7]:

$$t_m = b\delta(1 + 0.207\delta^3)/8. \quad (9)$$

The length t_{rh} is the (complex) radiation length given by $t_{rh} = Z_{rh}/(jkZ_{ch})$, where rh is the subscript for the hole end, and Z_{rh} the radiation impedance of the tonehole. Different expressions exist in the literature. For the sake of simplicity, we assume that it is equal to the radiation of a tube without flange (see e.g.[17]). At low frequencies, the order of magnitude of the uncertainty concerning the real length correction $t_{rh} = \mathrm{Re}(t_r)$ is $0.2b$, which is the difference between the two extreme cases (without flange and with infinite flange, respectively). If losses near the walls are ignored, the total equivalent height of the tonehole is defined as:

$$t_s = \mathrm{Im}(Z_s/(kZ_{ch})). \quad (10)$$

At low frequencies, it is equal to:

$$t_s = t_i + t + t_m + t_r. \quad (11)$$

The geometric values chosen in this paper are the tonehole radius $b = 4$ mm (the main tube radius is $a = 7.3$ mm), and height $t = 8.5$ mm; the matching length correction is $t_m = 0.3$ mm. The length correction for radiation is $t_r = 2.5$ mm (with a significant uncertainty of $0.2b = 0.8$ mm) and the internal length correction is $t_i = 2.1$ mm. The total equivalent height is therefore $t_s = 13.4$ mm. This quantity is of major interest for the computation of the input impedance of an instrument. Using the standard transmission line theory, the effect of a tonehole height difference by 1 mm can be computed: it implies a typical shift of the first impedance peak of a typical clarinet by 0.5% to 1% (i.e., 9 to 17 cents). Therefore the cumulative shift for several toneholes can be rather high.

It remains to derive the input impedance Z_{in}. in is the subscript of the tube input, and r that of the termination. The basic equation is:

$$\begin{pmatrix} P_{in} \\ U_{in} \end{pmatrix} = M_1 M_h M_2 \begin{pmatrix} P_r \\ U_r \end{pmatrix}. \quad (12)$$

M_1 and M_2 are the transfer matrices of the cylindrical sections of the tube ($i = 1, 2$):

$$M_i = \begin{pmatrix} A_i & B_i \\ C_i & A_i \end{pmatrix} = \begin{pmatrix} \cos k_a L_i & jZ_c \sin k_a L_i \\ jZ_c^{-1} \sin k_a L_i & \cos k_a L_i \end{pmatrix}. \quad (13)$$

The terminal impedance Z_r is projected back to the right of the tonehole, as follows:

$$Z_2 = \frac{A_2 Z_r + B_2}{C_2 Z_r + A_2}. \quad (14)$$

Similarly, the impedance Z_1 at the left of the tonehole is projected from Z_2 by using the matrix M_h and Eq. (2).

Finally the input impedance Z_{in} is projected from Z_1 by using the matrix M_1. A second choice of the lengths L_1 and L_2 lead to another value of the input impedance.

III. INVERSE PROBLEM

The aim of the inverse problem is to derive the two tonehole characteristics from the two input impedances Z_{in} and Z'_{in}. The apostrophe indicates the reverse situation. The two different situations are $L_1 < L_2$, and $L'_1 < L'_2$, when in the second case the tube is reversed such that $L'_1 = L_2$, and $L'_2 = L_1$. The tonehole is not located at the middle of the tube, in order to obtain two different input impedances when the tube is reversed. For the present method, the main tube is open: Z_r is the radiation impedance. It is assumed to be equal to its theoretical value without flange[17]. It was checked that the results are not very sensitive to the precise value of the radiation impedance. Using of the measured value of the radiation impedance does not change significantly the results. The important condition is that the radiation impedance is the same for the two situations. Now the input impedance is assumed to be known, and is projected back to the left of the tonehole, using the inverse matrix of M_1 as:

$$\begin{pmatrix} P_1 \\ U_1 \end{pmatrix} = \begin{pmatrix} A_1 & -B_1 \\ -C_1 & A_1 \end{pmatrix} \begin{pmatrix} P_{in} \\ U_{in} \end{pmatrix} \tag{15}$$

$$\Rightarrow Z_1 = \frac{A_1 Z_{in} - B_1}{-C_1 Z_{in} + A_1}. \tag{16}$$

Following Fig. 2, the equations for the 3 elements of the electrical equivalent circuit can be written: Defining $P = Z_h(U_1 - U_2)$; $P_1 = Z_1 U_1 = P + Z_a/2 U_1$; and $P_2 = Z_2 U_2 = P - Z_a/2 U_2$, the following equation is obtained:

$$\frac{1}{Z_h} = \frac{1}{Z_1 - Z_a/2} - \frac{1}{Z_2 + Z_a/2}. \tag{17}$$

A similar equation holds for the second situation (reversed tube), replacing Z_1 and Z_2 by Z'_1 and Z'_2, respectively.

$$\frac{1}{Z_h} = \frac{1}{Z'_1 - Z_a/2} - \frac{1}{Z'_2 + Z_a/2}. \tag{18}$$

The following quadratic equation is obtained by eliminating Z_h:

$$A Z_a^2/4 + B Z_a/2 + C = 0, \tag{19}$$

$$\begin{gathered} A = (Z'_1 - Z_1) - (Z'_2 - Z_2); \\ B = 2(Z'_1 Z'_2 - Z_1 Z_2); \\ C = Z'_2 Z_2 (Z'_1 - Z_1) - Z'_1 Z_1 (Z'_2 - Z_2) \end{gathered} \tag{20}$$

Eq. (19) can be solved for Z_a, then Z_h is derived from Eq. (17) or Eq. (18). However a simpler solution is obtained by expressing Z_h with respect to Z_a from Eq (17. A term Z_a^2 appears. Using the latter expression and Eq. 19), and eliminating Z_a^2, it can be written:

$$Z_a = -\frac{B}{A} - 2Z_h. \tag{21}$$

Then, introducing this result in the quadratic equation (19), the following result is obtained:

$$Z_h^2 = \frac{B^2}{4A^2} - \frac{C}{A}. \tag{22}$$

Two solutions exist for this equation. The solution with a negative real part can be eliminated because the physical system is passive. Z_s can be deduced from Eq. (6):

$$Z_s = Z_h + Z_a/4. \tag{23}$$

Throughout this paper, the results are focussed on 3 quantities: the total equivalent height of the tonehole t_s, given by Eqs. (10, 22, 23); the real part of the effective shunt impedance Z_h and the imaginary part of Z_a, from Eq. (21).

The results of the inverse problem were checked by using computed input impedances, and the order of magnitude of the numerical error is smaller than 10^{-14}. Fig. 3 shows the comparison between the direct and the inverse computations for the equivalent height of the tonehole t_s (see Eq.(10)). For Z_a, the numerical error is smaller than 10^{-12}. For other choices of termination impedance, such as an infinite impedance or the characteristic impedance, the entire computation remains valid.

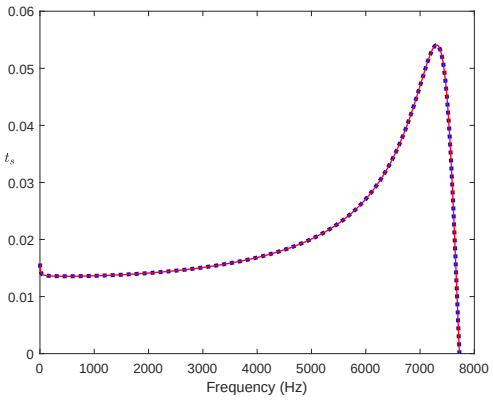

FIG. 3. (Color online) Equivalent height t_s of the tonehole (in m). Solid, red line: model; blue, dotted line: inverse problem (from Eq. (22)). Dimensions $a = 7.3$ mm, $b = 4$ mm, $t = 8.5$ mm, $L_1 = 44$ mm, $L_2 = 74$ mm.

When the frequency tends to zero, the small increase is due to the visco-thermal dispersion, which diminishes the sound speed, and increases the equivalent length. Furthermore, the strong variation at higher frequencies is due to the propagation of the planar mode in the tonehole (see the function tan(x) in Eq. (5)). The resonance near 7540 Hz corresponds to the minimum of the input impedance of the tonehole.

IV. SIMULATION OF THE EXPERIMENT

In order to simulate the experiment, errors are introduced on the data of the inverse problem. The input

impedance is first computed by using the model, and the values are treated as experimental data.

A. Effect of uncertainty on the main tube length

For the second case, an error of 0.2 mm is added to the length L_1. It includes the uncertainty of the measurement, and the uncertainty on the tube manufacture. For the second case, an error of 0.2 mm on the length L_1 is considered together with an opposite error on the length L_2 (the later case corresponds to an error on the location of the tonehole, without change in the total length $L_1 + L_2$).

For the equivalent height of the hole t_s, Fig. 4 shows the comparison between results for the two cases simulated and the theoretical result (without errors introduced). Between 1550 Hz and 1650 Hz, the error on the result is very large. Because this also happens at other higher frequencies, the figure is limited to 2000 Hz.

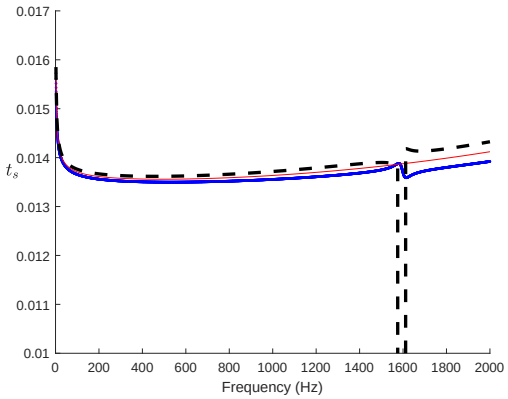

FIG. 4. (Color online) Equivalent height t_s (in m). Red, solid thin line: theory without length errors. Blue, thick, solid line: inverse problem (Eq. (22)) with 0.2 mm error on L_1. Black, dashed line: inverse problem with 0.2 mm error on L_1 and -0.2 mm error on L_2.

The frequency ranges with large error are close to the input impedance minima of the main tube (1560 Hz for Z_{in} and 1610 Hz for Z'_{in}). A simple qualitative interpretation is the following: suppose that the radiation impedance of the tube is 0 (whatever the frequency), and that the input impedance vanishes at a given frequency, therefore the eigenfrequencies of the tube in the two positions are equal, and the problem becomes ill-posed (one equation for two unknowns): the solutions tend to infinity. This reasoning is not exact, because the radiation impedance is small, but not 0. The variations of t_s are very small up to 1400 Hz, as well as the discrepancies with the theoretical values. Concerning the real part of the shunt impedance Z_h, it can be seen in Fig. 5 that the accuracy of the simulated results is satisfactory up to 1400 Hz.

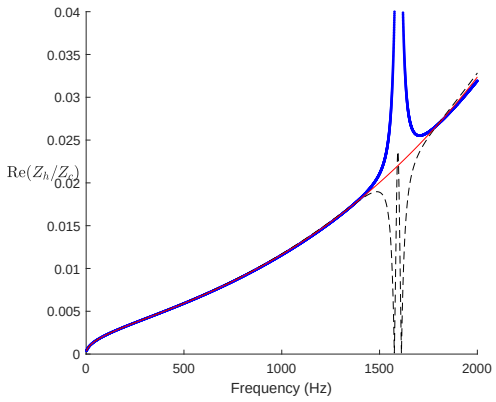

FIG. 5. (Color online) Real part of the reduced shunt impedance $Re(Z_h/Z_c)$ (dimensionless). See line definitions in the caption of Fig. 4.

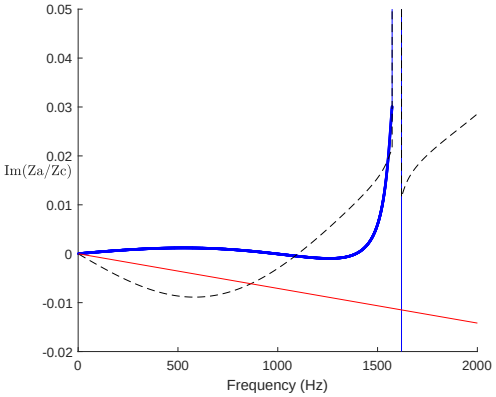

FIG. 6. (Color online) Imaginary part of the reduced series impedance $Im(Z_a/Z_c)$ (dimensionless). See line definitions in the caption of Fig. 4.

However, concerning the imaginary part of the series impedance Z_a, even a very small error on the lengths causes large errors on the result (see Fig. 6). Even the sign of the quantity is not determined. This result suggests that it is extremely difficult to expect a precise measurement of the series impedance. From this perspective, the method is less robust than the method of[10], even if the later is not very precise (the uncertainty is almost 35%). The present method is probably not suitable for measuring this element through experimentation.

B. Effect of the data uncertainty on the measured input impedance

A second attempt to simulate the experiment is based on the introduction of a random error on the modulus of the input impedance (for the two configurations of the main tube Z_{in} and Z'_{in})). The input impedance is

modified as follows:

$$\widetilde{Z_{in}} = Z_{in}\{1 + 0.005[rand(N) - 0.5]\}. \qquad (24)$$

The number N is the size of the input impedance vector. *rand* is a Matlab function that generates uniform pseudo-random numbers in the interval $[0, 1]$. The value 0.005 is determined by the measurement of many input impedances. It means that the error modelled ranges from -0.25% to 0.25% of Z_{in}. The three figures 7 to 9 show a confirmation of the previous observations: the measurement can be accurate up to 1600 Hz for the shunt impedance, but the measurement of the series impedance is not possible (see Figs. 7 to 9). The relative error on the equivalent height is less than 7%.

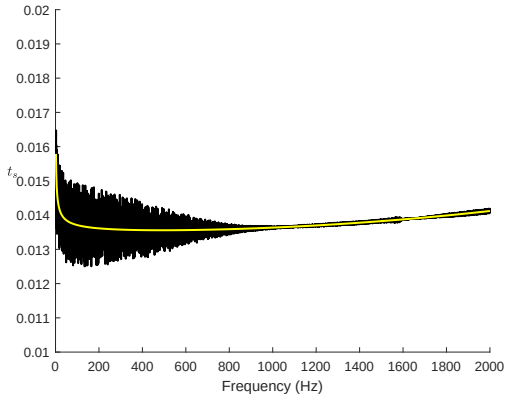

FIG. 7. (Color online) Tonehole equivalent height t_s (in m). Black lines: result of a simulation with a random error on the input impedance of the tube (Eq. 24). Yellow line: no random error.

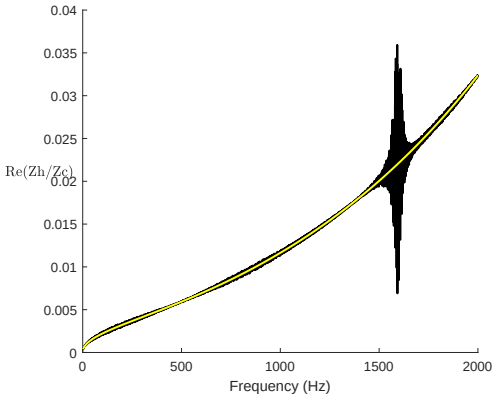

FIG. 8. (Color online) Real part of the reduced shunt impedance $Re(Z_h/Z_c)$ (dimensionless). Black lines: result of a simulation with a random error on the input impedance of the tube (Eq. 24). Yellow line: no random error.

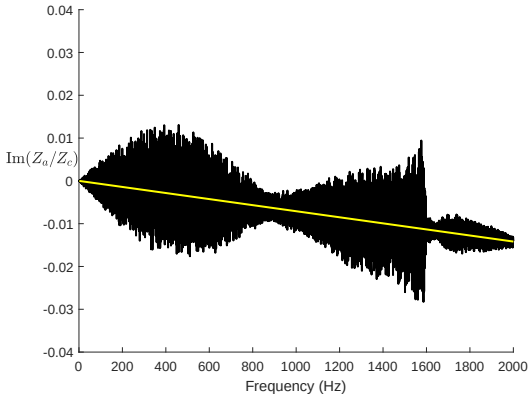

FIG. 9. (Color online) Imaginary part of the reduced series impedance $Im(Z_a/Z_c)$ (dimensionless). Black lines: result of a simulation with a random error on the input impedance of the tube (Eq. (24)). Yellow line: no random error.

C. Practical considerations for the dimensions of the main tube

A conclusion of the simulation study implies that the main tube has to be chosen to be as short as possible. In order to avoid the coupling of evanescent modes between the tonehole and the radiating termination, the distance L_1 between the tonehole and the termination can be chosen between 2 and 3 times the main tube diameter. Furthermore the value of the first minimum frequency implies a small total length $L_1 + L_2$. However it is essential that the two lengths are sufficiently different, in order to avoid the quadratic equation to become degenerate. A convenient choice is L_2 between 1/3 and 1/2 times the total length $L_1 + L_2$. We note that other terminations for he the tube lead to correct results, but, for instance, when the tube is closed, the first anti-resonance is rather low and this limits the frequency range of the measurement.

V. EXPERIMENTAL RESULTS FOR CYLINDRICAL TONEHOLES

A. Input impedance measurement

The previous analysis encourages us to study an experiment based upon the method presented in the present paper. The method is tested experimentally by using wood pieces, and the CTTM sensor[18] for the impedance measurement. A piezoelectric buzzer is used as a source. The pressure in the back cavity of the buzzer is measured by a microphone, which gives an estimation of the volume velocity. The measured pipe is connected to the front of the buzzer via a small open cavity in which a second microphone measures the pressure. The input impedance of the pipe is at first order proportional to the transfer function between the two microphones. The comparison with theoretical results for cylindrical tubes

(without toneholes) is satisfactory: the discrepancy for a closed tube is 4 cents for the resonance frequencies and 1 dB for the peak heights, except at very low frequencies. For this reason, measurements are done above 200 Hz.

B. Preliminary results concerning the repeatability of the measurement

We first study the repeatability for a tube and a tonehole with dimensions equal to those previously considered. For the frequency range 200 to 1400 Hz, the equivalent height t_s of the tonehole is found to be between 14.4 mm and 15.5 mm, while the theoretical value (from Eq. 10 is 13.4 mm. For 4 measurements after disassembly and assembly, the uncertainty is found to be about 1 to 2% (see Fig. 10). Furthermore Fig. 11 shows the comparison between the measurements of 4 tubes built with the same tools. The material of the tubes is a composite material built by Buffet-Crampon for the Greenline clarinet, and the holes were deburred. The results are distributed on both sides of the theoretical one. This is an effect of the manufacturing tolerance, which is of the same order of magnitude as the measurement uncertainty, or higher. For all experimental results, the Matlab function *smooth* has been used. We remark measurements are not necessarily taken on the same day and at the same temperature, but the computation took it into account.

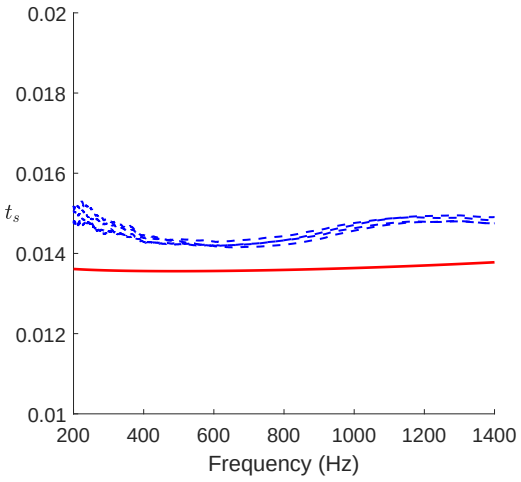

FIG. 10. (Color online) Tonehole equivalent height (in m) measured 4 times after disassembly. Blue, dashed lines: measurements. Red, solid line: theory. Dimensions $a = 7.3$ mm, $b = 4$ mm, $t = 8.5$ mm, $L_1 = 44$ mm, $L_2 = 74$ mm.

C. Comparison between two tubes of different lengths

Two tubes with the same length $L_2 = 44$ mm abd with a length $L_1 = 74$ mm and 118 mm are compared. The value of L_2 is chosen to be 3 times the tube diameter.

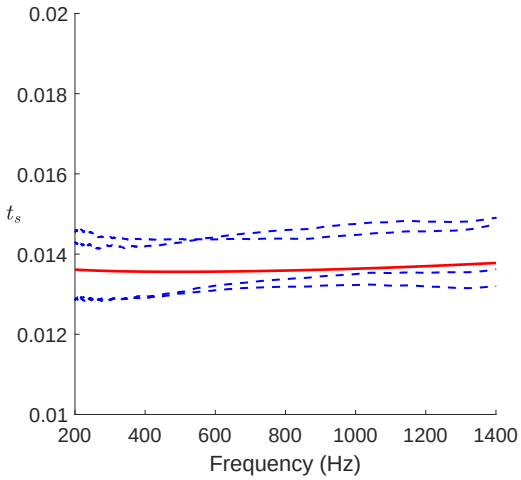

FIG. 11. (Color online) Tonehole equivalent height t_s (in m) for 4 tubes built with the same tool. Blue, dashed lines: measurements. Solid, red line: theory.

The dimensions of the tonehole are identical for the two tube lengths ($b = 4$ mm; $t = 8.5$ mm). Fig. 12 shows a small increase when the frequency approaches the eigenfrequency of the tubes. As explained above, the short tube yields better results on a wider frequency range. The discrepancy between the results of the two tubes is less than 3

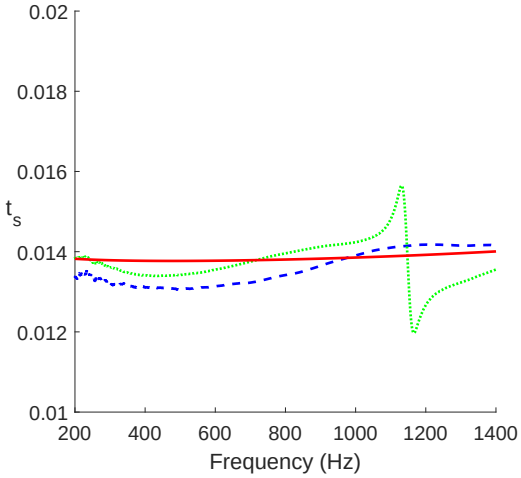

FIG. 12. (Color online) Measured value of the equivalent height t_s(in m) of the hole. Green, dashed lines: long tube. Blue, dottted line: short tube. Red, solid line: theory

Concerning the real part of the shunt impedance, it appears that the two tubes yield very similar values, except in the vicinity of the eigenfrequency. Fig. 13 shows that they are higher than the theoretical values. Remember that for a linear functioning, radiation losses are proportional to ω^2, while visco-thermal losses increase as

$\sqrt{\omega}$. We refer to[10] for a discussion about the theoretical aspects. Finally, the experiment confirms that the series impedance cannot be measured by the tube reversed method, as shown in Fig. 14.

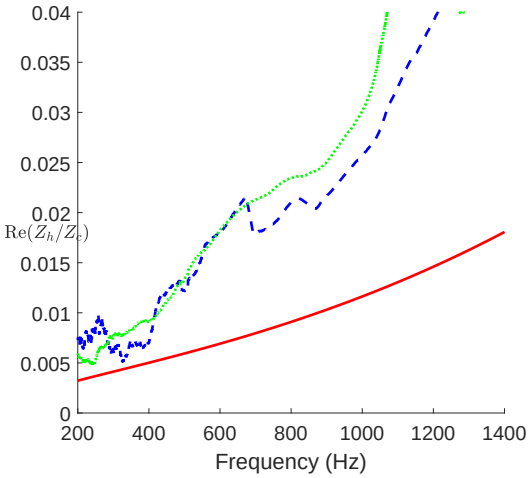

FIG. 13. (Color online) Measured value of the real part of the reduced shunt impedance $Re(Z_h/Z_c)$ (dimensionless). See the line definitions in the caption of Fig. 12.

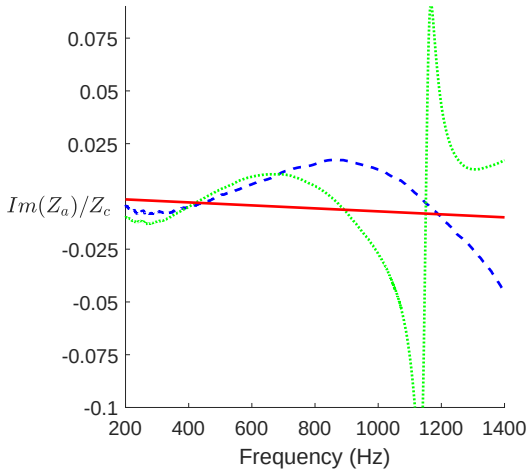

FIG. 14. (Color online) Measured value of the imaginary part of the reduced series impedance $Im(Z_a/Z_c)$ (dimensionless). See the line definitions in the caption of Fig. 12.

VI. EXPERIMENTAL RESULTS FOR UNDERCUT TONEHOLES

Undercutting tonholes was studied in[10] for high excitation level and in[19] (see also[20]) for rectangular geometry. Eight short tubes of length 118 mm have holes drilled at $L_1 = 44$ mm that have three different geometries: three are straight (but the hole is deburred), three are undercut with a cylinder length of 6.7 mm (tubes denoted UC1) and two are undercut with a cylinder length of 5.7mm (tubes denoted UC2). Figs. 15 and 16 show the effect of undercutting the tonholes. The quantity shown by Fig. 15 is slightly different from that shown previously (see e.g. Fig. 13), because considering the length correction in Eq. (10) implies a division by the cross-section area S_h, but for the case of undercut toneholes, the area is not constant. For this reason, we choose the acoustic mass (per unit density) m_s:

$$m_s = Z_h/(j\omega\rho). \tag{25}$$

The figures represent the average quantities for each geometry. The effect of undercutting is a decrease of $10m^{-1}$ to $20m^{-1}$ for the acoustic mass when the undercutting becomes wider. The jump below 400 Hz in Fig. 15 remains unexplained.

Two causes for this mass increase can be analysed. The widening implies a decrease of the acoustic mass of the plane mode, and also of the internal length correction due to the discontinuity between the main tube and the tonehole. The first of these causes can be modelled. Considering the acoustic mass for the cylindrical tonehole case, calculating the average value, we obtain 280 m^{-1}. For the cases of undercutting, we obtain 270 m^{-1} and 264 m^{-1}. An elementary model can be made in order to interpret these results. The shape of the most undercut tonehole (UC2) is close to a cylinder extended in a truncated cone joining the internal wall of the main tube. For the cases studied, the lengths of the cylinder ℓ and of the cone ℓ' are approximately equal to 5.5 and 5 mm, respectively. The radius of the cylinder is $b = 4$ mm, the small radius of the cone is $R_1 = b$ and its large radius is $R_2 = 5.4$ mm. The calculation of the mass of a tube with variable cross section is done by integrating the inverse of the area along the axis. For a cone, the result is published in[3], p. 325. It is that of a cylinder with a cross section equal to the geometric average of the radius: $S = \pi R_1 R_2$. The difference between the cylindrical tonehole and the undercutting one is:

$$\delta_m = \frac{\ell'}{\pi b^2}\left[1 - \frac{b}{R_2}\right]. \tag{26}$$

The result of this formula is $26m^{-1}$. This result, based on approximate geometric and acoustic models, is consistent with the experimental data. This is encouraging for the use of an accurate measurement method for the computation of the input impedance of an instrument.

Furthermore, Fig. 16 shows that the effect of undercutting on the real part of the shunt impedance is small, but significant: it causes a decrease in resistance by approximately 10 % as the undercut is increased from 0 to that of tubes UC2. It is difficult to interpret the differences between the three geometries and their variation with frequency, and the influence of nonlinear effects cannot be ignored. However, a linear reasoning can be applied here: undercutting a tonehole broadens the effective radius, and visco-thermal effects diminish.

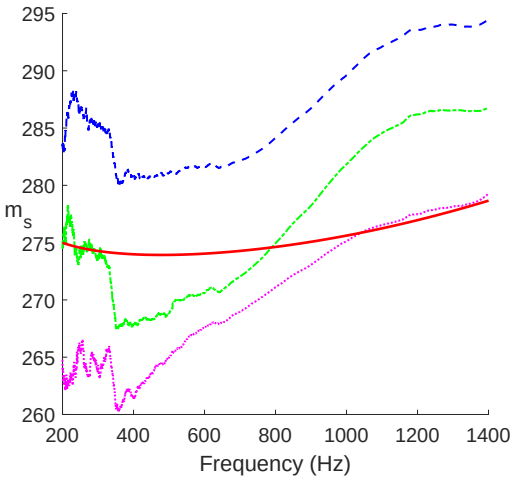

FIG. 15. (Color online) Measured value of the acoustic mass per unit density m_s of the hole. Red, solid line: theory of a cylindrical tonehole in m^{-1}. From top to bottom, 3 geometries of the tonehole: Blue, dashed line: no undercutting; Green, dash-dot line: undercut tubes UC1, Magenta, dotted line: undercut tubes UC2.

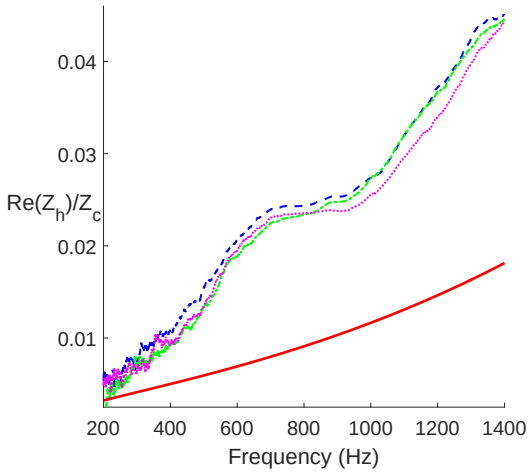

FIG. 16. (Color online) Measured value of the real part of the reduced shunt impedance $Re(Z_h/Z_c)$ (dimensionless). Red line: theory of a cylindrical tonehole. See line definitions in the caption of Fig. 15.

VII. CONCLUSION

The method presented in this paper allows an evaluation of the effect of the complex shunt impedance of an open tonehole. We recall that the aim is to insert the experimental value in the computation of the input impedance of an instrument. The effect of a hole modification on the input impedance of an instrument is significant: a difference of 1 mm for the equivalent height may imply a shift of the first impedance peak. The cumulative shift for several toneholes can be rather high (see e.g. an article on the clarinet tuning[16]).

It is important to use a short tube for this method, due to anti-resonances associated to the total tube length. We remark that a similar problem concerning the "forbidden" frequency ranges is encountered in other methods. Moreover the distance of the hole to the tube end needs to be short.

Concerning the real part of the shunt impedance, the results appear to be robust, and suggest further studies on the theoretical aspects, even for cylindrical toneholes in the linear regime.

Concerning the equivalent height of the tonehole (related to the imaginary part of the shunt impedance), the primary quantity studied here, the results seem to be very sensitive to small geometric differences. The relative variation of the equivalent height with frequency is small, and the absolute variation remains small. For a cylindrical tonehole, at approximately 500 Hz, the discrepancy between experiment and theory is very small for the equivalent height (0.5 mm), and is of the same order of magnitude as the result obtained in[10]. The paper is limited to the frequency range [200 Hz, 1400 Hz] for the measurements. It is concluded that the variation with frequency is mainly due to the measurement method. Assuming that the true value of the tonehole equivalent height is independent of frequency, the choice of an average of the values between 400 and 600 Hz as appropriate can be extended to any hole geometry. This result of the different cases examined in the present work can be used for including the acoustic characteristics of undercut toneholes in a computation of input impedances of an instrument.

The method is not convenient for measuring the series impedance. Actually this quantity is very small, but for this quantity the methods proposed in previous publications seem to be better. Concerning undercut toneholes, which are generally not symmetrical, in certain cases it could be useful to search for a circuit with 3 unknowns (see[4]). The aim of the present paper is not to improve a model, but it is useful in that it highlights some of the complications inherent in existing open tonehole models. The main improvement to existing models could be done on the radiation impedance of a tonehole, including the influence of the pads.

ACKNOWLEDGEMENTS

The authors gratefully thank the French Association Nationale de la Recherche et la Technologie for the PhD grant of Hector Garcia (CONVENTION CIFRE N° 2017 1600), as well as the french Agence Nationale de la Recherche, through the joint laboratory "Liamfi" between the Laboratoire de Mécanique et d'Acoustique and Buffet Crampon (ANR LCV2-16-007-01). Furthermore the authors thank the Consejo Nacional de Ciencia y Tecnología Políticas de Privacidad Acceso (Conacyt) for the International Scholarship 707987. The authors thank Thierry Mialet (Buffet Crampon company) for designing

and manufacturing the wood pieces used in this article. Erik Petersen provided a careful reading of the English of the paper and gave useful comments, and Fabrice Silva helped for the experiment: they deserve the thanks of the authors.

[1]E. Petersen, T. Colinot, J. Kergomard, P. Guillemain, " On the tonehole lattice cutoff frequency of conical resonators: applications to the saxophone", Acta Acust. 4 13 (2020). DOI: https://doi.org/10.1051/aacus/2020012

[2]D.H. Keefe, "Theory on the single woodwind tone hole", J. Acoust. Soc. Am. 72(3), 676–687 (1982).

[3]A. Chaigne, J. Kergomard, "Acoustics of musical instrumens", Springer Verlag, New York (2016).

[4]V. Dubos, J. Kergomard, A. Khettabi, J.P. Dalmont, D.H. Keefe, C. Nederveen, C." Theory of sound propagation in a duct with a branched tube using modal decomposition", Acust. Acta Acust. 85, 153–169 (1998).

[5]N. Marcuwitz, "Waveguide Handbook",Mc Graw Hill, New York (1948).

[6]J.W. Coltman, "Acoustical analysis of the Boehm flute", J. Acoust.Soc. Am.65(2), 499-506 (1979).

[7]C.J. Nederveen, J.K.M. Janssen, R.R. Van Hassel, "Corrections for woodwind tone-hole calculations". Acustica, 85 957-966 (1998).

[8]P. A. Dickens,"Flute acoustics, Measurement, modelling and design", Ph. D. Thesis, University of South Wales (2007).

[9]A. Lefebvre, G. Scavone, "Characterization of woodwind instrument toneholes with the finite element method" J. Acoust. Soc. Am. 131, 3153–3163 (2012).

[10]J.P. Dalmont, C.J. Nederveen, V. Dubos, S. Ollivier, V. Méserette, E. te Sligte," Experimental determination of the equivalent circuit of an open side hole: linear and non linear behaviour". Acta Acust. United Acust. 88, 567–575 (2002).

[11]A.H. Benade and J.S. Murday, "Measured end-correction for woodwind tonehole", J. Acoust. Sco. Am, 41, 1609-1609 (1967).

[12]A.H. Benade, "Fundamentals of Musical Acoustics", Oxford University Press (1976).

[13]D.H. Keefe, "Acoustic streaming, dimensional analysis, of nonlinearities, and tone hole mutual interactions in woodwinds", J. Acoust.Soc.Am. 73, 1804-1820 (1983).

[14]D.H. Keefe, "Experiments on the single woodwind tone hole", The Journal of the Acoustical Society of America 72, 688 (1982); https://doi.org/10.1121/1.388249

[15]J.P. Dalmont, "Acoustic measurement, part II: a new calibration method", J. Sound Vib., 243, 441-459 (2001).

[16]V. Debut, J. Kergomard, F. Laloë, "Analysis and optimisation of the tuning of the twelfthes for a clarinet resonator". Applied Acoustics 66, 365-409 (2005).

[17]F. Silva, P. Guillemain, J. Kergomard, B. Mallaroni, A.N. Norris, "Approximation formulae of the acoustic radiation impedance of a cylindrical pipe", J. Sound Vib., 322, 255-263 (2009).

[18]A. Macaluso, J.P. Dalmont,"Trumpet with near-perfect harmonicity: Design and acoustic results", J. Acoust. Soc. Am. 129, 404 (2011); https://doi.org/10.1121/1.3518769

[19]R. MacDonald, " A Study of the Undercutting of Woodwind Toneholes Using Particle Image Velocimetry", PhD Thesis, University of Edinburgh (2009). http://www.acoustics.ed.ac.uk/wp-content/uploads/Theses/Macdonald_Ro

[20]M. Temiz, I. Lopez Arteaga, A. Hirschberg,"Nonlinear behavior in tone holes in musical instruments: an experimetal study", Conference CFA/Vishno, Le Mans 1-6 (2016).

End of the submitted article

Appendix: Finite Element Model for the tube reversed method

A finite element model of the short tube was implemented in COMSOL Multiphysics. The geometry of the tube was made in accordance to the physical dimensions of the tube in a 3D model. The modeled tube is the same used and described as short tube in the submitted article section, it has a total length of $L = 118\ mm$, external diameter of 31.7 mm, internal diameter of 14.6 mm, the tonehole is placed at 44 mm of one of the ends and has an internal diameter of 8 mm. The air that surrounds the tube is modeled in a semi-sphere of 150 mm of radius, the center coincides with the inlet of the tube, which is also the input. An external layer of air is modeled as a Perfectly Matched Layer (PML) that correspond to an anechoic termination, in accordance with the anechoic chamber in which measurements where carried on (Fig. 2.1). Model and measurement were both at $20°C$.

The source of excitation is simulated as a *Port*[1] boundary condition that models a plane wave mode at 0.0635 Pa (70 dB). To compute the input impedance the average pressure and the velocity integral are computed at the inlet of the tube (Fig. 2.2). Two simulations are performed, one with the tonehole at 44 mm of the input and a the second one with the tonehole at 74 mm, i.e. the tube reversed condition.

[1] https://www.comsol.com/blogs/using-the-port-boundary-condition-in-acoustic-waveguide-models/

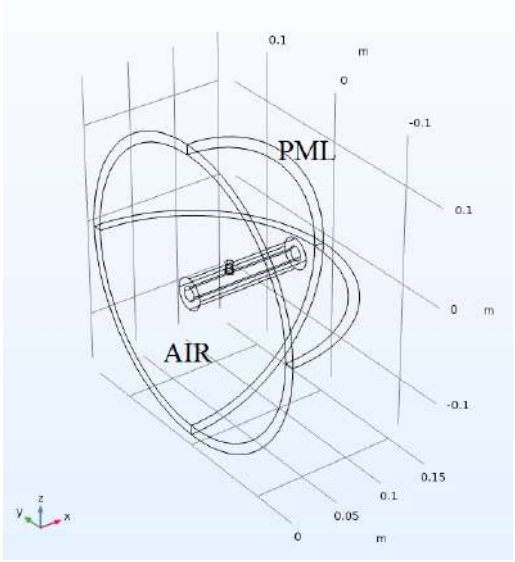

Figure 2.1: COMSOL model for the tube reversed method. Direct position of the tube $L_1 < L_2$.

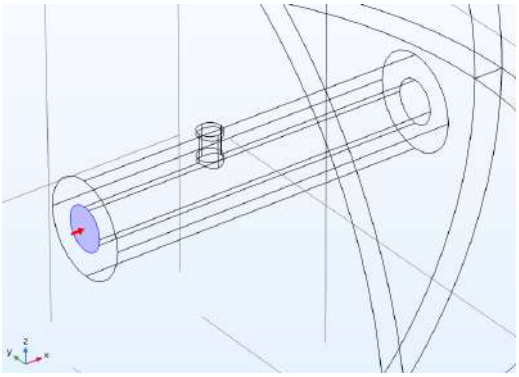

Figure 2.2: Source surface at the inlet. *Port* boundary condition with 0.0635 Pa amplitude.

The generated mesh includes a *Boundary Layer* that models the viscous-thermal layers to compute the losses and dispersion at the internal walls. Also, the PML anechoic condition is meshed in a regular manner as a *Mapped* distribution.

Data of the input impedance obtained through each simulation are processed as if the COMSOL results were the input impedance measurements.

Input impedance results

Input impedance obtained from the FEM model is compared with direct theoretical computations, this comparison is in Fig. 2.3

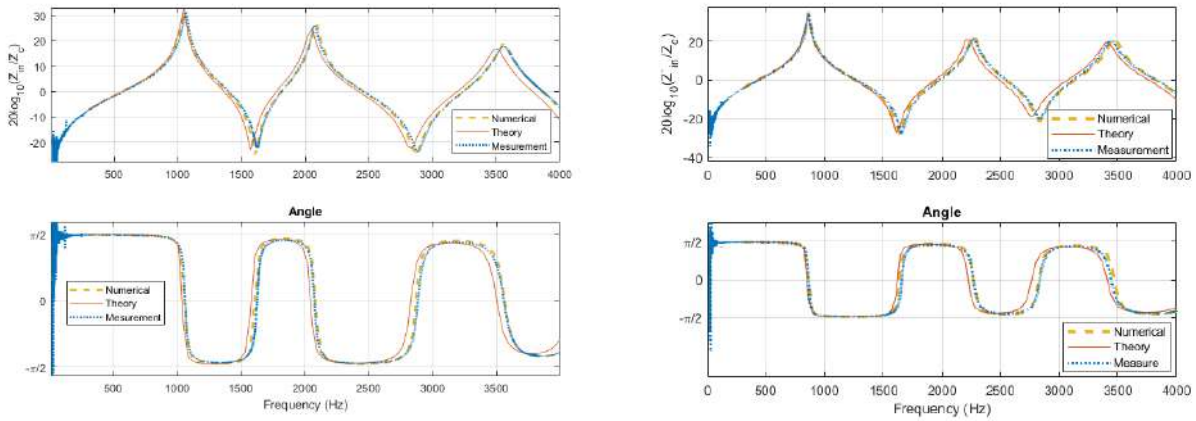

(a) (b)

Figure 2.3: Input impedance results for the(a)tube direct and (b) tube reversed.

In Fig. 2.3 it is observed that both the tube direct and the tube reversed simulations are in accordance with the theoretical model in low frequency and as the frequency rises, the difference rises as well. The difference between theory and measurement in the direct tube is 20 *cents* for the first peak, 13.9 *cents* for the second and 22.4 for the third. As the difference between measurement and COMSOL simulation is 20, 17 and 4 *cents* respectively. For the reversed tube, there is no difference between theory, measurement ans COMSOL simulation for the first peak, for the second peak the difference between theory and measurement is 31.2 *cents*, and of 11.4 *cents* between measurement and COMSOL, as for the third peak the difference between theory and measurement is 37 *cents* and between measurement and COMSOL is of 16.5 *cents*. In every case the difference in amplitude is less than 0.8 dB.

Derived quantities

A computation of the series and shunt impedances is performed with the FEM model data. In the same way it was performed from the experimental measurements. First result for the series impedance of the tonehole Z_a is shown in Fig. 2.4. It is observed that results from measurement and FEM data are in accordance.

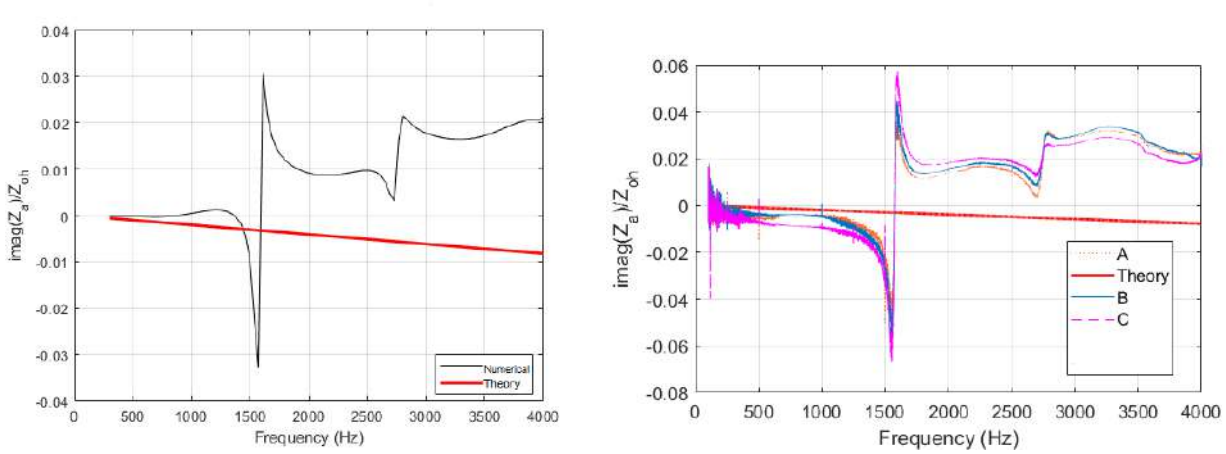

(a) (b)

Figure 2.4: Imaginary part of the series impedance Z_a computed with the inverse calculation. Through (a) FEM model data and (b) through measurement (A, B and C correspond to different measured tubes).

Fig. 2.5 shows the comparison for the real part of the shunt impedance Z_h. And, Fig. 2.6 shows the comparison for the imaginary part of the shunt impedance Z_h.

From Figs. 2.4 to 2.6 it is observed that either from the measurement results or from the FEM data there are frequencies that are not well resolved for the studied method. Therefore, an observation of the pressure at these frequencies using the FEM model is done. First the 1683 Hz frequency is observed in Fig. 2.7.

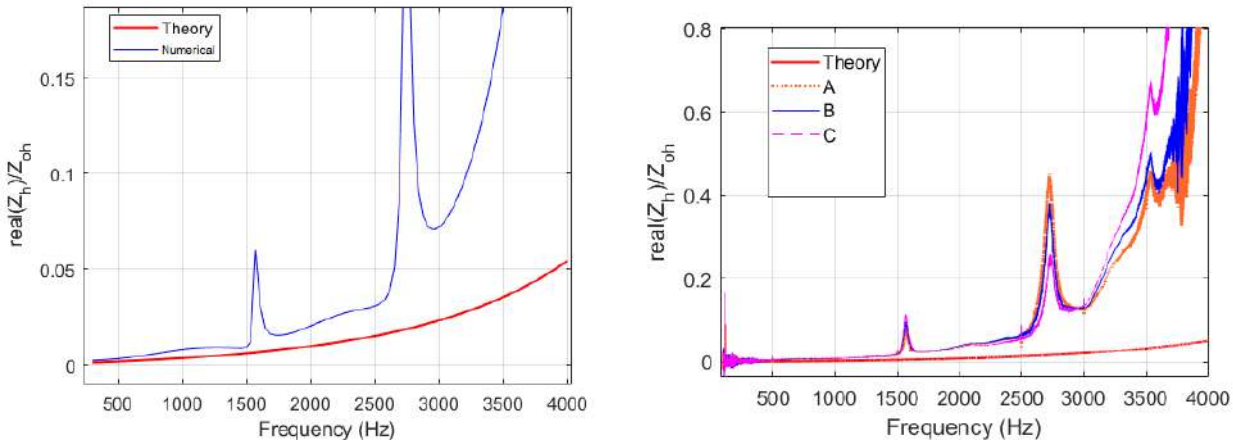

(a) (b)

Figure 2.5: Real part of the shunt impedance Z_h. Through (a) FEM model data and (b) through measurement (A, B and C correspond to different measured tubes).

In Fig. 2.7 it is observed the pressure plot of the tube at $1608Hz$ in both positions. While for the tube direct position there is a pressure minimum close to the tonehole, for the tube reversed position, there is a large pressure minimum zone that spans over the toneholes input.

Fig. 2.8 shows the pressure plot of the tube at 2878 Hz. Inversely from what it is observed in Fig. 2.7, there is pressure minimum at left form the tonehole in the tube reversed position, while there is a large pressure minimum zone underneath the tonehole in the tube direct position.

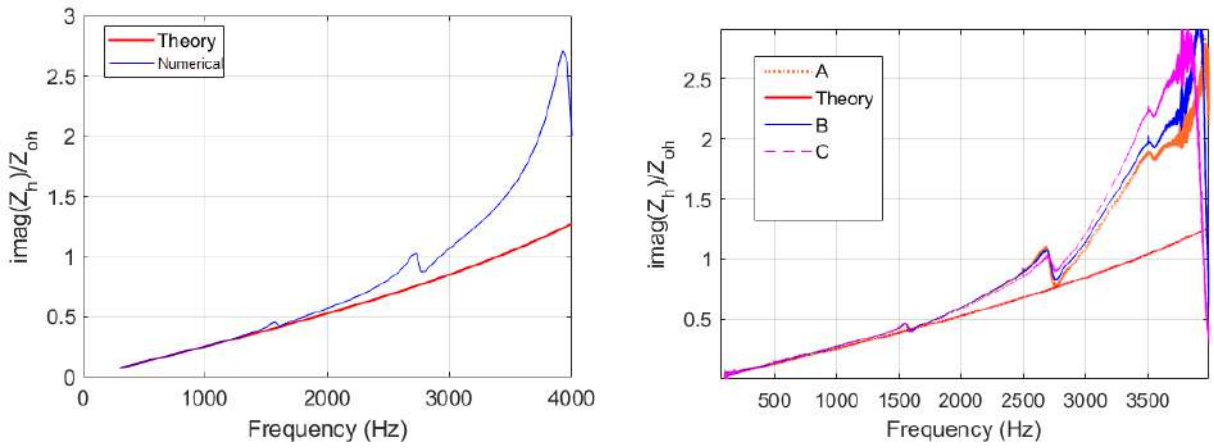

(a) (b)

Figure 2.6: Imaginary part of the shunt impedance Z_h. Through (a) FEM model data and (b) through measurement (A, B and C correspond to different measured tubes).

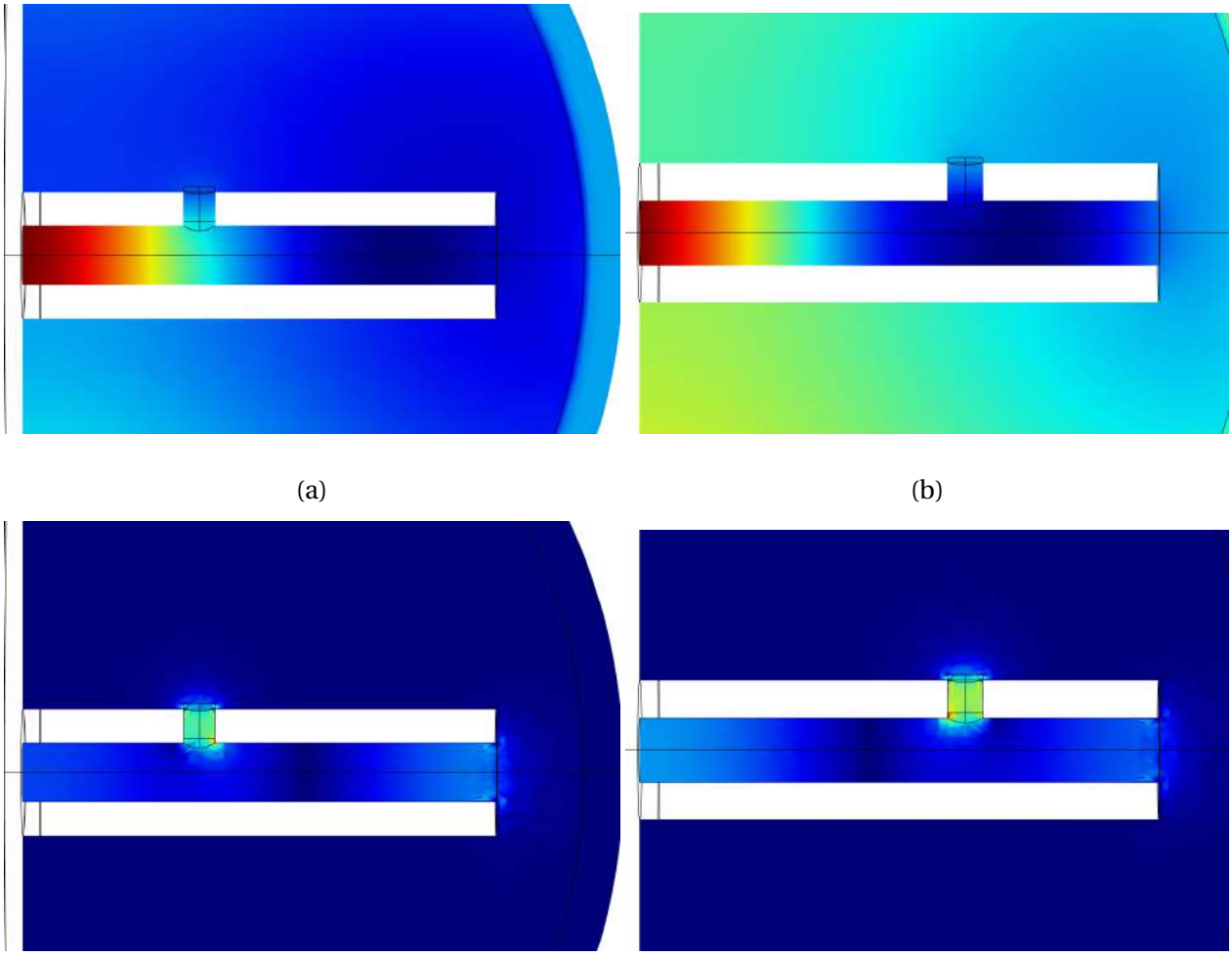

(a) (b)

(c) (d)

Figure 2.7: (a)(b)Pressure and (c)(d) velocity, input impedance minimum at 1608 Hz. (a)(c) tube direct position and (b)(d) tube reversed position.

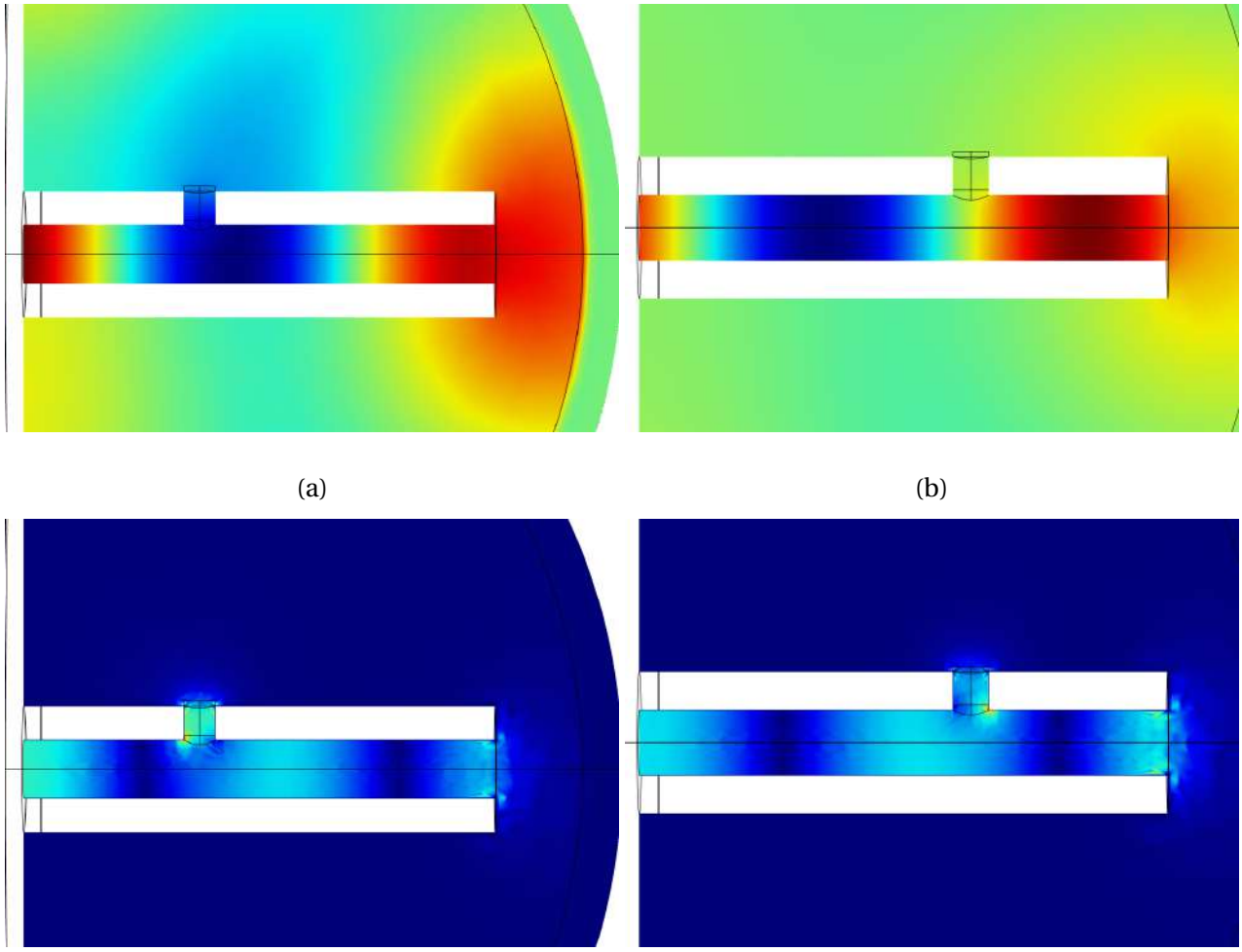

(a) (b)

(c) (d)

Figure 2.8: (a)(b)Pressure and (c)(d)velocity, input impedance minimum at 2878 Hz. (a)(c) Tube direct position; (b)(d) tube reversed position.

Conclusion

It can be concluded that

- Numerical FEM simulation provides accurate results that are comparable to those obtained through measurement.
- The method depends strongly in the tube total length and in the position of the tonehole.
- Results are not accurate after the tube's first input impedance minimum. Therefore, short tubes with less minima should be preferred.
- It seems not possible to obtain the series impedance Z_a with this method.
- The method cannot be precise at frequencies where impedances at both sides of the tonehole are very close or where there is a pressure minima close to the tonehole inlet.

Bibliography

[1] E. Petersen, *Comment le facteur d'instruments du musique a anche equilibre-t-il la production et le rayonnement?* PhD thesis, Aix-Marseille Univ, 2020.

[2] D. H. Keefe, "Theory of the single woodwind tone hole," *The Journal of the Acoustical Society of America*, vol. 72, no. 3, pp. 676–687, 1982.

[3] C. Nederveen, J. Jansen, and R. Van Hassel, "Corrections for woodwind tone-hole calculations," *Acta Acustica united with Acustica*, vol. 84, no. 5, pp. 957–966, 1998.

[4] V. Dubos, J. Kergomard, A. Khettabi, J.-P. Dalmont, D. Keefe, and C. Nederveen, "Theory of sound propagation in a duct with a branched tube using modal decomposition," *Acta Acustica united with Acustica*, vol. 85, no. 2, pp. 153–169, 1999.

[5] P. A. Dickens *et al.*, *Flute acoustics: measurements, modelling and design*. PhD thesis, PhD Thesis, University of New South Wales, 2007.

[6] A. Lefebvre and G. P. Scavone, "Characterization of woodwind instrument toneholes with the finite element method," *The Journal of the Acoustical Society of America*, vol. 131, no. 4, pp. 3153–3163, 2012.

[7] J.-P. Dalmont, C. J. Nederveen, V. Dubos, S. Ollivier, V. Meserette, E. te Sligte, *et al.*, "Experimental determination of the equivalent circuit of an open side hole: linear and non linear behaviour," *Acta Acustica united with acustica*, vol. 88, no. 4, pp. 567–575, 2002.

[8] N. Marcuvitz, “Handbook, waveguide vol. 10,” 1951.

[9] J. W. Coltman, “Acoustical analysis of the boehm flute,” *The Journal of the Acoustical Society of America*, vol. 65, no. 2, pp. 499–506, 1979.

[10] D. H. Keefe, “Acoustic streaming, dimensional analysis of nonlinearities, and tone hole mutual interactions in woodwinds,” *The Journal of the Acoustical Society of America*, vol. 73, no. 5, pp. 1804–1820, 1983.

[11] J.-P. Dalmont, “Acoustic impedance measurement, part i: A review,” *Journal of Sound and Vibration*, vol. 243, no. 3, pp. 427–439, 2001.

[12] D. H. Keefe, “Experiments on the single woodwind tone hole,” *The Journal of the Acoustical Society of America*, vol. 72, no. 3, pp. 688–699, 1982.

[13] A. H. Benade and J. Murday, “Measured end corrections for woodwind tone-holes,” *The Journal of the Acoustical Society of America*, vol. 41, no. 6, pp. 1609–1609, 1967.

[14] A. H. Benade, *Fundamentals of musical acoustics*. Courier Corporation, 1990.

[15] A. Chaigne and J. Kergomard, *Acoustics of musical instruments*. Springer, 2016.

[16] V. Debut, J. Kergomard, and F. Laloë, “Analysis and optimisation of the tuning of the twelfths for a clarinet resonator,” *Applied acoustics*, vol. 66, no. 4, pp. 365–409, 2005.

[17] F. Silva, P. Guillemain, J. Kergomard, B. Mallaroni, and A. N. Norris, “Approximation formulae for the acoustic radiation impedance of a cylindrical pipe,” *Journal of Sound and Vibration*, vol. 322, no. 1-2, pp. 255–263, 2009.

[18] C. A. Macaluso and J.-P. Dalmont, “Trumpet with near-perfect harmonicity: Design and acoustic results,” *The Journal of the Acoustical Society of America*, vol. 129, no. 1, pp. 404–414, 2011.

[19] R. MacDonald, “Study of the undercutting of woodwind toneholes using particle image velocimetry,” 2009.

[20] M. Temiz, I. L. Arteaga, and A. Hirschberg, “Non-linear behaviour of tone holes in musical instruments: an experimental study,” in *French Acoustic Congress (CFA 2016)*, pp. 377–382, Université du Maine, 2016.

Chapter 3

Method of the input and transfer impedances

3.1 Introduction

In this chapter another method to characterize the tonehole impedance is presented. As the method of the reversal tube presented in chapter 2, this is an indirect determination.

This method was developed by Dalmont et al. (2002) [1] for the experimental characterization of an open tonehole on a section of another tube. This system can be considered as a two-port. The method was used for a tonehole with a cylindrical geometry. Nevertheless, it can be applied to any geometry provided that the hole is symmetrical. This method relies on the measurement of an input impedance and a transfer impedance. Fig. 3.1 shows a schematic representation of the air confined in a perpendicular tonehole on a straight cylindrical tube. The main tube has radius a, and lengths, L_1 at left, and L_2 at right of the tonehole, $L_1 = L_2$. The tonehole has radius b, and height t. A source is placed at the left side of the main tube (L_1 termination), where the input pressure is $P_{in}(\omega)$, and the volume velocity is $U_{in}(\omega)$. At the right side of the main tube there are an output pressure $P_{end}(\omega)$ and a volume velocity $U_{end}(\omega)$.

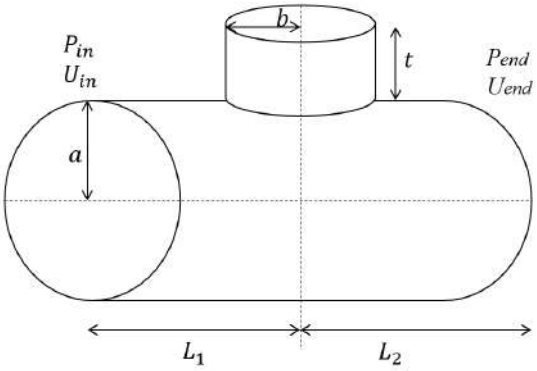

Figure 3.1: Schematic representation of a perpendicular tonehole in the middle of a cylindrical tube [2].

Sections 3.2 to 3.7 are a theoretical analysis of the method. In the sections 3.2 and 3.3 the method is presented, in sections 3.4 and 3.5 a theoretical simulation of the experiment is done to study the influence of the incertitude on the tube length an in the input impedance. Section 3.6 is a theoretical comparison between the methods presented in Chapters 2 and 3. And, section 3.7 is the conclusion os this theoretical analysis.

Sections 3.8 and 3.9 are results of a study of the method presented in this chapter through the Finite Element Method (FEM) and through the result of measurements.

3.2 Direct problem: model

In this section, the input impedance Z_{in} and the transfer impedance Z_T of a cylindrical tube with one tonehole at the middle are computed according to the steps summarized in schematic below (see Appendix for definitions).

Summary of the direct problem.

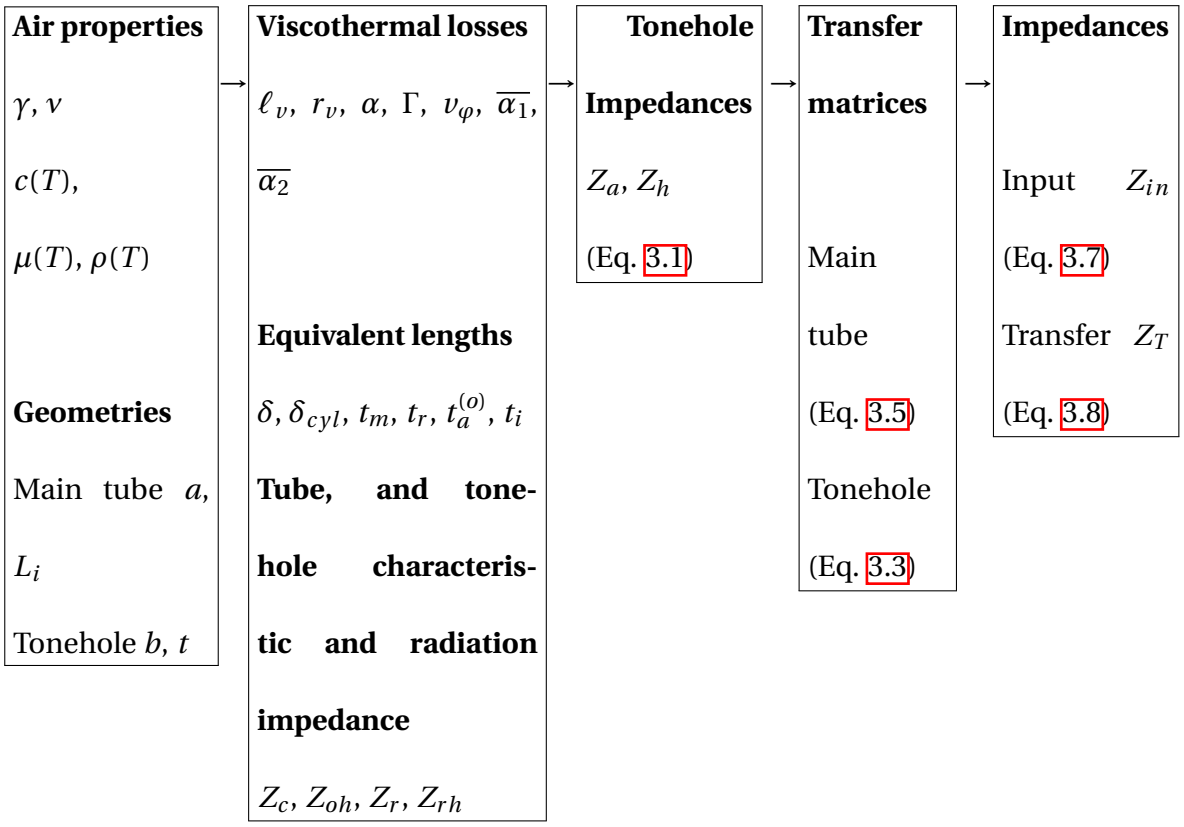

As previously said, the tonehole can be considered as a two-port system, which in return, can be also represented by a T-shaped circuit, such as the one presented in Fig. 1 in chapter 2. The circuit has to be connected to another circuit describing the tube. As it can be seen in Fig. 2 in chapter 2, there are two impedances to be determined Z_a, and Z_h, therefore two equations are needed.

In the case where the tonehole is symmetrical, the series impedance in the T-shaped circuit is the same at the two sides ($Z_a/2$), as depicted in Fig. 2 chapter 2. A direct calculation that assumes physical values, and specific conditions such as tube length and tonehole geometry, is performed in order to obtain the input and transfer impedances. First, the series impedance Z_a is computed by using Eq. 3.1 [3] with the wavenumber k, the main tube's radius a, and the equivalent length of the main tube t_a. Then, the shunt impedance Z_h is determined through: the characteristic impedance of the tonehole Z_{oh}, the physical length t, and the equivalent lengths of the matching

volume t_m, the inner part t_i and of the radiation t_r of the tonehole (Eq. 3.2), losses in Z_a are ignored (t_a is real and $k = \omega/c$).

$$Z_a = jkZ_c t_a \qquad and \qquad Z_h = Z_s - Z_a/4 \tag{3.1}$$

where

$$Z_s = jZ_{oh}(kt_i + \tan[k_b t + k(t_m + t_r)]). \tag{3.2}$$

In Eq. 3.2 k_b is the wavenumber that considers viscothermal losses in the tonehole and it is defined as $k_b = \frac{\Gamma_b}{j}$, where the propagation constant Γ_b is, among others, function of the tonehole radius b (see Appendix). In Eqs. 3.1 and 3.2, k is the wavenumber for a plane wave in free space ($k = \omega/c$), $Z_c = \rho c/\pi a^2$ is the characteristic impedance of the main tube, $Z_{oh} = \rho c/\pi b^2$ is the characteristic impedance of the tonehole. Values of the inner t_i, and series t_a equivalent lengths depend on the tonehole geometry, and there is a slight dependence on the frequency only. The transfer matrix of the tonehole (Eq. 3.3 which it is the same that Eq. 2.3 in Chapter 2), which is related to the circuit shown in Fig. 2 in chapter 2, is computed through Eqs. 3.1, and 3.2. Because of the tonehole symmetry, $D_h = A_h$.

$$M_h = \begin{pmatrix} 1 + Z_a/2Z_h & Z_a/2(2 + Z_a/2Z_h) \\ 1/Z_h & 1 + Z_a/2Z_h \end{pmatrix} = \begin{pmatrix} A_h & B_h \\ C_h & A_h \end{pmatrix} \tag{3.3}$$

As described before, there is a source located at the left side of the main tube, and the opposite end is closed (Fig. 3.1), then the volume velocity is $U_{end} = 0$ at the end of the tube, and the impedance at the output tends to infinity $Z_{end} \to \infty$.

In terms of transfer matrices, the system shown in Fig. 3.1 can be represented by two transfer matrices of the cylindrical sections of the tubes M_1 and M_2 (Eq. 3.5), the transfer matrix of the tonehole M_h (Eq. 3.3) and by the values of the pressure, and volume velocity at the input, and at

the end of the tube (Eq. 3.4). The main tube is cylindrical, thus the transfer matrices are symmetrical i.e. $A_1 = D_1$ and $A_2 = D_2$

$$\begin{pmatrix} P_{in} \\ U_{in} \end{pmatrix} = (M_1)(M_h)(M_2) \begin{pmatrix} P_{end} \\ 0 \end{pmatrix} = \begin{pmatrix} A_1 & B_1 \\ C_1 & A_1 \end{pmatrix} \begin{pmatrix} A_h & B_h \\ C_h & A_h \end{pmatrix} \begin{pmatrix} A_2 & B_2 \\ C_2 & A_2 \end{pmatrix} \begin{pmatrix} P_{end} \\ 0 \end{pmatrix}, \tag{3.4}$$

where the matrices M_1 and M_2 are defined by [4]:

$$M_i = \begin{pmatrix} \cos k_a L_i & j Z_c \sin k_a L_i \\ j Z_c^{-1} \sin k_a L_i & \cos k_a L_i \end{pmatrix}, i = 1, 2. \tag{3.5}$$

The wavenumber k_a in Eq. 3.5 includes viscothermal losses, it is defined as $k_a = \frac{\Gamma_a}{j}$, where the propagation constant Γ_a is, among others, function of the tube radius a (see Appendix). In the case where the tonehole is exactly in the middle of the main tube, $L_1 = L_2$, and therefore $M_1 = M_2$.

In a single matrix notation Eq. (3.4) becomes:

$$\begin{pmatrix} P_{in} \\ U_{in} \end{pmatrix} = M \begin{pmatrix} P_{end} \\ 0 \end{pmatrix} = \begin{pmatrix} A & B \\ C & D \end{pmatrix} \begin{pmatrix} P_{end} \\ 0 \end{pmatrix}. \tag{3.6}$$

In Eq. 3.6 the transfer matrix of the system M includes properties of the cylindrical sections as well as the tonehole. Then, the input and transfer impedance can be computed through the matrix elements as:

$$Z_{in} = \frac{P_{in}}{U_{in}} = \frac{A}{C}. \tag{3.7}$$

And, in a similar way, the transfer impedance is:

$$Z_T = \frac{P_{end}}{U_{in}} = \frac{1}{C}. \tag{3.8}$$

3.3 Inverse Problem

In this section, it is shown how the series and shunt impedances Z_a and Z_h respectively can be deduced from computed or measured input and transfer impedances Z_{in} and Z_T respectively. This is done through several steps detailed in this section and summarized in the schematic below (see Appendix for precise definitions).

Summary of the inverse problem.

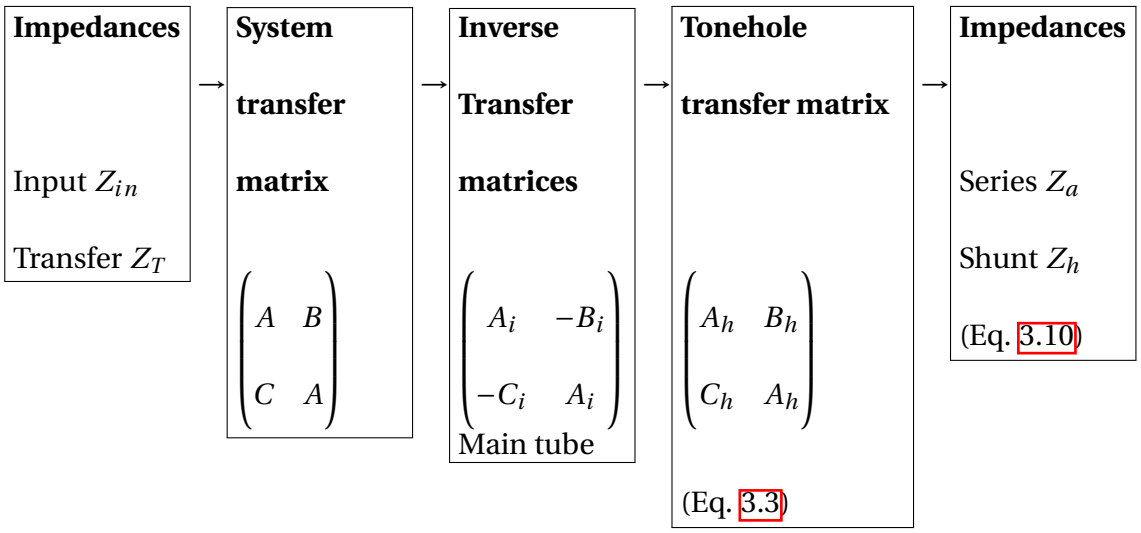

For the purpose of experimentally obtaining the series and shunt impedances of the system (Fig. 3.1), it is necessary to measure the input, and transfer impedances. This is done, through the measurement of the pressure P_{in}, and the estimation of the volume velocity U_{in} at the entrance of the tube (source position), and the pressure P_{end} at the closed end (Fig. 3.1). Then, using Eq. 3.8 the value of C is determined as $C = 1/Z_T$ and then the value of A can also be determined through Eq. 3.7 as $A = Z_{in} \cdot C$. Also, since the system is symmetrical, then $A = D$, and finally B can be determined by the reciprocity property as $B = (AD - 1)/C$. The system is measured by the use of an Impedance Sensor (*Capteur Z*[1] by its name in French), which measures pressures in three positions, and computes the impedances Z_{in}, and Z_T (see Chapter 1 for an explanation of the sensor's principle).

[1] CTTM Centre de Transfert de Technologie du Mans.

The transfer matrix of the tonehole M_h is obtained from the system's transfer matrix, by multiplying left and right the transfer matrix by the inverse transfer matrices of the cylindrical parts of the main tube (Eq. 3.5) of lengths L_1, and L_2 (Eq. 3.9), in this case, the inversion of matrices is equivalent to interchange the values of the lengths by $-L_1$ and $-L_2$, respectively.

$$M_h = \begin{pmatrix} A_h & B_h \\ C_h & A_h \end{pmatrix} = \left(M_1^{-1}\right) \begin{pmatrix} A & B \\ C & A \end{pmatrix} \left(M_2^{-1}\right) \tag{3.9}$$

Through the expression for the transfer matrix of the tonehole, the series impedance Z_a, and the shunt impedance Z_h can be deduced by matching terms of the matrix M_h in Eq. 3.3, and after some algebra we have:

$$Z_h = \frac{1}{C_h} \qquad and \qquad \frac{Z_a}{2} = \frac{A_h - 1}{C_h}. \tag{3.10}$$

In order to check the consistency of the formula of the direct and inverse problems, Fig. 3.2 shows the results of comparing the real and imaginary part of the series and shunt impedances for the direct (Eqs. 3.1 and 3.2) and inverse procedures (Eq. 3.10) in the case when Z_{in} and Z_T are calculated through Eqs. 3.7 and 3.8. There is an agreement close to machine precision in the calculations direct, and inverse of the shunt impedance, and of the imaginary part of the series impedance. There is a numerical error in the real part of the series impedance in the range $0-4kHz$, in the order magnitude of 10^{-13} which also increases with the frequency . Therefore these numerical errors are negligible.

Since results confirm the expected accordance between the direct and the inverse problems, a simulation of experiment is performed in the next section, adding uncertainties to input variables of the inverse problem, in order to observe consequences of possible errors made during the real

experiment, and therefore evaluate in advance the sensitivity of possible sources of error.

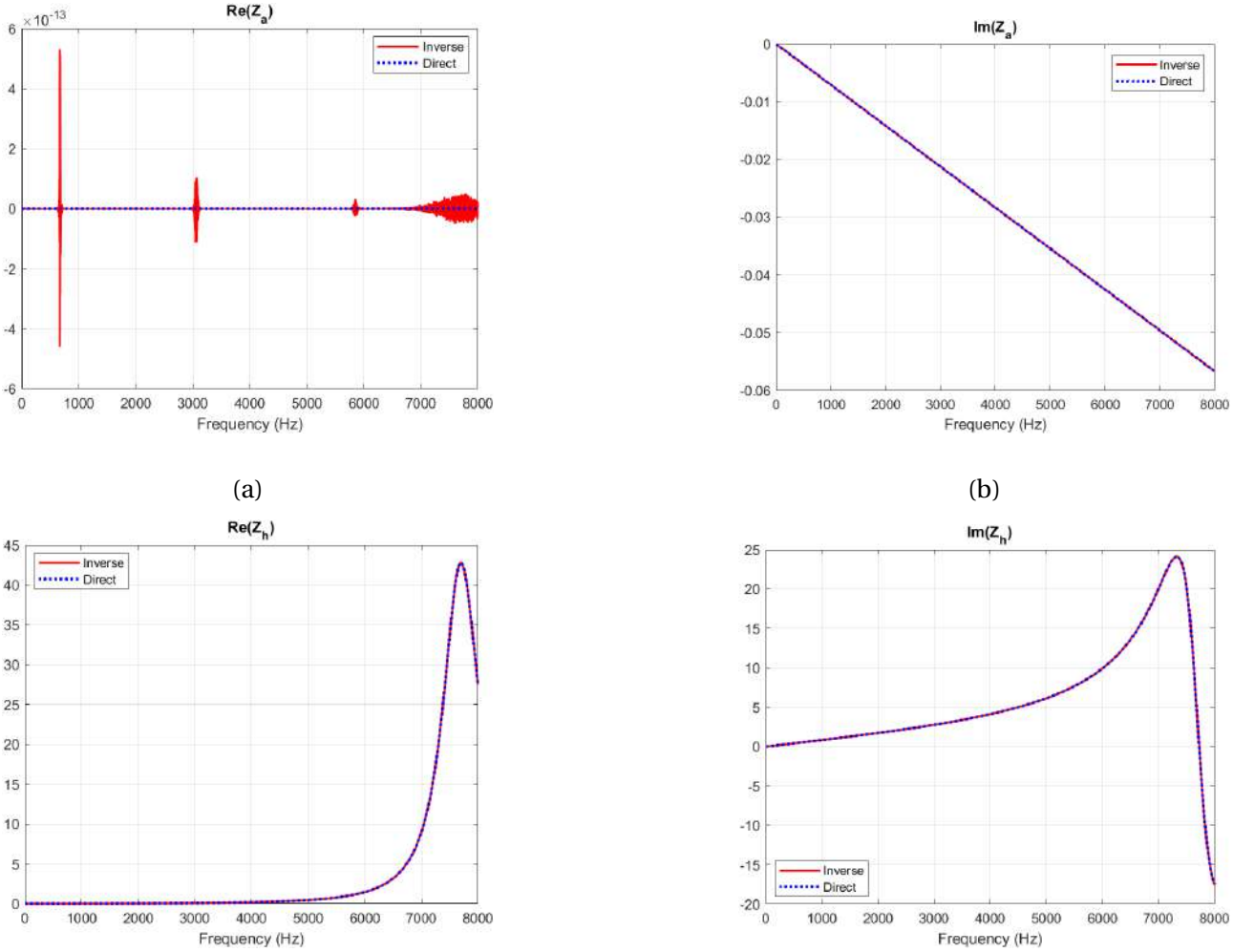

Figure 3.2: Comparison between the direct (analytical approach), and inverse computations of the real and imaginary parts of the series Z_a and shunt Z_h impedance in the case when Z_{in} and Z_T are calculated by Eqs. 3.7 and 3.8. It is to be noted that the real part of the series impedance Z_a is zero in the direct computation (Eq. 3.1), therefore the inverse computation shows only numerical errors.

3.4 Simulation of the experiment: effect of uncertainties on the main tube length

In order to simulate the experiment, the inverse problem is studied with errors introduced on some parameters (main tube length in this section). As a starting point, a direct calculation of the series Z_a, and shunt Z_h impedance is done through the model (Eqs. 3.1 and 3.2). Then, the system's transfer matrix (Eq. 3.6) is computed through Eqs. 3.5 and 3.3, by multiplying the three obtained matrices as described in Eq. 3.4. Then Eqs. 3.7 and 3.8 allow to deduce the input Z_{in} and transfer Z_T impedances. Z_{in} and Z_T are the input quantities of the inverse method. Contrary to the previous section, the inverse method is applied by considering uncertainties in the length of the tube in order to assess the influence of inevitable errors in a real experimental setup. The series and shunt impedances are then computed, and the deviations obtained are then analyzed.

Table 3.1: Input parameters for the direct method

Temperature	$T = 20°\ C$
Main tube radius	$a = 7.3\ mm$
Tonehole radius	$b = 4\ mm$
Tonehole height	$t = 8.5\ mm$
Main tube length	$L = 118\ mm$

The influence of the uncertainty in the lengths L_1 and L_2 of the main tube is first considered. The tonehole remains in the middle, and all the other parameters remain unchanged (Table 3.1). The choice of the uncertainty (Table 3.2) is made in accordance with making tolerance. The smallest scale in the machines to make the tubes is one-tenth of a millimeter. Then ϵ in Table 3.2 are

chosen accordingly.

Table 3.2: Length of the main tube and uncertainties

Main tube length (mm)	ϵ (mm)
118+2ϵ	0.2
118+2ϵ	−0.2

3.4.1 Analytical and numerical errors induced by the length uncertainties

The uncertainty (ϵ) from Table 3.2 are added to the length L_1 and L_2 of the tube cylindrical sections (Eq. 3.5), obtaining Eq. 3.11. For simplicity losses in the main tube are ignored in the forthcoming analysis; $k\epsilon$ is a small quantity, because the wavelength has the order of magnitude of the total length.

$$\tilde{M}_i = \begin{pmatrix} \cos[k(L_i+\epsilon)] & jZ_c \sin[k(L_i+\epsilon)] \\ jZ_c^{-1} \sin[k(L_i+\epsilon)] & \cos[k(L_i+\epsilon)] \end{pmatrix}. \tag{3.11}$$

By using Taylor's theorem, the matrix $\tilde{M}_i$ can be approximated at order one to:

$$\tilde{M}_i \approx \widehat{M}_i = \begin{pmatrix} \cos kL_i & jZ_c \sin kL_i \\ jZ_c^{-1} \sin kL_i & \cos kL_i \end{pmatrix} - k\epsilon_i \begin{pmatrix} \sin kL_i & -jZ_c \cos kL_i \\ -jZ_c^{-1} \cos kL_i & \sin kL_i \end{pmatrix}. \tag{3.12}$$

Let Q_i be the inverse matrix of M_i, ($Q_i = M_i^{-1}$), then the matrices associated with an uncertainty ϵ in the lengths L_1 and L_2 at order 1 are: $\widehat{Q}_i = Q_i + \epsilon Q_i'$, where $'$ symbol denoted the derivative. Therefore the transfer matrix equation for the tonehole with an uncertainty (ϵ) in the lengths L_1 and L_2 is:

$$\widehat{M_h} = \widehat{Q_1} M \widehat{Q_2} = (Q_1 + \epsilon Q_1')M(Q_2 + \epsilon Q_2'), \tag{3.13}$$

where M is the transfer matrix of the system as in Eq. 3.6 that is computed with the measurement of Z_{in} and Z_T, and M_h is the tonehole transfer matrix (Eq. 3.3). The first-order tonehole transfer matrix with uncertainties in the length at both sides of the tonehole is then:

$$\widehat{M_h} \approx Q_1 M Q_2 + \epsilon Q_1' M_1 M_h M_2 Q_2 + \epsilon Q_1 M_1 M_h M_2 Q_2' \tag{3.14}$$

Since $Q_i = M_i^{-1}$ then Eq. 3.14 becomes:

$$\widehat{M_h} \approx M_h + \epsilon Q_1' M_1 M_h + \epsilon M_h M_2 Q_2'. \tag{3.15}$$

On one hand, by using the fact that:

$$Q_1' M_1 = \begin{pmatrix} -k\sin kL_1 & -jkZ_c\cos kL_1 \\ -jkZ_c^{-1}\cos kL_1 & -k\sin kL_1 \end{pmatrix} \begin{pmatrix} \cos kL_1 & jZ_c\sin kL_1 \\ jZ_c^{-1}\sin kL_1 & \cos kL_1 \end{pmatrix}. \tag{3.16}$$

Then:

$$Q_1' M_1 = \begin{pmatrix} 0 & -jkZ_c \\ -jkZ_c^{-1} & 0 \end{pmatrix}. \tag{3.17}$$

On the other hand, we have:

$$M_2 Q_2' = \begin{pmatrix} \cos kL_2 & jZ_c\sin kL_2 \\ jZ_c^{-1}\sin kL_2 & \cos kL_2 \end{pmatrix} \begin{pmatrix} -k\sin kL_2 & -jkZ_c\cos kL_2 \\ -jkZ_c^{-1}\cos kL_2 & -k\sin kL_2 \end{pmatrix}. \tag{3.18}$$

And then:

$$M_2 Q_2' = \begin{pmatrix} 0 & -jkZ_c \\ -jkZ_c^{-1} & 0 \end{pmatrix}. \tag{3.19}$$

Therefore, products $Q_1' M_1$ and $M_2 Q_2'$ does not depend on the lengths L_1 and L_2.

Then by substituting the results of Eqs. 3.17 and 3.19, then the matrix 3.14 is:

$$\widehat{M_h} \approx M_h - k\epsilon \begin{pmatrix} 0 & jZ_c \\ jZ_c^{-1} & 0 \end{pmatrix} M_h - k\epsilon M_h \begin{pmatrix} 0 & jZ_c \\ jZ_c^{-1} & 0 \end{pmatrix}. \tag{3.20}$$

Considering that $A_h = D_h$, and by substituting we have that the matrix Eq. 3.14 is written as:

$$\widehat{M_h} \approx M_h - jk\epsilon \begin{pmatrix} Z_c C_h & Z_c A_h \\ Z_c^{-1} A_h & Z_c^{-1} B_h \end{pmatrix} - jk\epsilon \begin{pmatrix} Z_c^{-1} B_h & Z_c A_h \\ Z_c^{-1} A_h & Z_c C_h \end{pmatrix}. \tag{3.21}$$

Then the elements of the matrix are:

$$\widehat{A}_h = A_h - jk(\epsilon Z_c C_h + \epsilon Z_c^{-1} B_h), \tag{3.22}$$

$$\widehat{B}_h = B_h - 2jk\epsilon Z_c A_h, \tag{3.23}$$

and

$$\widehat{C_h} = C_h - 2jk\epsilon Z_c^{-1} A_h. \tag{3.24}$$

Therefore, in the case where under the condition $k\epsilon \ll 1$, the error on the shunt impedance is independent of the lengths L_1 and L_2.

$$\frac{\widehat{Z_h}}{Z_h} = \frac{C_h}{\hat{C}_h} = 1 + 2jk\epsilon Z_c^{-1} \frac{A_h}{C_h}. \tag{3.25}$$

Concerning the series impedance Z_a, an approximation allows a similar analysis:

$$B_h = Z_a(1 + Z_a/4Z_h) \simeq Z_a. \tag{3.26}$$

Thus

$$\frac{\widehat{Z_a}}{Z_a} = 1 - 2jk\epsilon Z_c \frac{A_h}{B_h}. \tag{3.27}$$

Furthermore the relative error is large, because $Z_c/B_h \simeq Z_c/Z_a$ is very large.

Fig. 3.3 shows impedance curves and equivalent height for different uncertainties in the length, error curves are presented for the numerical computations (Eq. 3.11). The uncertainties and tube

lengths are in Table 3.2. In Fig. 3.3b it is observed that the differences in the real part of the shunt impedance computed Z_h when the error in the length is introduced is barely noticeable, in contrast with the imaginary part of the series impedance (Fig. 3.3a) where the difference is greater as the frequency rises.

The equivalent length of the tonehole shown in Fig. 3.3c is computed through:

$$t_s = Im(Z_s/(jkZ_{oh})). \tag{3.28}$$

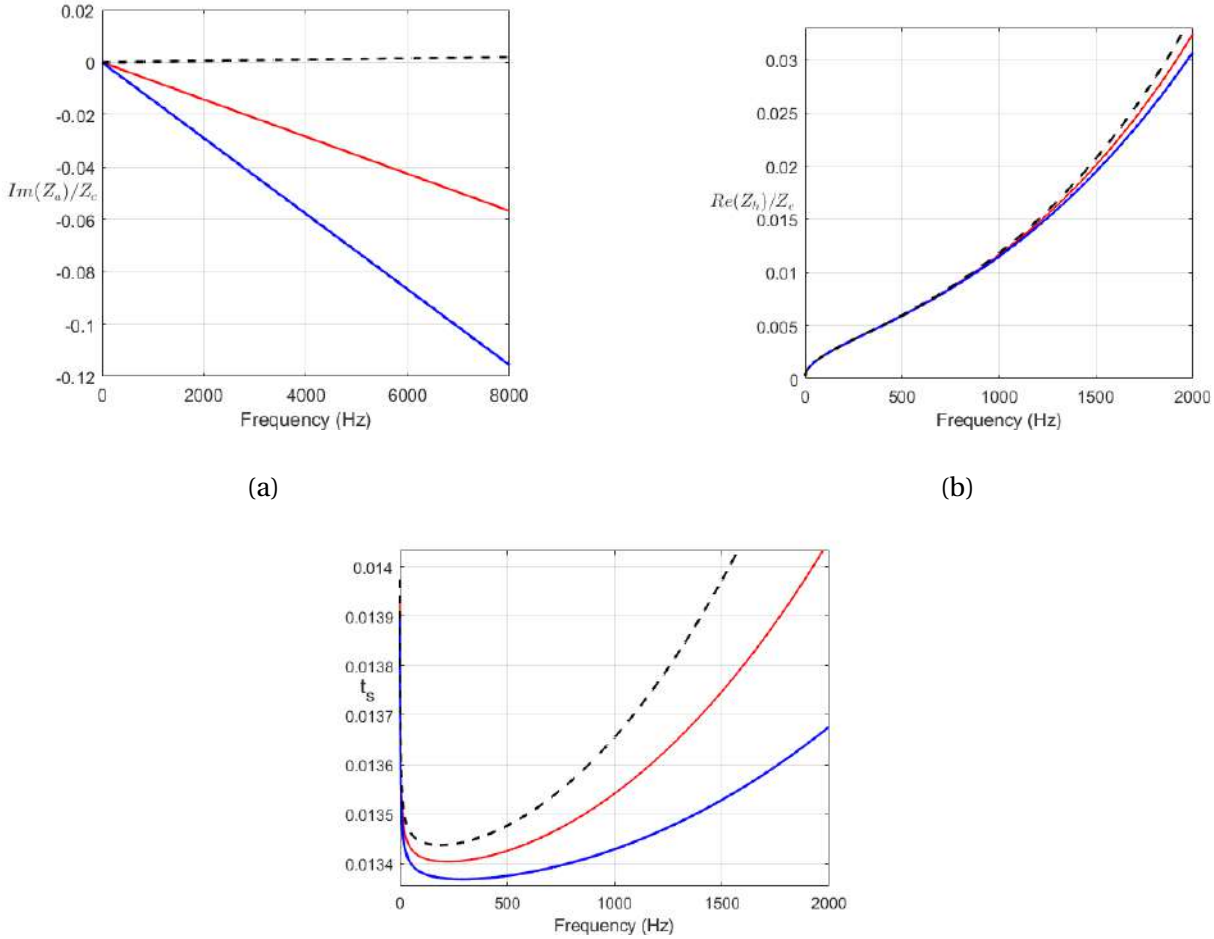

Figure 3.3: Computation for uncertainties in the main tube length, (a) imaginary part of the series impedance Z_a, (b)imaginary part of the shunt impedance Z_h and (c) equivalent height t_s. Red, solid thin line: theory without length errors. Blue thick solid line: inverse problem with $\epsilon = 0.2$ mm. Black dashed line: inverse problem $\epsilon = -0.2$ mm.

Simulations of the same errors where done on three tubes of different lengths 60 mm, 118 mm and 162 mm of total length. It was observed that the error does not depends on the tube length for a given uncertainty. In every case, the error is smaller at low frequency and increases with frequency. As a conclusion, it is important to keep the incertitude on the length small despite the total length of the tube.

3.5 Simulation of the experiment: effects of the influence of uncertainties in the input impedance

In this section only the error due to an uncertainty in the measurement of the input impedance is considered, because of the assumption that the error as a consequence of an uncertainty in the length (section 3.4), and the one due to the impedance measurement, are both small and they can be added at the end of the analysis.

In preliminary measurements (see Chapter 1), it was noted that the uncertainty in the impedance measurements can be modeled as a random error regarding the impedance magnitude. After analyzing similar measurements the magnitude of this uncertainty is estimated 1%. Then, the perturbed impedance for the inverse procedure is computed through Eq. 1.3. For the method of the reversal tube (see Chapter 2), two tubes of different lengths where simulated and analyzed in order to observe differences due to the main tube length in the computations of the tonehole impedances. For this method, the expected error in the computed tonehole impedance, for three tubes of lengths $L = 60\ mm$, $L = 118\ mm$, and $L = 162\ mm$ is observed in Figs. 3.4 to 3.6.

The imaginary part of the series impedance ($imag\{Z_a\}$) for the three simulated tubes is in Fig. 3.4. It is seen that results are very look alike for the tubes of length 118 and 162 mm, and significantly different for the tube of 60 mm. For the tube of length $L = 162\ mm$ the error is bigger at 2000 Hz, this error continues increases towards a maximum at 2270 Hz, which is also an input impedance maximum, in comparison with the $L = 118\ mm$ tube, that has a similar maximum peak at 3070 Hz. The tube of 60 mm has a big resonance at approximately 1000 Hz, but the next resonance is after 5000 Hz, which means that between 1000 and 5000 Hz the error due to the incertitude of the measurement of the input impedance is small between these given frequencies.

In Fig. 3.5 it is observed that the error in the real part of the shunt impedance ($real\{Z_h\}$) is different depending on the tube length. For the tube of length $L = 162\ mm$, it seems that the bandwidth of the error is narrower. And the tube of 60 mm shows only one peak of error instead of two as in the other lengths.

Figs. 3.6 shows the error in equivalent height t_s (Eq. 3.28) for the three simulated tubes. It is observed that despite the length of the tube, the errors are in accordance in the frequency range from 0 to 2000 Hz, the frequency of the peak being different depending on the length. This is due to the fact that the longer tubes have the first impedance maximum at similar frequencies, 665 Hz, for the tube of $L = 118\ mm$ and 550 Hz for the tube of $L = 162\ mm$. For the small tube (60 mm) the error is observed at 1000 Hz. At the first impedance maximum where also the error is maximum.

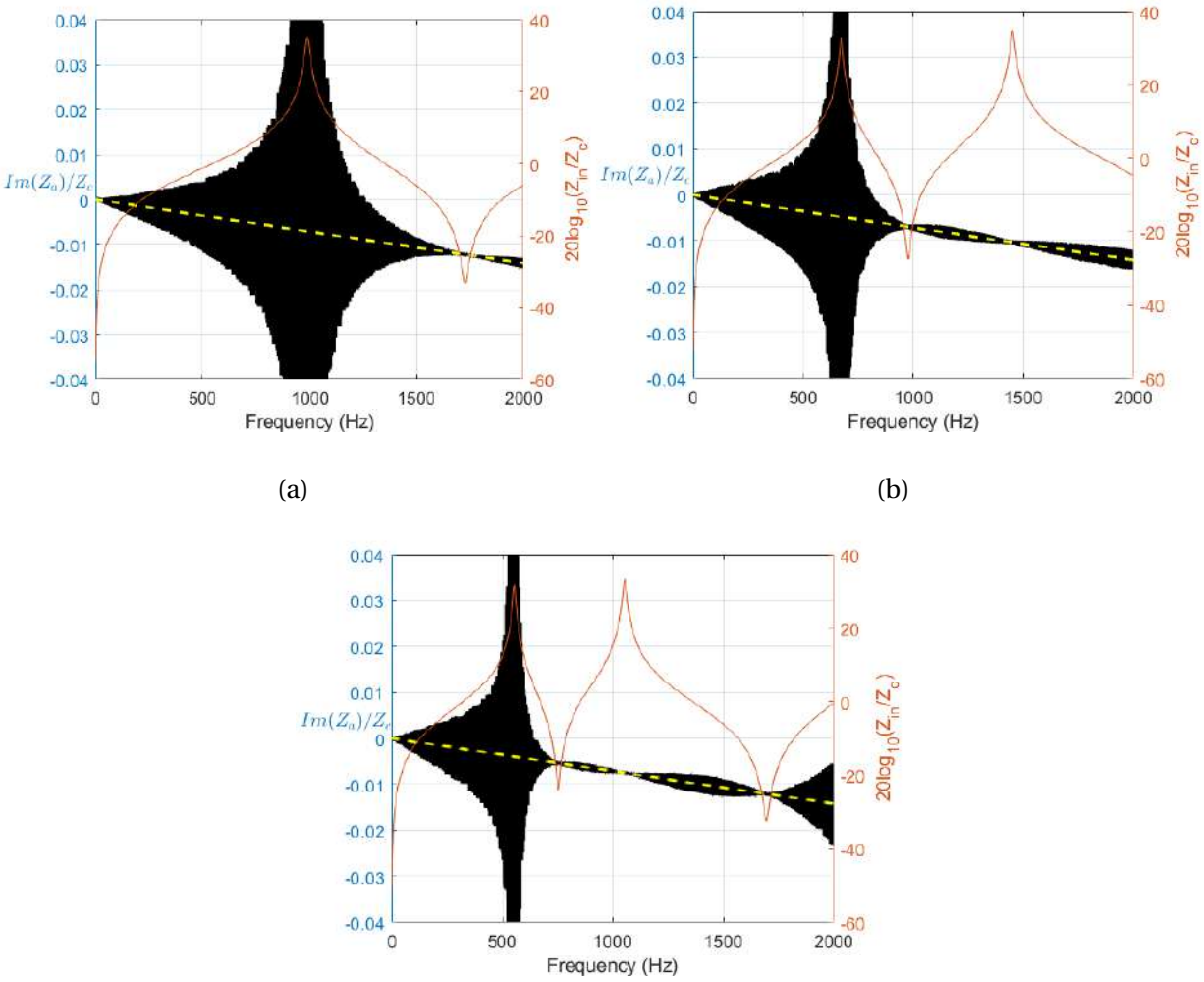

(a)

(b)

(c)

Figure 3.4: Imaginary part of the series impedance Z_a for the lengths (a) $L = 60\ mm$, (b) $L = 118\ mm$ and (c) $L = 162\ mm$. Black lines: result of the inverse method when a random error is added on the computed input and transfer impedances Z_{in} and Z_T. Yellow line: no random error added. Orange curve, input impedance with scale at right.

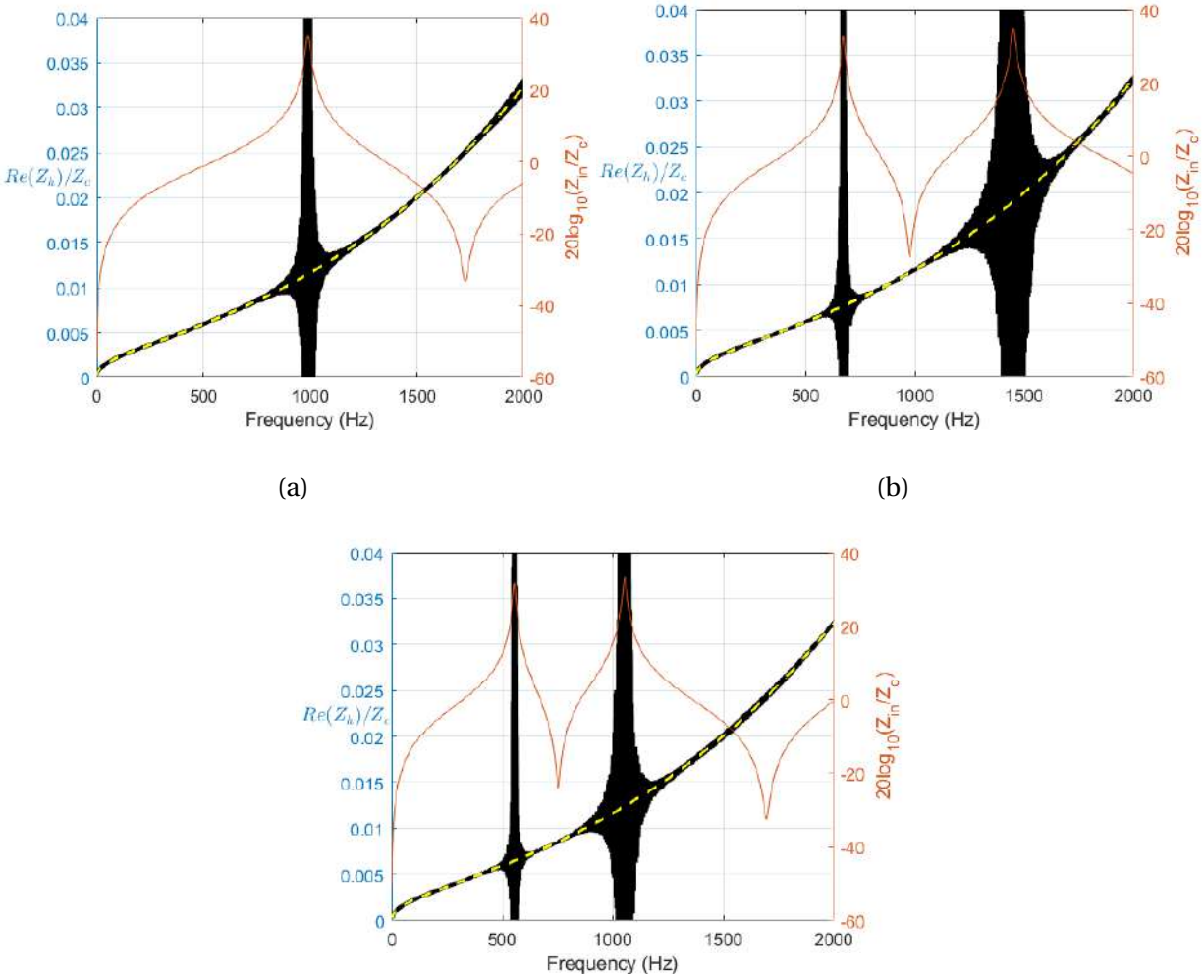

(a)

(b)

(c)

Figure 3.5: Real part of the shunt impedance Z_h for the lengths (a) $L = 60\ mm$, (b) $L = 118\ mm$ and (c) $L = 162\ mm$. Black lines: result of the inverse method when a random error is added on the computed input and transfer impedances Z_{in} and Z_T. Yellow line: no random error added. Orange curve, input impedance with scale at right.

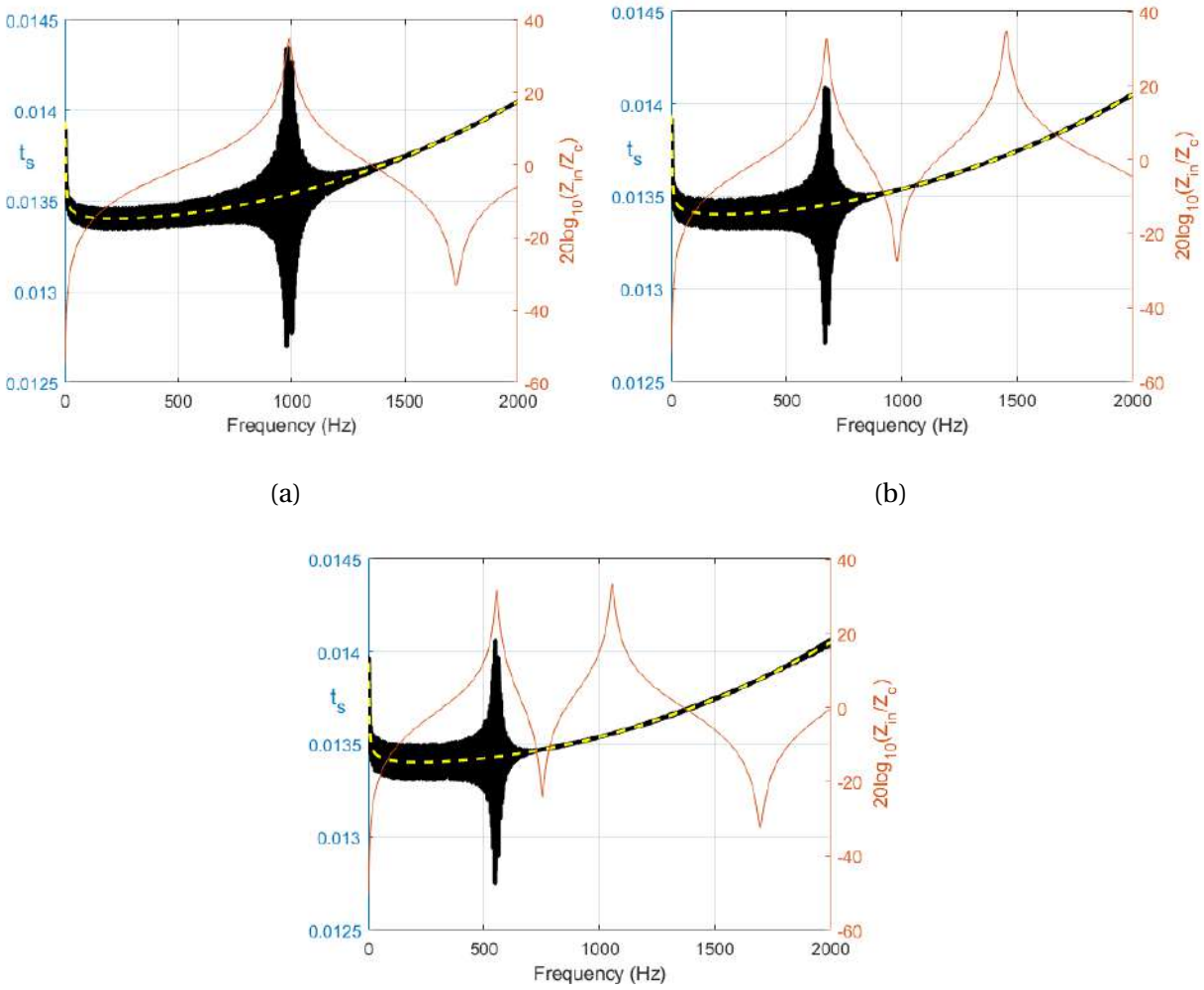

(a)

(b)

(c)

Figure 3.6: Tonehole equivalent height t_s (in m) for the lengths (a) $L = 60\ mm$, (b) $L = 118\ mm$ and (c) $L = 162\ mm$. Black lines: result of the inverse method when a random error is added on the computed input and transfer impedances Z_{in} and Z_T. Yellow line: no random error added. Orange curve, input impedance with scale at right.

3.6 Comparison between the two methods

in this section we compare the results of the method of the input and transfer impedances with the tube reversed method. We use the simulation of the experiment. For the first, the location of the tonehole is exactly at the middle of the tube. The lengths L_1 and L_2 are necessarily equal, as well as the error. For the second, the tonehole cannot be close to the middle. The three figures 3.7, 3.8 and 3.9 show the main drawback of the reversed tube method: it is the effect of the anti-resonance of the input impedance near 1600 Hz. However, below this frequency, the results of the two methods seem to be very similar, and the discrepancy between them is very small. For the particular case considered, the discrepancy between the results of the inverse and direct problems is very small, but the error on the series impedance is close to 50$\dot{\Omega}$This is a realistic order of magnitude, which confirms the difficulty ot the measurement.

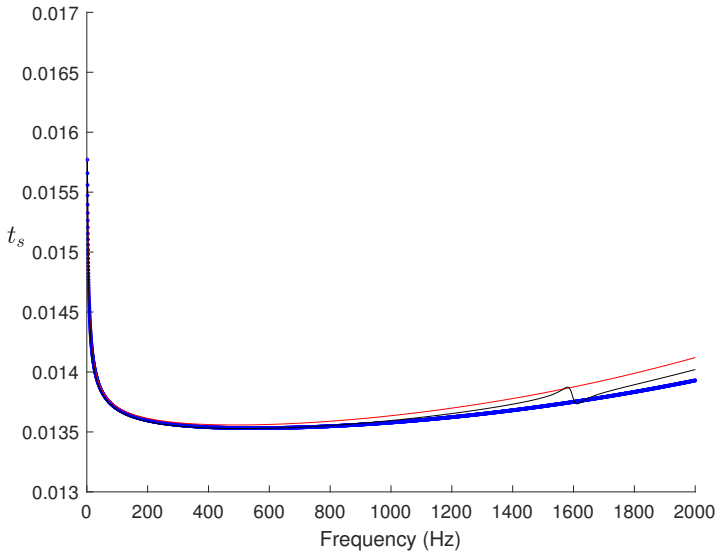

Figure 3.7: (Color online) Equivalent height t_s (in m). Red, solid line: theory without length errors. Blue and black, solid lines: inverse problem with 0.2 mm error on $L_1 + L_2 = 118$ mm. Blue line: method of the input and transverse impedances ($L_1 = L_2 = 59$ mm). Black line: reverse tube method ($L_1 = 44mm, L_2 = 74$ mm).

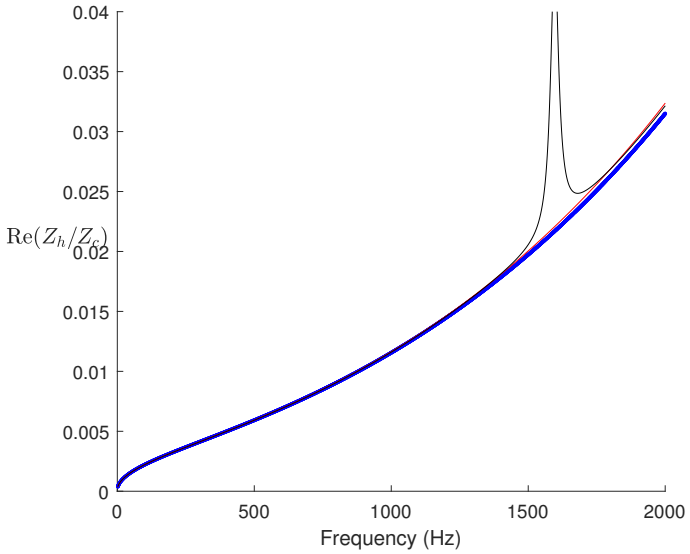

Figure 3.8: (Color online) Real part of the shunt impedance Z_h. See line definitions in the caption of Fig. 3.7.

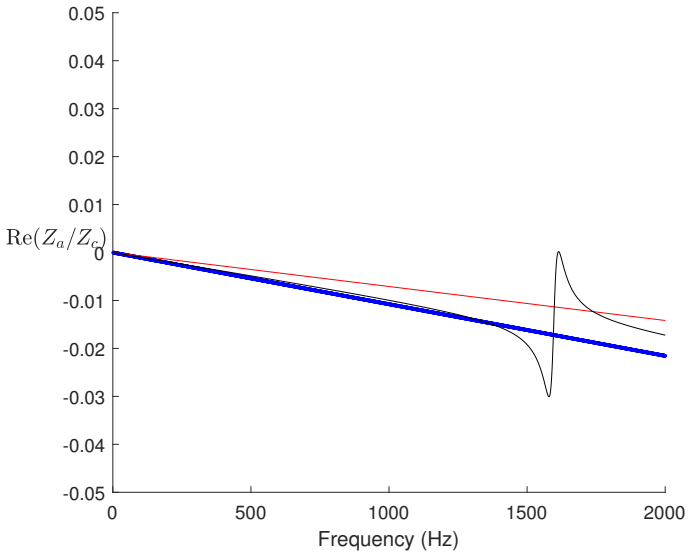

Figure 3.9: (Color online) Imaginary part of the series impedance Z_a. See line definitions in the caption of Fig. 3.7. .

3.7 Conclusion of the theoretical part

- From the simulation of the experiment in which an uncertainty in the length is studied (Section 3.4) it is observed that while the impact of a positive value of the uncertainty $\epsilon > 0$, produces a diminishing value of the imaginary part of the series impedance and on the equivalent length, a negative value of ϵ will produce that the imaginary part of the series impedance changes to a positive value, which is not in accordance with the physical problem (Fig. 3.3).

- Even though the error in the shunt impedance is found to be small (Figs. 3.3b and 3.3c), is very likely that the error in the series impedance will be large in comparison (Fig. 3.3a) and therefore there is a chance that it will be difficult to measure the series impedance Z_a with a good degree of accuracy.

- Regarding the real part of the shunt impedance, there is no appreciable difference in the computation between 0 and 2000 Hz for neither of the error in the length simulated.

- When there is an uncertainty in the input impedance measurement (without uncertainty in the length) (Section 3.5) there are frequencies for which the error in the computed quantities (Z_a, Z_h and t_s) is quite big, these are coincident with the maximum peaks in the input impedance Z_{in}. Therefore, a short tube which has less maximum peaks will be preferred.

- Short tubes will give better results in the low frequency range. Provided that the low frequency range is of primary importance in a musical instrument, a short tube of 60 mm will be used in the experimental part of this work with this method.

3.8 Finite Element Model and measurements for the method of the input and transfer impedances

3.8.1 Losses in the Finite Element Method

In order to use results of the Finite Element Method and to compare them to experimental results. We have to make sure that acoustic variables obtained form the FEM simulation have the same parameters as the theoretical model. Since results of the simulation are to be computed with the theoretical model in order to implement the inverse calculation to obtain tonehole parameters.

As explained in Sect. 3.3 for the method of the input and transfer impedances, it is necessary to compute the transfer matrices of the cylindrical tube sections at left and right of the tonehole. By multiplying the transfer matrix of the tube with tonehole left and right by the inverse transfer matrices of the cylindrical sections, the tonehole transfer matrix elements can be obtained (Eq. 3.9). In terms of a Finite Element Model, a tube with lateral tonehole open to the air, a 3D model has to be used. Nevertheless, the theory of the losses and dispersion in a cylindrical tube used in the theoretical part of this study, is a 1D model. Therefore, a comparison between the theoretical 1D model and a 3D FEM model in cylindrical tubes is performed.

The first quantity to be compared is the wavenumber inside the tube k_a, which includes viscothermal losses and is defined as $k_a = \frac{\Gamma_a}{j}$, where the propagation constant Γ_a is among others, function of the tube radius (See Appendix). The Finite Element Method (FEM) model is performed in COMSOL Multiphysics, it consists of a straight cylindrical tube of 30 mm of total length and internal radius of 7.3 mm which coincides with the tubes made by Buffet Crampon for the measurements. The wavenumber obtained from the FEM model is computed from the values of the average pressure at the inlet P_{in} (source position), at the closed end of the tube P_{end} and tubes

total length L (Eq. 3.29).

$$k_a = \frac{1}{L}\arccos\left(\frac{P_{in}}{P_{end}}\right) \tag{3.29}$$

Fig. 3.10 shows results for the comparison of the wavenumber in the theoretical 1D and numerical 3D models. The difference in the real part is in Fig. 3.10a, it is below 0.2%. For the imaginary part the difference is 4% at low frequencies and it diminishes to 1% at 4 kHz.

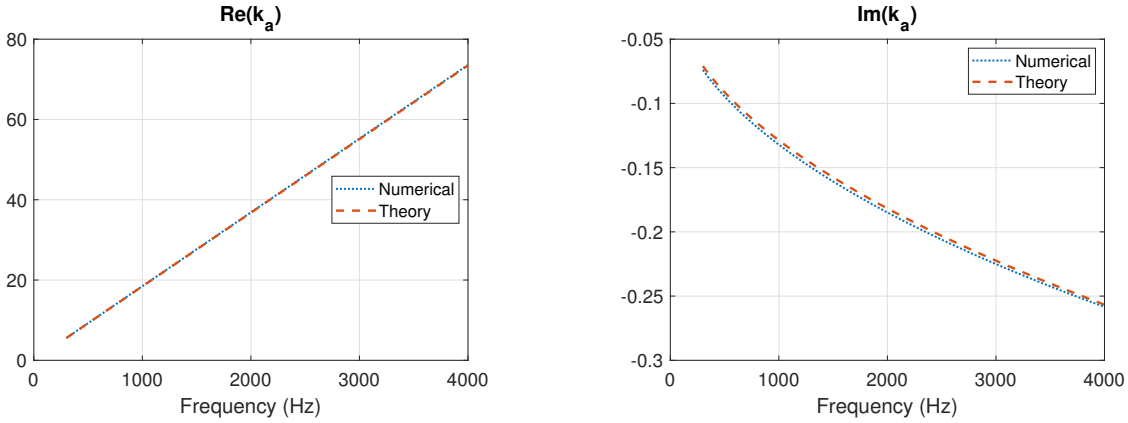

(a) (b)

Figure 3.10: (a) Real and (b) imaginary part of the wavenumber k_a with viscothermal losses comparison between theoretical 1D model and a 3D numerical model through COMSOL.

The second quantity to be compared is the characteristic impedance with viscothermal losses Z_o. In the theoretical 1D model is defined as $Z_o = \frac{\rho c}{S}\left[1 + \frac{\overline{\alpha_1}(1-j)}{r_v} - j\frac{\overline{\alpha_2}}{r_v^2}\right]$ [4] (see Appendix). In the simulated 3D numerical model the impedance is computed as:

$$Z_o = j\sin(k_a L)\left(\frac{P_{end}}{U_{in}}\right) \tag{3.30}$$

Where L is the total tube length, and U_{in} is the volume velocity at the inlet.

Results of the comparison are in Fig. 3.11. In this case the difference in the real part at low frequency is about 0.075% and it diminishes to 0.035% at 4 kHz. As for the imaginary part, the difference is between zero and 2% up to 3 kHz, after this frequency the difference increases rapidly to 15% at 4 kHz.

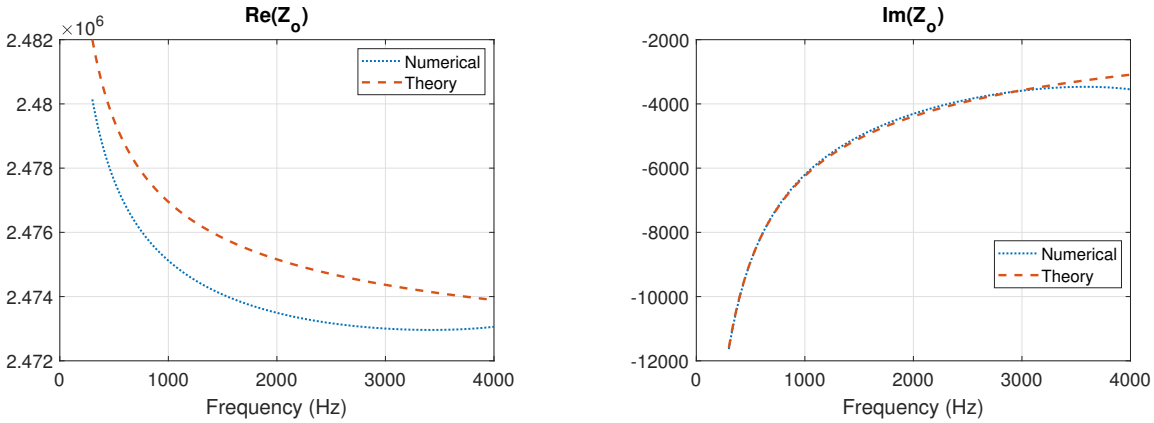

(a) (b)

Figure 3.11: (a) Real and (b) imaginary part of the characteristic impedance Z_o with viscothermal losses comparison between theoretical 1D model and a 3D numerical model through COMSOL.

3.9 Measurement vs FEM

In this section a comparison between theory, measurement and the FEM model for a cylindrical tube with a tonehole in the middle is done. We compare the input and transfer impedances, in the case of the transfer impedance we use the direct measurement performed with the impedance sensor through the use of a third microphone described in Sec. 1.3.4.

Fig. 3.12 shows the comparison between theory, measurement and FEM model for a tube of 104 mm of total length with tonehole in the middle. Fig. 3.12a shows the modulus of the input impedance in dB. Numerical simulation results were only computed up to 1400 Hz due to a lack

of time in the use of the computer[2]. For the first and second peaks, there is no difference in frequency nor in amplitude between measurement and FEM model. The difference between these two and the theory in the first peak is 37 $cents$ and 6 dB. The difference in the second peak is 40 $cents$ and 3.7 dB. The third measured peak has no relation with the theory whatsoever. Fig. 3.12c shows the phase of the input impedance, it is observed that after 2 kHz theory and measurements increasingly diverge.

Fig. 3.12b shows the comparison between theory, measurement and FEM model of the tube of 104 mm of total length and with tonehole in the middle, for the modulus of the transfer impedance. For the first peak the difference in frequency between measurement and numerical simulation is 3 $cents$ and 3 dB, the difference between measurement and theory is 37 $cents$ and 14.1 dB. There is a peak at 1029 Hz in the measurement that it is not expected by the theory nor by the FEM model, at this frequency there is a difference of about 6 dB between theory and the numerical model. For the second peak, the difference between measurement and theory is 40.4 $cents$ and 12.6 dB. There is a fourth peak in the measurement not expected by the theory at 2391 Hz. For the third peak of the theory there is no relation at all with the measurement. Fig. 3.12d shows that there is very little relation in the phase between the measurement and both theory and numerical model.

A shorter tube is also measured and modeled. This is a cylindrical tube of 60 mm of total length with a tonehole in the middle. A FEM model is performed in the same way it was done for the 104 mm length. The tonehole has the same geometry in both cases. Th difference between Figs. 3.12 and Fig. 3.13, besides the tube length, is the third microphone used, the first is a 1/4" and the second is a probe microphone (1.25 mm).

[2]This simulation took about 13 hours to be completed in desktop PC.

Fig. 3.13 shows the comparison between theory, numerical simulation and measurement of the input and transfer impedances for a 60 mm length tube with a 4 mm raidus tonehole in the middle. The difference between measurement and numerical simulation for the first peak of the input impedance (Fig. 3.13a) is 21 $cents$ and 0.5 dB in amplitude. The difference between theory and measurement is 56 $cents$ and 5 dB in amplitude. For the second peak of the input impedance the difference between measurement and FEM model in 3.6 $cents$ and 0.1 dB in amplitude; the difference between measurement and theory is 8.7 $cents$ and 2.5 dB in amplitude. Fig. 3.13c shows that phases are in accordance for the three presented cases.

As for the transfer impedance (Fig. 3.13b) the difference between measurement and FEM model is 20 $cents$ and 0.9 dB, and 56 $cents$ and 13 dB between the measurements and the theory for the first peak. There is a peak that is only present in the measurement at 1615 Hz, at this frequency the difference between the numerical simulation and the theory is about 6 dB. For the second peak of the transfer impedance, the difference between measurement and numerical simulation is 3.6 $cents$ in frequency and 2.8 dB in amplitude, the difference between measurement and theory is 8.7 $cents$ and 11.1 dB in amplitude. There is another peak in the measurement at 3969 Hz that is not present in the other two curves, at this frequency the difference between FEM model and theory is about 6 dB, as in the previous case. Fig. 3.13d shows that there is agreement in the phases of the theory and the FEM model, but there is no agreement whatsoever with the measurement.

Result observed in Figs. 3.12b and 3.13b are consistent with the results of the measurement of the transfer impedance in a straight cylindrical tube in Sect. 1.3.4 and seen in Fig. 1.13. Therefore, the unknown problem in the measurement of the transfer impedance it is not due to neither the microphone type, the holder, or the presence of the tonehole.

After analyzing the comparison between theory, FEM and measurement, it is noted that it might be possible to utilize measurement results up to 1200 Hz. Since up to this frequency the difference with the FEM model is less than 3 dB and about 4 $cents$. Fig. 3.14 shows the modulus and phase of the measurement up to 1200 Hz that will be used in the reconstruction.

3.9.1 Reconstruction

After the comparison of the measurement and the numerical simulation, it can be concluded that there is a problem in the measurement of the transfer impedance. Nevertheless, it is also observed that there is a frequency range that is close to the numerical simulation results and it might be suitable for the reconstruction through the input and transfer impedances method.

To compute the tonehole impedances the inverse problem described in Sec. 3.3 is used. First input and transfer impedances are measured, this was done experimentally with the use of the impedance sensor and the probe microphone (Sect. 1.3.4). Measurement results are in Fig. 3.14.

There is a difference between the measurement and the numerical simulation, that can be explained by the lack of knowledge of the use of the sensibility of the probe microphone in the impedance sensor software. Fig. 3.15 shows this difference, in the case of the input impedance (Fig. 3.15a) the difference is less than 10% up to 900 Hz. In the case of the transfer impedance (Fig. 3.15b) there is a maximum difference of 30% up to 950 Hz.

The reconstruction of the tonehole impedances performed withe the experimental data in Fig. 3.14 is observed in Fig. 3.16. In the case of the imaginary part of the series impedance, despite

the fact that there is consistency in the negative sign of the result, the difference with the expected value from the theory is in the order of 10^6, which implies that it might not be possible to obtain this value through this measurement. The difference with the theory of the reconstructed real part of the shunt impedance goes from 68% in low frequency to 74% at 1200 Hz. As for the imaginary part of the shunt impedance, the difference with theory is 68% in low frequency and it diminishes to 62% at 1200 Hz.

A comparison with theoretical values is in Fig. 3.17. It has to be mentioned that the theoretical values seen in Fig. 3.17 are computed according to previous studies. Nevertheless, no previous study has been performed in tubes with the geometrical characteristics of those used in this study.

3.9.2 Computing of the tonehole input impedance from the FEM model

One of the advantages of the Finite Element Method is that values of the pressure and the volume velocity almost at any part in the model. The accuracy of the result will depend on how accurate is the model in the desired section of the model. But it also has to be bared in mind that a very detailed model will lead to the need of higher hardware computation use, and this may prevent the model to be solve at all.

Nevertheless, a computation of the input impedance of the tonehole was obtained form the FEM model by the use of a surface in which the average pressure and the integral of the velocity are computed. Fig. 3.18 shows the surface used for computing the input impedance.

Fig. 3.19 shows results of the real and imaginary part of the tonehole input impedance computed through the FEM model of the 60 mm length tube. It is compared to the theory of the shunt

impedance. Nevertheless, is has to be noted that theoretical calculation of the shunt impedance includes equivalent lengths of the inner and matching volume corrections, which are very likely that are not taken into account in FEM model data. In the real part of the input impedance (Fig. 3.19a) the difference is about 90% in low frequencies and about 80% at high frequencies. Nevertheless, it has to be noted that there is a forbidden frequency at 2845 Hz which coincides with the second maximum of the tubes input and transfer impedances (Fig. 3.13), at this frequency there a pressure node at the tonehole. As for the imaginary part of the tonehole impedance (Fig. 3.19b) the difference between curves is about 22% for the studied frequency range, apart from the forbidden frequency of 2845 Hz.

3.9.3 Conclusion of the FEM model and measurements

- The losses and dispersion in the numerical model through COMSOL are in accordance with 1D model of losses in the literature.
- There is an unknown reason for which unexpected peaks are observed in the transfer impedance measurement. This prevents the method to be implemented experimentally in a wide frequency range.
- In the comparison between the FEM model and measurement, it is found that there is a difference of less than 10% in the real part of the input impedance between measurement and numerical simulation. While for the imaginary part of the input impedance this difference is less than 30% below 900 Hz.
- There is a reconstruction of the tonehole impedances performed through measurements. Nevertheless, values obtained are more than 60% lower than those expected from the theory. It might not be possible to achieve actual values in the conditions of the present study.

- The Finite Element Method could be an alternative to obtain the tonehole impedances, but the model has to be improved and several data has to be collected to obtain a result that is in accordance with measurement results.

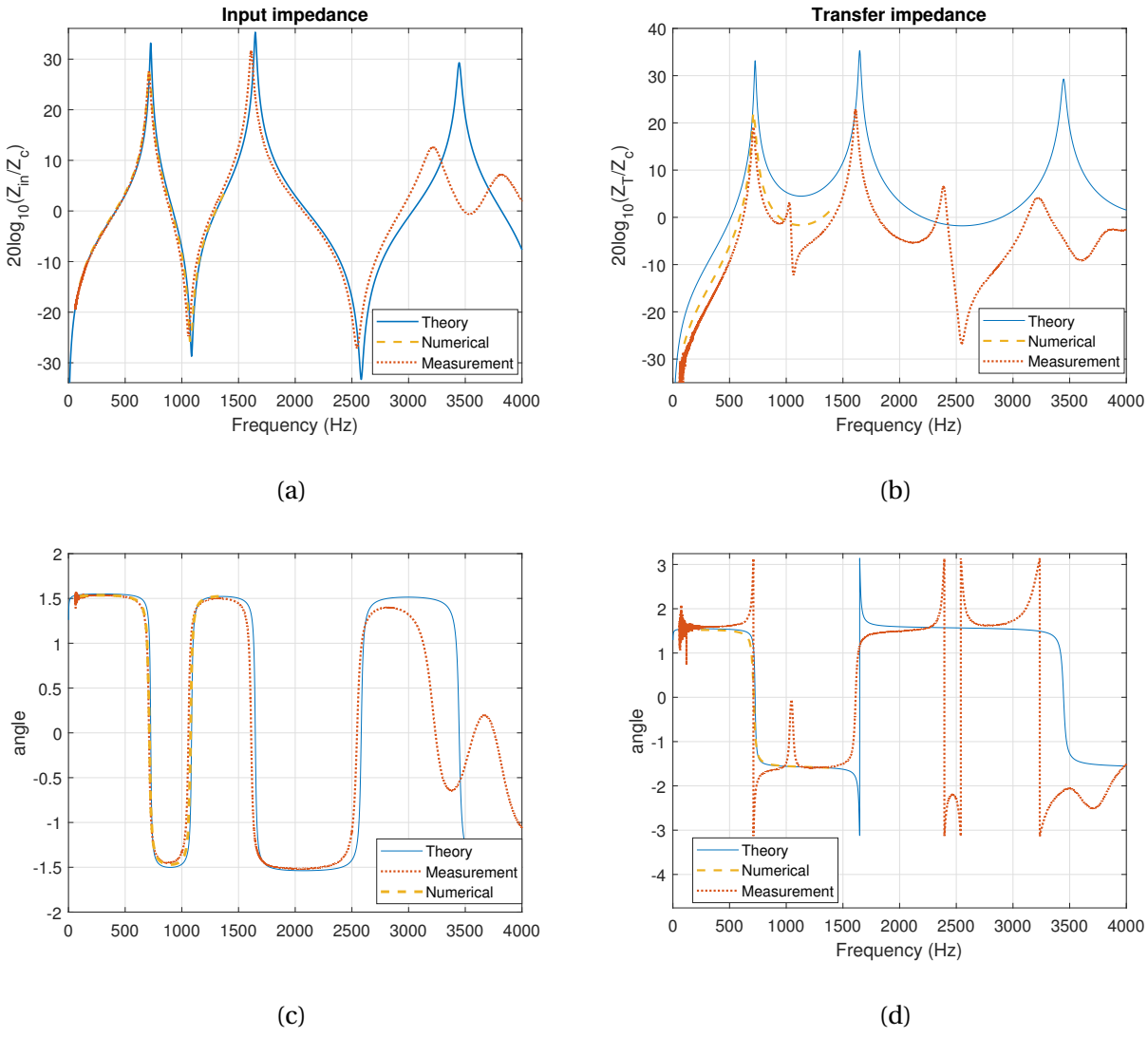

Figure 3.12: Comparison between Theory, Measurement and Numerical simulation through COMSOL for a 104 mm of length with tonehole in the middle. Input impedance (a) modulus and (c) phase; and transfer impedance (b) modulus, and (d) phase. Measurement done with impedance sensor and 1/4" microphone G.R.A.S (see Sec. 1.3.4). FEM results only computed up to 1400 Hz.

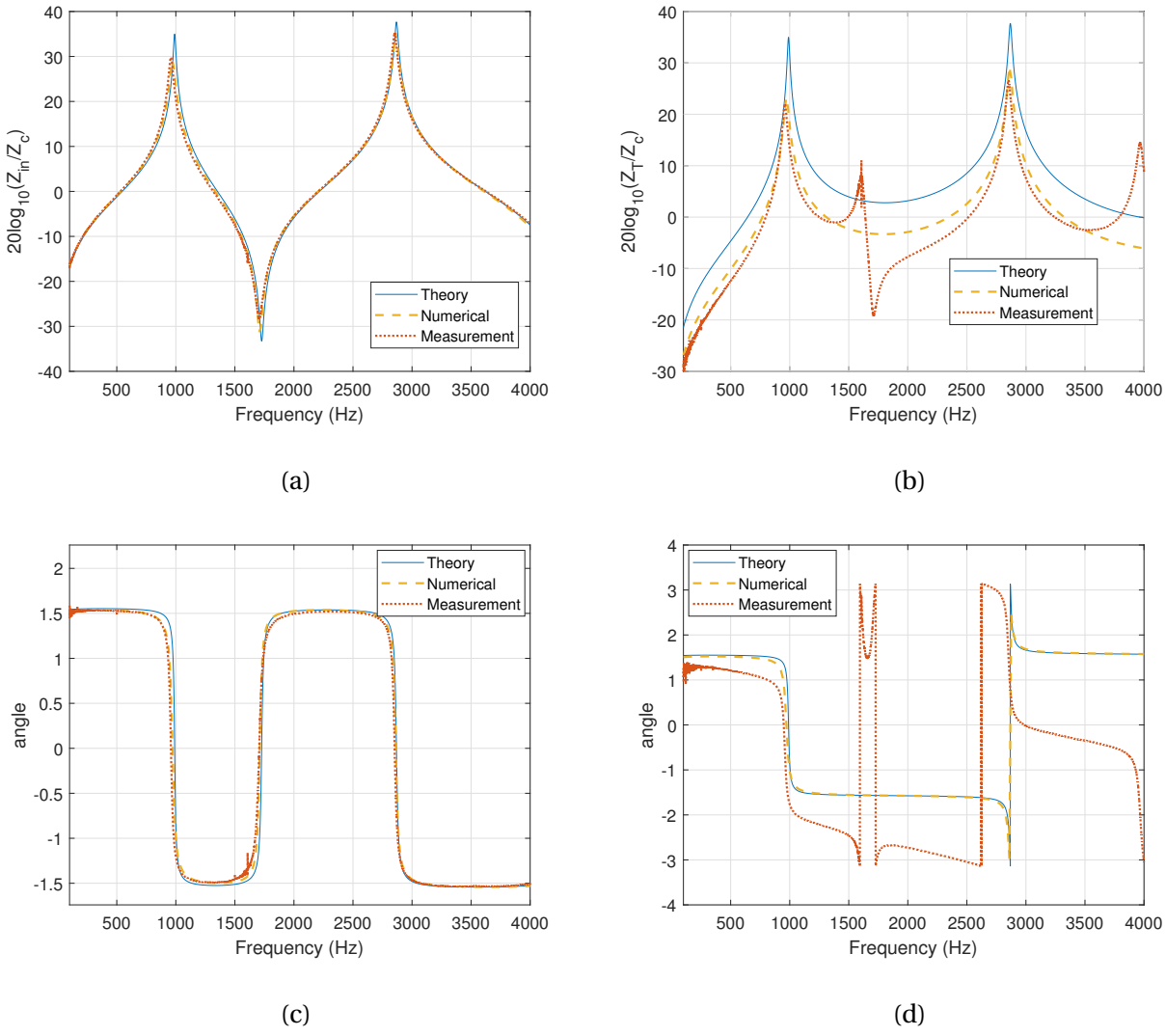

Figure 3.13: Comparison between Theory, Measurement and Numerical simulation through COMSOL for a 60 mm of length with tonehole in the middle. Input impedance (a) modulus and (c) phase; and transfer impedance (b) modulus, and (d) phase. Measurement done with impedance sensor and Probe microphone G.R.A.S (see Sec. 1.3.4).

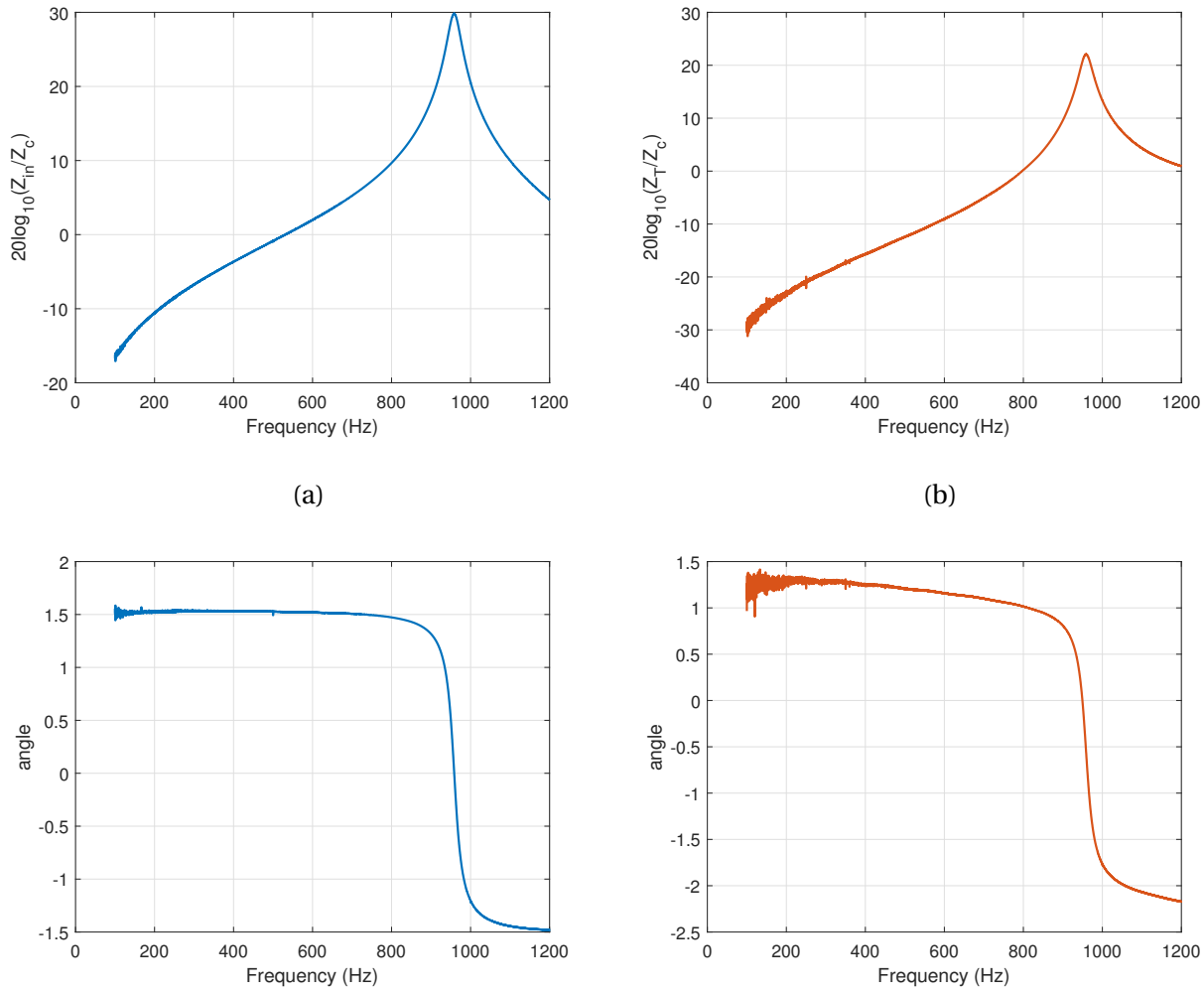

Figure 3.14: Measurement of the Input impedance (a) modulus, (c) phase; and transfer impedance (b) modulus and (d) phase. Measurement done with impedance sensor and probe microphone G.R.A.S (see Sec. 1.3.4).

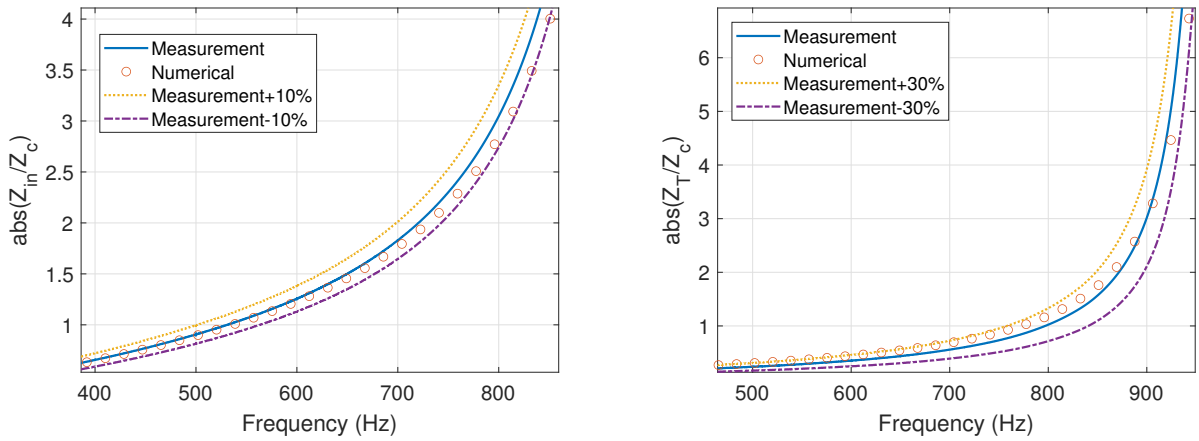

(a) (b)

Figure 3.15: Difference between the measurement and the numerical simulation, Input Impedance (a) and transfer impedance (b). Measurement done with impedance sensor and probe microphone G.R.A.S (see Sec. 1.3.4).

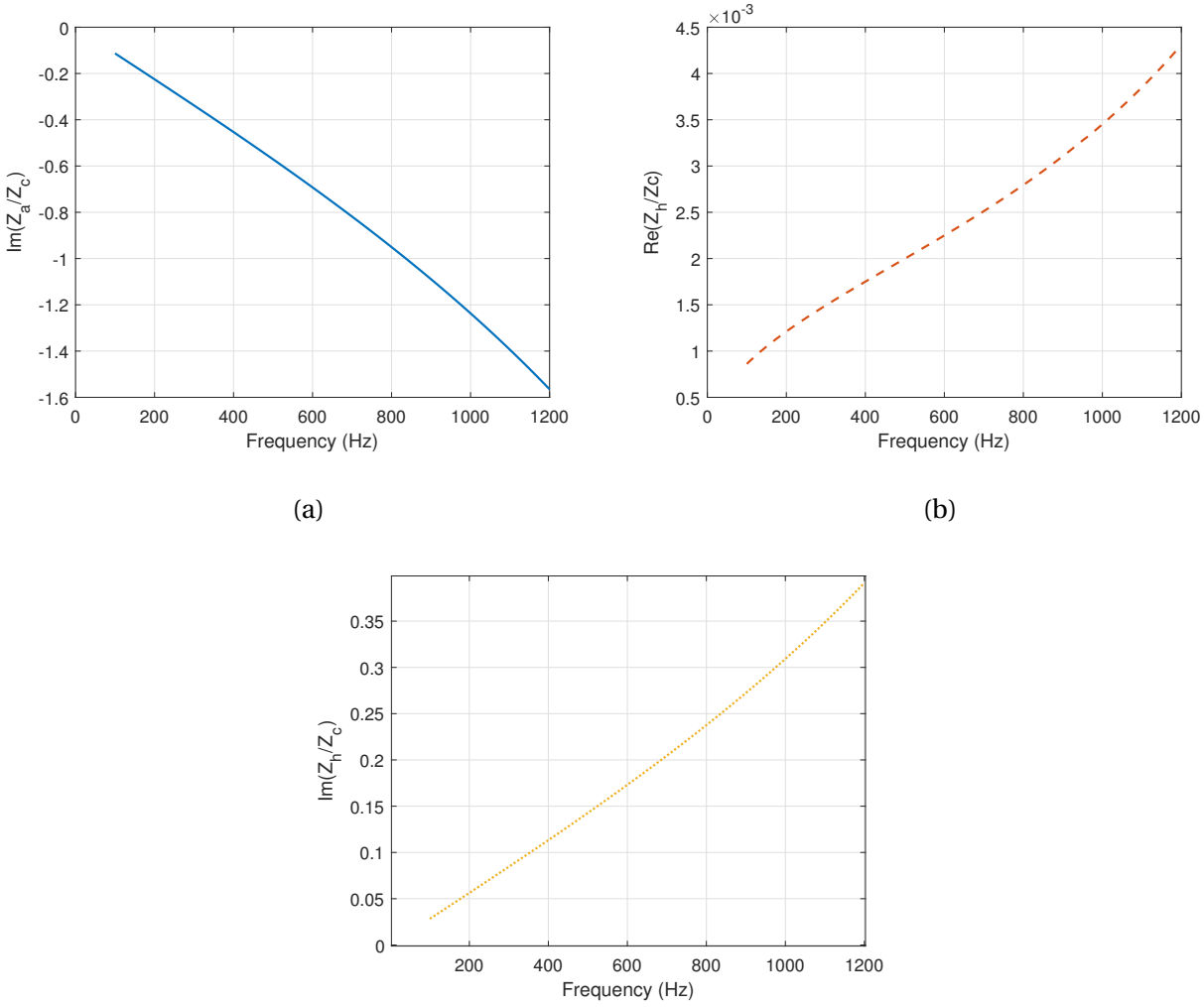

Figure 3.16: Inverse problem computation for series and the shunt impedances obtained from measurement (Fig. 3.14). (a) Imaginary part of the series impedance Z_a. (b) Real part of the shunt impedance. (c) Imaginary part of the shunt impedance Z_h.

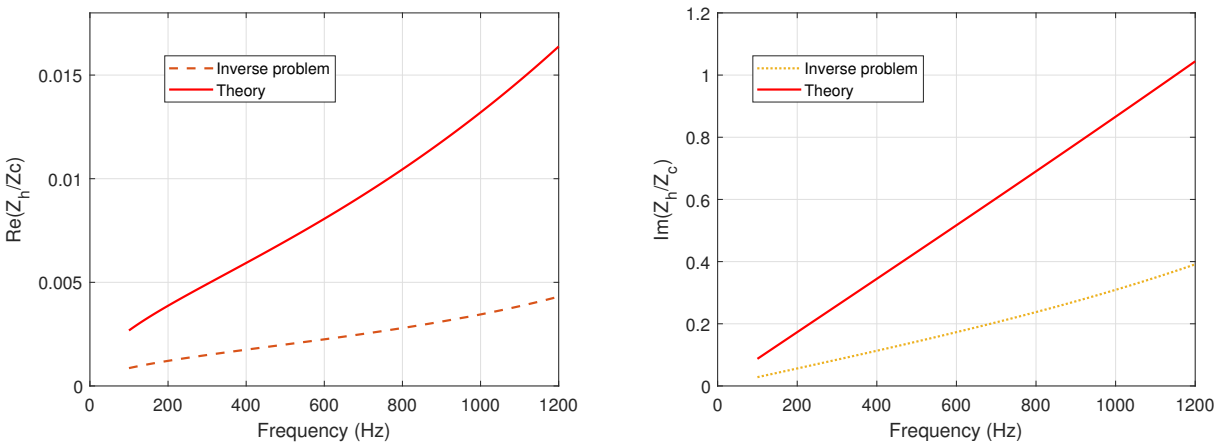

(a) (b)

Figure 3.17: Inverse problem computation for the shunt impedance obtained from measurement (Fig. 3.14). (a) Real part of the shunt impedance Z_h and (b) imaginary part of the shunt impedance Z_h.

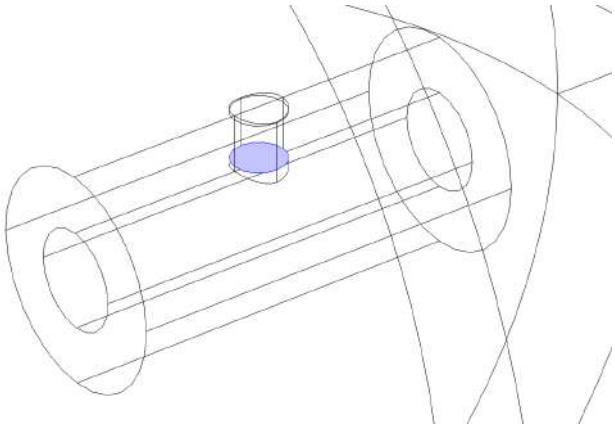

Figure 3.18: COMSOL FEM model of the 60 mm length tube with 4 mm radius tonehole in the middle. Surface marked is used to compute the input impedance of the tonehole.

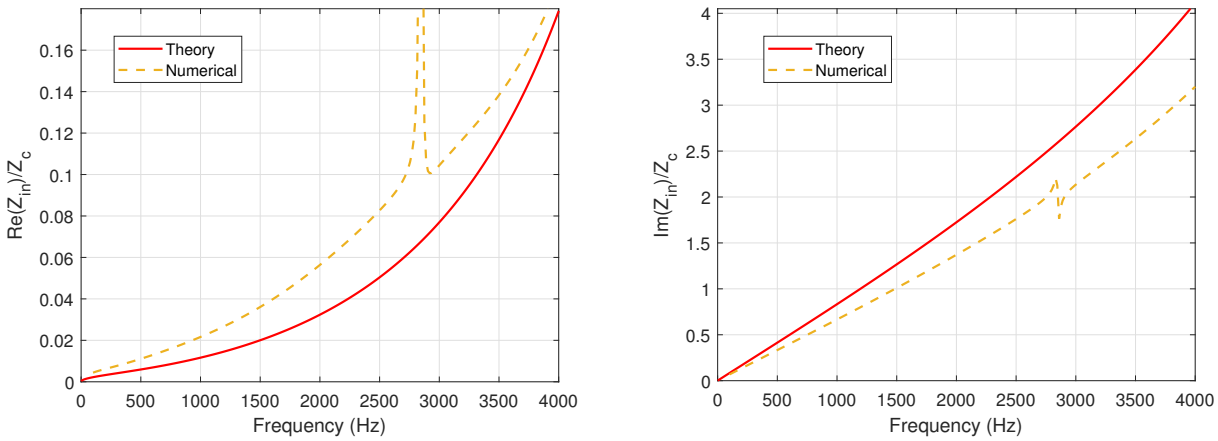

(a) (b)

Figure 3.19: Comparison between theory and directly computing of the tonehole input impedance with the surface in Fig. 3.18. (a) Real part of the input impedance and (b) imaginary part of the tonehole impedance.

Bibliography

[1] J.-P. Dalmont, C. J. Nederveen, V. Dubos, S. Ollivier, V. Meserette, E. te Sligte, *et al.*, "Experimental determination of the equivalent circuit of an open side hole: linear and non linear behaviour," *Acta Acustica united with acustica*, vol. 88, no. 4, pp. 567–575, 2002.

[2] A. Chaigne and J. Kergomard, *Acoustics of musical instruments*. Springer, 2016.

[3] A. Lefebvre and G. P. Scavone, "Characterization of woodwind instrument toneholes with the finite element method," *The Journal of the Acoustical Society of America*, vol. 131, no. 4, pp. 3153–3163, 2012.

[4] A. Chaigne, *Ondes acoustiques*. Editions Ecole Polytechnique, 2001.

Chapter 4

Conclusion and perspectives

4.1 Conclusion

The impedance sensor *Capteur-Z* showed to be an accurate tool for the measurement of the input impedance in the conditions of the present study. For instance, in repeated measurements carried on a steel straight tube, without disassembling, it was concluded that there is an associated incertitude of 1% in the input impedance measurement (Sect. 1.2, Fig. 1.4).

Since the input and transfer impedance method requires the use of a third microphone at the end of the tube, the terminal impedance of microphone caps was studied and compared to a rigid terminations and with the theoretical values (Sect. 1.3.3). It was concluded that the probe microphone holder has the terminal impedance closest to the rigid end experimental and theoretical results. In opposition to the 1/4" microphone holder, which is not in accordance to the expected theoretical values nor to the measurement of a perfectly rigid end termination (Fig. 1.10). This work suggests that it is mandatory to take into account the measured reflection coefficient of the closed end in future experiments.

The transfer impedance, which is also an important quantity in the input and transfer impedance method, was computed and compared in straight tubes (Sect. 1.4). It was concluded that it is not possible to directly measure this quantity with the impedance sensor and a third microphone, there are unexpected frequency peaks that are not seen in the theory nor in the numerical simulation, even if the microphone holder resembles a rigid termination (Figs. 1.13).

The study of the radiation impedance of an open end tube, showed that theory is only accurate in low frequency, below 1 kHz (Sect. 1.4 Figs. 1.14 and 1.15). And there is a shift in the real part of the input impedance with respect to the studied theory [1] (Fig. 1.15).

Regarding the input impedance of closed and open end straight tubes similar to those manufactured by Buffet Crampon, the numerical simulation through COMSOL Multiphysics, showed to be an accurate and promising tool for computing this quantity. There is an agreement between numerical simulation and theory in the case of a one closed end tube (Sect. 1.5.4 Fig. 1.16). Results of numerical simulation also showed to be accurate and in agreement with measurements for the one open end tube (Figs. 1.19, 1.21 and 1.22). In this case the available analytical solution is not in agreement, because this type of tube termination is not very well known theoretically.

For the development of the reversed tube method, the new method introduced during this PhD, aims to obtain the tonehole impedances by only measuring the input impedance in two different conditions instead of the input and transfer impedances. It was shown the benefits of using a short tube due to antiresonances associated to the total tube length (Sect. 2.5.3 Figs. 1.12 and 2.14). Shorter tubes should be used in future measurements. For this method, the relative variation of the equivalent tonehole's height with frequency is small, and the absolute variation remains small (Figs. 2.10 and 2.11). The method is not convenient for measuring the series impedance of

the tonehole, but proved to have good results for the shunt impedance in the low frequency range (200-1400 Hz). It was shown that the reversed tube method allows an evaluation of the effect of the complex shunt impedance of an open tonehole (Fig. 2.6). Also, the results of the equivalent height of the tonehole seem to be very sensitive to small geometric difference, such as the toneholes with undercut (Fig. 2.15).

Finite Element Method simulation showed that the "forbidden" frequencies in the reversed tube method are mainly due to nodes in pressure at the tonehole in the direct position of the tube, combined with a pressure minimum at the tonehole in the reversed position, and *vice versa* (Figs. 2.23 and 2.24).

For the theoretical analysis of the input and transfer impedance method, it was found that on one hand, when an positive incertitude ($\epsilon > 0$) in the length is introduced, it produces a diminishing value of the imaginary part of the series impedance and on the equivalent length. On the other hand, when a negative value of the uncertainty ϵ is introduced, it will produce that the imaginary part of the series impedance changes to a positive value, which is not in accordance with the theoretical results (Sect. 3.3 Fig. 3.3).

Similarly to the reversed tube method, proposed and studied in chapter 2, it is very likely that, with the input and transfer impedances method it will be very difficult to obtain the series impedance since the computed error is large in the theoretical analysis (around 100% Fig. 3.8a). Nevertheless, the computed error in the shunt impedance was found to be relatively small (less than 10%, Figs. 3.7a and 3.9a). Also, through the simulations of the experiment it was found that small tubes, with few maxima and minima will provide better results (Figs. 3.4 to 3.6).

In the experimental results of the input and transfer impedance method, it is confirmed that it is not possible to accurately measure the transfer impedance in a wide frequency range and this prevents the computation of the tonehole impedances through this method (Sects. 1.3.4, 3.7 Figs. 1.13, 3.12 and 3.13). An experimental reconstruction was performed for a reduced frequency range (100-1200 Hz) and it was found that there is a difference of the order of magnitude of 10^4% in the computation of the series impedance. Also, the experimental reconstruction of the shunt impedance, showed a disagreement of about 70% with the theoretically expected values (Sect. 3.8.1 Figs. 3.14 to 3.17) but, since there are no other experimental results for this kind of tubes with this method it is not possible to know if the problem comes from the fact that the transfer impedance is not accurately measured.

The theoretical comparison between the aforementioned methods showed good agreement in the simulated results. Nevertheless, improvements in the experimental development of both methods is needed in order to achieve good comparable results.

The Finite Element Method simulations through COMSOL Multiphysics, showed good agreement in low frequencies, in particular compared with measurements (Sect. 1.5, Chapter 2 Appendix, Sects. 3.6 and 3.7). Therefore this tool could be used as an alternative to the measurements to obtain the tonehole impedances. Nevertheless, more attention model improvement should be done, in order to achieve results in a higher frequency range.

4.2 Perspectives

In order to continue and improve the results of the present study, an experimental set up that accurately measures the transfer impedance has to be used. It has been proven that without this quantity, achieving accurate results will be very difficult.

In order to obtain better results with the reversed tube method, shorter lengths of tube should be tested in order to increase the frequency range in which accurate results can be achieved. The method should be tested for other undercuts and toneholes with keys and pads such as those found in woodwinds.

The Finite Element model has proven to be a useful tool in this type of study. Nevertheless, better models that are in agreement with measurements have to be performed. For this, higher computing power has to be implemented. Also, this method can be used to achieve results in the nonlinear regime.

Despite it was a goal at the beginning of this study, no results on the nonlinear regime of the tonehole was achieved by the lack of material and time. This is very important if results are to be implement in design and optimization of woodwind instruments software. The use of an artificial mouth that controls the blow pressure and the reed aperture will be very useful in the comparison on the effect of the undercut in the produced sound by means of bifurcation diagrams.

Bibliography

[1] F. Silva, P. Guillemain, J. Kergomard, B. Mallaroni, and A. N. Norris, “Approximation formulae for the acoustic radiation impedance of a cylindrical pipe,” *Journal of Sound and Vibration*, vol. 322, no. 1-2, pp. 255–263, 2009.

Appendix A

Nonlinear behavior of the tonehole

Several studies have been conducted on the nonlinear behavior of the tonehole. Most of them devoted to metamaterials [1], [2], Helmholtz resonators [3], [4], [5] or microperforated plates [6], [7], [8]. Nevertheless, similar characteristics are expected to be found in musical instrument toneholes, to know: the high sound pressure level at the interior and at the exterior of the hole, the formation of jets and vortices, the particle velocity and its relation to the tonehole effective height in the form of the imaginary part of the shunt impedance.

The nonlinear phenomenon related to the toneholes - this is, it depends on the sound intensity - in relation to the fact that the air velocity in small holes can be relatively high. When the velocity in a tonehole is high, a jet is formed when the air exits the tonehole and the kinetic energy of the jet is dissipated by the vortices generated by the mixing of the jet with the air at the exterior. The consequence is an effect of saturation: beyond certain level it is difficult for the air to exit the tonehole which behaves at the limit as if it were closed [9].

The acoustical linear behavior in wind instruments is restricted to low levels. In the case of clarinets, measured in the external camp, we could say that less than 0.1 Pa (74 dB) is considered

low level. In playing conditions musicians can easily overpass the 2 Pa (100 dB). It is therefore, interesting for instrument makers to better understand the behavior of the toneholes at high levels where the nonlinear behavior of the tonehole can be important in the produced sound of the instrument.

The typical amplitude of the standing acoustic wave corresponding to the fundamental oscillation frequency of a clarinet is in the range of 1 to 5 kPa (internal pressure) [10]. In a clarinet, typical tonehole diameter is comparable to the wall thickness. Ingard and Labate [11] showed by flow visualization that in that case the pulsating flow separates from the wall to form free jets, one directed out of the pipe and one directed into the pipe. Ingard and Ising [12] conducted experiments on a tapered orifice with sharp edge and showed that the transfer impedance has a nonlinear, amplitude dependent, real part. Keefe [13] showed that acoustic streaming and convective nonlinearities are components of the sound field in woodwinds under playing conditions. He also showed that the presence of the nonlinear sound field correlated with changes in timbre and the stability of oscillation, and is more pronounced for toneholes whose height is much smaller than its diameter. He observed that nonlinearities are most important for the low register tones of a woodwind.

Several studies, mainly experimental, have been performed with the aim of obtaining a dependence between the change in the holes acoustic impedance and the nonlinearities. Very few are devoted to musical instruments, but to Helmholtz resonators and perforated plates. The main focus is the real part of the orifice impedance, which is related to the acoustic resistance (the dissipation in the hole) since the main purpose of resonators and plates is sound absorption. However, the dependence of the imaginary part of the impedance, related to the effective length of the hole, has also been investigated.

Sivian [14] investigated plates of less than 1 mm thick that where part of a Helmholtz resonator. He obtained particle velocities up to 40 m/s, it was found that the transition to a nonlinear regime comes with an intense increase in the acoustic resistance and it begins at an inlet velocity amplitude as low as 1 m/s. Between 1940 and 1950 Ingard and several co authors [11] [5] [12] published that also the imaginary part of the hole impedance changes in the nonlinear regime, they showed that the imaginary part decreases as the particle velocity increases. It was concluded that the nonlinearity of the hole impedance depends on the interaction between the sound and the vortex fields, and the nonlinear losses may be related to the energy required to generate vortices and jets. In a later article, Ingard et al. [5] showed that for holes with a wall thickness of less than 2 mm nonlinear process becomes noticeable when the amplitude of displacement in the hole is equal to the wall thickness. For a wall thickness greater or equal to 2 mm the amplitude of the particle velocity in the hole does not depend on the thickness nor the diameter. When changing the diameter of the hole, they observed that when the diameter increased and the height of the hole decreased, the nonlinear resistance was increased. In this work Ingard obtained a power dependence of the nonlinear resistance on the velocity with a power of 1.7.

Bies and Wilson [4] measured the acoustic impedance of a Helmholtz resonator installed in a tube. The sound pressure in the tube was 170 dB and the particle velocity in the orifice was 100 m/s, it was found that the acoustic resistance increased with an increase in the velocity at the neck, regardless the position of the resonator in the tube. While for the imaginary part of the hole impedance, interpreted as a length correction, it was found a decrease in the length with an increase in the particle velocity in the neck.

Panton and Goldman [15] introduced dimensionless parameters considering the acoustic impedance of the orifice. For linear regimes: the relative thickness and the shear number. When there is a non-

linear regime: Strouhal number and the dimensionless velocity are added. The Strouhal number represents a measure of the nonlinearity of the flow, where a small Strouhal number is indicative of significant nonlinearity [16]. They found that the nonlinear process is noticeable at a dimensionless velocity of about 3 and above. It was noted that the dependence of the acoustic resistance on the dimensionless velocity in logarithmic coordinates for velocities greater than 10 becomes almost linear and they are related by the air density.

In a literature review, Hirshberg et al. [10] discuss the vortex shedding at the tonehole. There is flow separation from the walls inside the instrument when the acoustical displacement of air particles is comparable or larger than the radius of curvature of the edges of the tonehole. The shear layers formed by this flow separation are unstable and roll up into vortices. Authors mention the experiment proposed by Benade and carried out by Keefe in 1983: two clarinets with equal input acoustical impedance but thin or thick walls have drastically different properties; the thin walled clarinet cannot be played with a regular mouthpiece, which highlights the importance of the nonlinear effects at the toneholes.

In 2000 Dikey et al. [2] used the dimensionless approach to investigate the concentric Helmholtz resonator with eight orifices at 135 dB from 100 to 800 Hz, this ensured a sheared number greater than 10. They found a power relation between the acoustic resistance and the velocity with the power 1.72. They concluded that there is frequency invariance obtained not only for the orifice resistance but for the length correction of the orifice, the length correction decreased with an increase of the velocity at the orifice.

In a theoretical analysis of a nonlinear absorption of a Helmholtz resonator Zinn [3] concluded that the resistance in the neck of the resonator, linearly increases with the velocity. He also noted

that when the oscillating flow passes through the orifice, its cross section contracts, just as it does when a steady flow passes through the orifice. Quantitatively this phenomenon is determined by the vena contracta factor C_v, whose typical value is 0.64. As a result, the measured velocity in the center of orifice increases by 1.56 times. Jing and Sun [1] also investigated theoretically and by measurement the nonlinearities in an orifice of 4 mm diameter at 150 and 200 Hz with variable level up to 144 dB, results showed a value of the vena contracta between 0.63 and 0.75. depending on the sound pressure level.

Temiz et al. [6] investigated four perforated plates with orifice diameters from 0.3 to 4.2 mm, for every plate the perforation coefficient was 0.74%, the study was carried on between 60 and 240 Hz. Authors noted two nonlinear behaviors in the transfer impedance of the orifice: the quasi-steady flow separation at Strouhal numbers less than one, the local vortex shedding for Strouhal number around four and the linear behavior at Strouhal numbers greater than 10.

As noted by Komkin et al. [7] despite the long history of the study of the effects of nonlinearity in the impedance of orifices, there has been almost no work devoted to analyze the effect of the orifice diameter on its nonlinear impedance. They study the variation of an orifice from 3 to 15 mm with pressure levels up to 135 dB, it was shown that with an increase in the sound pressure level, the attached length of the orifice decreases significantly at the beginning, then comes to a new constant level, and the smaller the orifice diameter, the lower this level. It was also found that the nonlinear resistance of the orifice, in contrast to the linear resistance, increases in proportion to the orifice diameter [8]. In a more recent publication Komkin et al. [7] studied the acoustic impedance of orifices, they showed experimentally that in order to obtain reliable estimates of the orifice impedance the particle velocity in the orifice should be determined by measurements. They observed three characteristic areas in the analysis, linear, transitional and developed nonlin-

earity. It was shown that the diameter of the orifice does not affect its acoustic impedance in the developed nonlinear regime. This impedance depends only on the particle velocity of the orifice, and this dependence is nonlinear.

We can conclude form the outlined studies, that there is a nonlinear dependence between the impedance and the particle velocity. These characteristic could play an important role in the final produced sound from the clarinet when played at high sound pressure levels.

Appendix B

Air physical properties

Table B.1: Air's physical properties [17]

Speed of sound	$c = 331.45\sqrt{\frac{t+273.16}{273.16}}\ \left[\frac{m}{s}\right]$
Density	$\rho = 1.2929\frac{273.16}{t+273.16}\left[\frac{kg}{m^3}\right]$
Ratio of specific heats	$\gamma = C_p/C_v = 1.402$
Characteristic viscous length	$\ell_v = \frac{\mu}{\rho c}\ [m]$
Prandtl number	$Pr = \ell_v/\ell_t = (r_v/r_t)^2 = 0.71$
Square root of the Prandtl's number	$\nu = 0.843$
Viscosity	$\mu = 1.708 \times 10^{-5}(1+0.0029t)\left[kg\ m^{-1}s^{-1}\right]$

Radiation impedance [23]

$$Zr = Zc\frac{j\delta ka + 0.5d_2(jka)^2}{1+0.5(n_1+d_1)jka+0.5d_2(jka)^2} \tag{B.1}$$

Where, for an unbaffled tube:

$$\delta = 0.6133\ \ n_1 = 0.167\ \ d_1 = 1.393\ \ d_2 = 0.457 \tag{B.2}$$

and for the baffled tube :

$$\delta = 0.8236\ \ n_1 = 0.182\ \ d_1 = 1.825\ \ d_2 = 0.649 \tag{B.3}$$

Table B.2: Viscothermal losses [17]

Characteristic impedance	$Z_c = \frac{\rho c}{S}\left[1 + \frac{\overline{\alpha_1}(1-j)}{r_v} - \frac{\overline{\alpha_2} j}{r_v^2}\right]$
Phase velocity	$\frac{\omega}{v_\varphi} = \frac{\omega}{c}\left[1 + \frac{\alpha_1}{r_v}\right]$
$\overline{\alpha_1}$	$\frac{1}{\sqrt{2}}\left(1 - \frac{\gamma-1}{\nu}\right)$
$\overline{\alpha_2}$	$1 - \frac{\gamma-1}{\nu} + \frac{\gamma-1}{2\nu^2} + \frac{3(\gamma-1)^2}{2\nu^2}$
α	$\frac{\omega}{c}\left[\frac{\alpha_1}{r_v} + \frac{\alpha_2}{r_v^2}\right]$
α_1	$\frac{1}{\sqrt{2}}\left(1 + \frac{\gamma-1}{\nu}\right)$
α_2	$1 + \frac{\gamma-1}{\nu} - \frac{\gamma-1}{2\nu^2} - \frac{(\gamma-1)^2}{2\nu^2}$
	$r_v = R\sqrt{\frac{\omega}{c\ell_v}}$
	$r_t = R\sqrt{\frac{\omega}{c\ell_t}}$
Propagation constant	$\Gamma_a = \alpha + j\omega/v_\varphi$

Table B.3: Equivalent lengths for an open tonehole

Main tube	$t_a = -(b\delta^2)/(1.78\tanh(1.84\,t/b) + 0.94 + 0.540\delta + 0.285\delta^2)$	[18]
Matching volume	$t_m = b\delta(1 + 0.207\delta^3)/8$	[19]
Drilled tonehole	$\delta_{cyl} = 0.822 - 0.47(b/(a+t))^{0.8}$	[20]
Radiation impedance	$Z_{rh} = Z_{oh}[0.25(kb)^2 + jk\delta_{cyl}b]$	[21]
Radiation equivalent length	$t_r = \tan^{-1}[Z_{rh}/(jZ_{oh})]/k$	[22]
Inner equivalent length	$t_i = (0.82 - 0.193\delta - 1.09\delta^2 + 1.27\delta^3 - 0.71\delta^4)b$	[18]

Bibliography

[1] X. Jing and X. Sun, "Sound-excited flow and acoustic nonlinearity at an orifice," *Physics of Fluids*, vol. 14, no. 1, pp. 268–276, 2002.

[2] N. Dickey, A. Selamet, and J. Novak, "The effect of high-amplitude sound on the attenuation of perforated tube silencers," *The Journal of the Acoustical Society of America*, vol. 108, no. 3, pp. 1068–1081, 2000.

[3] B. T. Zinn, "A theoretical study of non-linear damping by helmholtz resonators," *Journal of Sound and Vibration*, vol. 13, no. 3, pp. 347–356, 1970.

[4] D. A. Bies and O. Wilson Jr, "Acoustic impedance of a helmholtz resonator at very high amplitude," *The Journal of the Acoustical Society of America*, vol. 29, no. 6, pp. 711–714, 1957.

[5] U. Ingard, "On the theory and design of acoustic resonators," *The Journal of the acoustical society of America*, vol. 25, no. 6, pp. 1037–1061, 1953.

[6] M. A. Temiz, I. Lopez Arteaga, G. Efraimsson, M. Åbom, and A. Hirschberg, "The influence of edge geometry on end-correction coefficients in micro perforated plates," *The Journal of the Acoustical Society of America*, vol. 138, no. 6, pp. 3668–3677, 2015.

[7] A. Komkin, A. Bykov, and M. Mironov, "Experimental study of nonlinear acoustic impedance of circular orifices," *The Journal of the Acoustical Society of America*, vol. 148, no. 3, pp. 1391–1403, 2020.

[8] A. Komkin, A. Bykov, and M. Mironov, "Acoustic resistance of an orifice at high sound pressure levels," *Acoustical Physics*, vol. 64, no. 5, pp. 563–566, 2018.

[9] J.-P. Dalmont, "Acoustique des instruments à anches," in *Musique et Technique 2010*.

[10] A. Hirschberg, J. Gilbert, A. Wijnands, and A. Valkering, "Musical aero-acoustics of the clarinet," *Le Journal de Physique IV*, vol. 4, no. C5, pp. C5–559, 1994.

[11] U. Ingård and S. Labate, "Acoustic circulation effects and the nonlinear impedance of orifices," *The Journal of the Acoustical Society of America*, vol. 22, no. 2, pp. 211–218, 1950.

[12] U. Ingard and H. Ising, "Acoustic nonlinearity of an orifice," *The journal of the Acoustical Society of America*, vol. 42, no. 1, pp. 6–17, 1967.

[13] D. H. Keefe, "Experiments on the single woodwind tone hole," *The Journal of the Acoustical Society of America*, vol. 72, no. 3, pp. 688–699, 1982.

[14] L. Sivian, "Acoustic impedance of small orifices," *The Journal of the Acoustical Society of America*, vol. 7, no. 2, pp. 94–101, 1935.

[15] R. L. Panton and A. L. Goldman, "Correlation of nonlinear orifice impedance," *The Journal of the Acoustical Society of America*, vol. 60, no. 6, pp. 1390–1396, 1976.

[16] D. Rockliff, *Application of particle image velocimetry to the measurement of non-linear effects generated by high-intensity acoustic fields*. PhD thesis, University of Edinburgh, 2002.

[17] A. Chaigne and J. Kergomard, *Acoustics of musical instruments*. Springer, 2016.

[18] V. Dubos, J. Kergomard, A. Khettabi, J.-P. Dalmont, D. Keefe, and C. Nederveen, "Theory of sound propagation in a duct with a branched tube using modal decomposition," *Acta Acustica united with Acustica*, vol. 85, no. 2, pp. 153–169, 1999.

[19] C. Nederveen, J. Jansen, and R. Van Hassel, "Corrections for woodwind tone-hole calculations," *Acta Acustica united with Acustica*, vol. 84, no. 5, pp. 957–966, 1998.

[20] A. Lefebvre and G. P. Scavone, "Characterization of woodwind instrument toneholes with the finite element method," *The Journal of the Acoustical Society of America*, vol. 131, no. 4, pp. 3153–3163, 2012.

[21] J.-P. Dalmont, C. Nederveen, and N. Joly, "Radiation impedance of tubes with different flanges: numerical and experimental investigations," *Journal of sound and vibration*, vol. 244, no. 3, pp. 505–534, 2001.

[22] J.-P. Dalmont, C. J. Nederveen, V. Dubos, S. Ollivier, V. Meserette, E. te Sligte, *et al.*, "Experimental determination of the equivalent circuit of an open side hole: linear and non linear behaviour," *Acta Acustica united with acustica*, vol. 88, no. 4, pp. 567–575, 2002.

[23] F. Silva, P. Guillemain, J. Kergomard, B. Mallaroni, and A. N. Norris, "Approximation formulae for the acoustic radiation impedance of a cylindrical pipe," *Journal of Sound and Vibration*, vol. 322, no. 1-2, pp. 255–263, 2009.

Bibliography

[1] Noureddine Atalla and Franck Sgard. *Finite element and boundary methods in structural acoustics and vibration*. CRC Press, 2015.

[2] Arthur H Benade. *Fundamentals of musical acoustics*. Courier Corporation, 1990.

[3] Arthur H Benade and JS Murday. Measured end corrections for woodwind tone-holes. *The Journal of the Acoustical Society of America*, 41(6):1609–1609, 1967.

[4] David A Bies and OB Wilson Jr. Acoustic impedance of a helmholtz resonator at very high amplitude. *The Journal of the Acoustical Society of America*, 29(6):711–714, 1957.

[5] J Bretos, C Santamarıa, and J Alonso Moral. Vibrational patterns and frequency responses of the free plates and box of a violin obtained by finite element analysis. *The Journal of the Acoustical Society of America*, 105(3):1942–1950, 1999.

[6] Encyclopaedia Britannica. The history of western wind instruments, 2021. URL: https://www.britannica.com/art/wind-instrument/The-history-of-Western-wind-instruments.

[7] Gregory Bunting, Scott T Miller, Clark R Dohrmann, and Timothy Walsh. Solving complex acoustic problems using high performance computations. *Acoustics Today*, 16(SAND2020-3661J), 2020.

[8] Antoine Chaigne. *Ondes acoustiques*. Editions Ecole Polytechnique, 2001.

[9] Antoine Chaigne and Jean Kergomard. *Acoustics of musical instruments*. Springer, 2016.

[10] A Kimi Coaldrake. A finite element model of the japanese koto constructed from computed tomography scans. *The Journal of the Acoustical Society of America*, 148(5):3153–3170, 2020.

[11] John W Coltman. Acoustical analysis of the boehm flute. *The Journal of the Acoustical Society of America*, 65(2):499–506, 1979.

[12] J-P Dalmont. Acoustic impedance measurement, part i: A review. *Journal of Sound and Vibration*, 243(3):427–439, 2001.

[13] Jean-Pierre Dalmont. Acoustique des instruments à anches. In *Musique et Technique 2010*.

[14] Jean-Pierre Dalmont, Cornelis J Nederveen, Véronique Dubos, Sébastien Ollivier, Vincent Meserette, Edwin te Sligte, et al. Experimental determination of the equivalent circuit of an open side hole: linear and non linear behaviour. *Acta Acustica united with acustica*, 88(4):567–575, 2002.

[15] Laboratoire de Mécanique et d'Acoustique. Home page, 2021. URL: http://www.lma.cnrs-mrs.fr/spip/?lang=en.

[16] Tirso De Olazábal and Raquel C de Arias. *Acústica musical y organología*. Ricordi, 1954.

[17] Vincent Debut, Jean Kergomard, and Franck Laloë. Analysis and optimisation of the tuning of the twelfths for a clarinet resonator. *Applied acoustics*, 66(4):365–409, 2005.

[18] Paul A Dickens et al. *Flute acoustics: measurements, modelling and design*. PhD thesis, PhD Thesis, University of New South Wales, 2007.

[19] NS Dickey, A Selamet, and JM Novak. The effect of high-amplitude sound on the attenuation of perforated tube silencers. *The Journal of the Acoustical Society of America*, 108(3):1068–1081, 2000.

[20] Vincent Dubos, J Kergomard, A Khettabi, J-P Dalmont, DH Keefe, and CJ Nederveen. Theory of sound propagation in a duct with a branched tube using modal decomposition. *Acta Acustica united with Acustica*, 85(2):153–169, 1999.

[21] MJ Elejabarrieta, A Ezcurra, and C Santamaría. Vibrational behaviour of the guitar soundboard analysed by the finite element method. *Acta Acustica united with Acustica*, 87(1):128–136, 2001.

[22] MJ Elejabarrieta, A Ezcurra, and C Santamarıa. Coupled modes of the resonance box of the guitar. *The Journal of the Acoustical Society of America*, 111(5):2283–2292, 2002.

[23] Hanna Gothall. How to inspect your mesh in comsol multiphysics. Technical report, COMSOL, 2017.

[24] Alexis Guilloteau. Conception d'une clarinette logique. *Design of a logical clarinet"), Ph. D. thesis, Aix-Marseille Université, Marseille, France*, 2015.

[25] A Hirschberg, Joel Gilbert, APJ Wijnands, and AMC Valkering. Musical aero-acoustics of the clarinet. *Le Journal de Physique IV*, 4(C5):C5–559, 1994.

[26] U Ingård and S Labate. Acoustic circulation effects and the nonlinear impedance of orifices. *The Journal of the Acoustical Society of America*, 22(2):211–218, 1950.

[27] Uno Ingard. On the theory and design of acoustic resonators. *The Journal of the acoustical society of America*, 25(6):1037–1061, 1953.

[28] Uno Ingard and Hartmut Ising. Acoustic nonlinearity of an orifice. *The journal of the Acoustical Society of America*, 42(1):6–17, 1967.

[29] Mads Herring Jensen. Theory of thermoviscous acoustics: Thermal and viscous losses. Technical report, COMSOL, 2014.

[30] Xiaodong Jing and Xiaofeng Sun. Sound-excited flow and acoustic nonlinearity at an orifice. *Physics of Fluids*, 14(1):268–276, 2002.

[31] Douglas H Keefe. Experiments on the single woodwind tone hole. *The Journal of the Acoustical Society of America*, 72(3):688–699, 1982.

[32] Douglas H Keefe. Theory of the single woodwind tone hole. *The Journal of the Acoustical Society of America*, 72(3):676–687, 1982.

[33] Douglas H Keefe. Acoustic streaming, dimensional analysis of nonlinearities, and tone hole mutual interactions in woodwinds. *The Journal of the Acoustical Society of America*, 73(5):1804–1820, 1983.

[34] Hyacinthe Klosé. *Celebrated Method for the Clarinet: Complete Edition*. Carl Fischer Music Dist, 1946.

[35] AI Komkin, AI Bykov, and MA Mironov. Acoustic resistance of an orifice at high sound pressure levels. *Acoustical Physics*, 64(5):563–566, 2018.

[36] Alexandr Komkin, Aleksei Bykov, and Mikhail Mironov. Experimental study of nonlinear acoustic impedance of circular orifices. *The Journal of the Acoustical Society of America*, 148(3):1391–1403, 2020.

[37] Marc Pachebat Le Roux Jean Christophe and Dalmont Jean Pierre. Un capteur de nouvelle génération pour la mesure d'impédance acoustique en contexte industriel.

[38] Antoine Lefebvre. Computational acoustic methods for the design of woodwind instruments. 2011.

[39] Antoine Lefebvre and Gary P Scavone. Characterization of woodwind instrument toneholes with the finite element method. *The Journal of the Acoustical Society of America*, 131(4):3153–3163, 2012.

[40] LMA. Inauguration liamfi, 2019. URL: http://www.lma.cnrs-mrs.fr/spip.php?article809.

[41] Charles A Macaluso and Jean-Pierre Dalmont. Trumpet with near-perfect harmonicity: Design and acoustic results. *The Journal of the Acoustical Society of America*, 129(1):404–414, 2011.

[42] Robert MacDonald. Study of the undercutting of woodwind toneholes using particle image velocimetry. 2009.

[43] Erdogan Madenci and Ibrahim Guven. *The finite element method and applications in engineering using ANSYS®*. Springer, 2015.

[44] N Marcuvitz. Handbook, waveguide vol. 10, 1951.

[45] Mircea Mihălcică, Mariana D Stanciu, and Sorin Vlase. Frequency response evaluation of guitar bodies with different bracing systems. *Symmetry*, 12(5):795, 2020.

[46] de la Recherche et de l'Innovation Ministère de l'Enseignement supérieur. Conventions industrielles de formation par la recherche (cifre), 2021. URL: https://www.enseignementsup-recherche.gouv.fr/cid22130/les-cifre.html.

[47] CJ Nederveen, JKM Jansen, and RR Van Hassel. Corrections for woodwind tone-hole calculations. *Acta Acustica united with Acustica*, 84(5):957–966, 1998.

[48] Cornelis Johannes Nederveen. Acoustical aspects of woodwind instruments. 1969.

[49] Ronald L Panton and Allen L Goldman. Correlation of nonlinear orifice impedance. *The Journal of the Acoustical Society of America*, 60(6):1390–1396, 1976.

[50] Erik Petersen. *Comment le facteur d'instruments du musique a anche equilibre-t-il la production et le rayonnement?* PhD thesis, Aix-Marseille Univ, 2020.

[51] Erik Petersen, Tom Colinot, Jean Kergomard, and Philippe Guillemain. On the tonehole lattice cutoff frequency of conical resonators: applications to the saxophone. *Acta Acustica*, 4(4):13, 2020.

[52] Edward Alexander Keane Ridley. Birth of the'boehm'clarinet. *The Galpin Society Journal*, pages 68–76, 1986.

[53] Dawn Rockliff. *Application of particle image velocimetry to the measurement of non-linear effects generated by high-intensity acoustic fields*. PhD thesis, University of Edinburgh, 2002.

[54] Péter Rucz, Fülöp Augusztinovicz, Judit Angster, Tim Preukschat, and András Miklós. A finite element model of the tuning slot of labial organ pipes. *The Journal of the Acoustical Society of America*, 137(3):1226–1237, 2015.

[55] HL Schwab and KC Chen. Finite element analysis of a guitar soundboard. *Catgut Acoust. Soc. Newsletter*, 24:13–15, 1975.

[56] Orphée Shop. Orphée music shop, 2021. URL: http://en.orpheemusic.com/clarinet.html.

[57] Fabrice Silva, Ph Guillemain, Jean Kergomard, Bastien Mallaroni, and Andrew N Norris. Approximation formulae for the acoustic radiation impedance of a cylindrical pipe. *Journal of Sound and Vibration*, 322(1-2):255–263, 2009.

[58] LJ Sivian. Acoustic impedance of small orifices. *The Journal of the Acoustical Society of America*, 7(2):94–101, 1935.

[59] Buffet Crampon Societe. Buffet crampon about us, 2021. URL: https://www.buffet-crampon.com/en/about-us/.

[60] G.R.A.S Sound and Vibration. Gras 40sc ccp probe microphone, 2021. URL: https://www.grasacoustics.com/products/special-microphone/probe-microphones/product/189-40sc.

[61] G.R.A.S Sound and Vibration. Gras 46bf-1 1/4" lemo free-field, 2021. URL: https://www.grasacoustics.com/products/measurement-microphone-sets/traditional-power-supply-lemo/product/686-46bf-1.

[62] MA Temiz, I Lopez Arteaga, and A Hirschberg. Non-linear behaviour of tone holes in musical instruments: an experimental study. In *French Acoustic Congress (CFA 2016)*, pages 377–382. Université du Maine, 2016.

[63] Muttalip Aşkın Temiz, Ines Lopez Arteaga, Gunilla Efraimsson, Mats Åbom, and Avraham Hirschberg. The influence of edge geometry on end-correction coefficients in micro perforated plates. *The Journal of the Acoustical Society of America*, 138(6):3668–3677, 2015.

[64] Michael Thrasher. The clarinetist-composers of nineteenth-century italy: An examination of style, repertoire, and pedagogy. *Proceedings of the Thirteenth Annual ClarinetFest (Atlanta, GA, 2006, accessed 30 January 2007)*, 2006.

[65] Robin Tournemenne and Juliette Chabassier. A comparison of a one-dimensional finite element method and the transfer matrix method for the computation of wind music instrument impedance. *Acta Acustica united with Acustica*, 105(5):838–849, 2019.

[66] Ben T Zinn. A theoretical study of non-linear damping by helmholtz resonators. *Journal of Sound and Vibration*, 13(3):347–356, 1970.

Résumé de la thèse en français :

Cette thèse Cifre est réalisée avec le facteur d'instruments à vent Buffet Crampon. Nous étudions la caractérisation acoustique des trous latéraux ouverts dans la clarinette, ou trous de notes. La jonction entre la cheminée de ces trous et le corps principal de l'instrument peut être chanfreinée lors de la fabrication. On parle alors de sous-coupage des trous. La motivation du facteur d'instruments à sous-couper certains trous est d'améliorer la justesse, la puissance et la facilité d'émission.

Depuis des décennies, le fonctionnement acoustique des trous latéraux peut être décrit de manière simplifiée par un modèle linéaire. Ce modèle s'intègre au formalisme des lignes de transmission utilisé pour modéliser la propagation acoustique dans les guides d'onde 1D. Le trou est représenté comme un élément localisé, caractérisé par une portion de circuit acoustique en T, associant dans le domaine fréquentiel une impédance en série et une impédance en parallèle.

Déterminer expérimentalement ces deux quantités est un enjeu important : cela permet à la fois d'intégrer dans le modèle l'effet de la complexité géométrique des différents types de sous-coupage pratiqués, mais également de modéliser des trous latéraux d'un instrument dont on ignore la géométrie.

Pour réaliser cet objectif, deux méthodes sont étudiées et comparées dans cette thèse : une première méthode proposée par J-P Dalmont et col. (2002), et une méthode originale que nous proposons. Cette dernière est basée sur la mesure de deux impédances d'entrée là où à la première méthode repose sur la mesure des impédances d'entrée et de transfert. Une simulation de l'expérience est réalisée où la sensibilité à des incertitudes géométriques ou de mesure est évaluée afin de dimensionner au mieux l'expérience. La mise en œuvre expérimentale permet de souligner les avantages et les faiblesses de cette nouvelle méthode par rapport à l'état de l'art. En particulier, on retient les résultats obtenus sur la détermination de l'impédance en parallèle. La capacité de la méthode à estimer de manière robuste sa partie réelle d'abord. Les résultats obtenus suggèrent d'ailleurs la nécessité de nouvelles études théoriques sur la modélisation des mécanismes dissipatifs. Nous notons également la capacité de la méthode à traduire de faibles variations géométriques au travers de l'estimation de la partie imaginaire de l'impédance en parallèle.

Des simulations numériques par la méthode des Elements Finis sont également réalisées pour éclairer le résultat des expériences (en particulier dans des configurations où l'approche expérimentale est mise en difficulté) mais aussi pour évaluer la pertinence de cet outil pour les travaux ultérieurs sur ces sujets.

A terme, ces modèles doivent intégrer des outils numériques d'aide à la conception en facture instrumentale.

Abstract

This Cifre PhD thesis is done with the wind instrument maker Buffet Crampon. We study the acoustic characterization of the open side holes in the clarinet, or toneholes. The junction between the chimney of these holes and the main body of the instrument can be chamfered during the manufacturing process. This is called undercutting the toneholes. The motivation of the instrument maker to undercut certain toneholes is to improve the tuning, the power and the ease of playing.

For decades, the acoustic functioning of toneholes can be described in a simplified way by a linear model. This model fits the transmission line formalism used to model acoustic propagation in 1D waveguides. The hole is represented as a localized element, characterized by a portion of an acoustic T-shaped circuit, associating in the frequency domain a series impedance and a parallel (shunt) impedance.

Determining experimentally these two quantities is an important issue : it allows both to integrate in the model the effect of the geometrical complexity of the different types of undercutting practiced, but also to model toneholes of an instrument whose geometry is unknown.

To achieve this objective, two methods are studied and compared in this thesis : a first method proposed by J-P Dalmont et al. (2002), and an original method that we propose. The latter is based on the measurement of two input impedances where the first method is based on the measurement of input and transfer impedances. A simulation of the experiment is performed where the sensitivity to geometrical or measurement uncertainties is assessed in order to best size the experiment. The experiment carried out allows to highlight the advantages and weaknesses of this new method compared to the state of the art. In particular, the results obtained on the determination of the shunt impedance are interesting. First of all, the ability of the method to estimate its real part in a robust way is stressed. The results obtained suggest the need for further theoretical studies on the modeling of dissipative mechanisms. We also note the ability of the method to account small geometrical variations through the estimation of the imaginary part of the shunt impedance.

Numerical simulations by the Finite Element Method are also carried out to shed some light on the results of the experiments (in particular in configurations where the experimental approach is challenged) but also to evaluate the relevance of this tool for further work on these topics.

Eventually, these models are expected to be part of numerical tools to help makers in the design of instruments.